National Library of Canada
Acquisitions and Bibliographic Services Branch
395 Wellington Street
Ottawa, Ontario
K1A 0N4

Bibliothèque nationale du Canada
Direction des acquisitions et des services bibliographiques
395, rue Wellington
Ottawa (Ontario)
K1A 0N4

Your file Votre référence

Our file Notre référence

NOTICE

The quality of this microform is heavily dependent upon the quality of the original thesis submitted for microfilming. Every effort has been made to ensure the highest quality of reproduction possible.

If pages are missing, contact the university which granted the degree.

Some pages may have indistinct print especially if the original pages were typed with a poor typewriter ribbon or if the university sent us an inferior photocopy.

AVIS

La qualité de cette microforme dépend grandement de la qualité de la thèse soumise au microfilmage. Nous avons tout fait pour assurer une qualité supérieure de reproduction.

S'il manque des pages, veuillez communiquer avec l'université qui a conféré le grade.

La qualité d'impression de certaines pages peut laisser à désirer, surtout si les pages originales ont été dactylographiées à l'aide d'un ruban usé ou si l'université nous a fait parvenir une photocopie de qualité inférieure.

Canada

THE GEOLOGY AND GEOCHEMISTRY OF GOLD MINERALIZATION IN THE BETTS BIG POND AREA, NEWFOUNDLAND

By

James Lavigne

A thesis submitted to the
School of Graduate Studies and Research
in partial fulfillment of the requirements
for the degree of Master of Science

Ottawa-Carleton Geoscience Centre
Department of Geology
University of Ottawa

January 1993

ISBN 0-315-89666-3

Canada

UNIVERSITÉ D'OTTAWA
UNIVERSITY OF OTTAWA

ABSTRACT

The ultramafic member of the Lower Ordovician Betts Cove Ophiolite Complex forms an elongate fault bounded belt on the eastern side of the Baie Verte Peninsula. The rocks in the southern part of the ultramafic belt consist of layered cumulates. The northern part of the belt dominantly consists of talc-carbonate rocks. A number of Au vein occurrences are located in the metasomatized rocks in the northern part of the belt.

The Betts Big Pond area encompasses the transition between the least altered layered cumulate rocks of the southern part of the ultramfic belt and the metasomatized rocks of the northern part of the ultramafic belt and includes serpentinite, serpentine-carbonate rocks, and talc-carbonate rocks. Au concentrations up to 1300 ppb occur in hematite bearing talc-carbonate rocks in the northern part of the Betts Big Pond area. Except for the occurrence of hematite and possibly barite, Au-bearing talc-carbonate rocks are mineralogically and chemically similar to non-Au-bearing talc-carbonate rocks. C and O isotopic compositions of magnesite from Au-bearing, non-Au-bearing talc-carbonate rocks, and serpentine-carbonate rocks are similar. Slightly anomalous Au concentrations are associated with magnetite-rich Fe-Cu sulphide bearing serpentinite.

The occurrence of Au in talc-carbonate rocks is consistent

with its deposition from $Au(HS)_2^-$ due to fluid oxidation as a result of the carbonatization of magnetite in the absence of Fe-bearing serpentine. The Au occurrence in serpentinite is consistent with Au deposition from $Au(HS)_2^-$ as the serpentinizing fluid reacted with a chromite lens.

The Long Pond and Arrowhead Pond veins in the northern part of the Betts Cove Complex are interpreted to have formed from fluids of mutually similar composition. C and O isotopic compositions of vein carbonates from the northern Betts Cove Complex are similar to the isotopic composition of C and O of magnesite from talc-carbonate rocks and serpentine-carbonate rocks of the Betts Big Pond area. Talc-carbonate rocks within the alteration halo surrounding Au-vein mineralization at Arrowhead Pond is enriched in SiO_2. Otherwise it is chemically similar to talc-carbonate rocks adjacent to the halo and talc-carbonate rocks in the Betts Big Pond area. The similarity in chemical and isotopic compositions as well as geological constraints suggets that Au-vein mineralization may have been emplaced at a similar time as Au-mineralization in talc-carbonate rock in the Betts Big Pond area.

Fluid conditions during serpentinization may have been favourable for the dissolution of Au as $Au(HS)_2^-$. Magmatic sulphides dissolved during serpentinization may have yielded Au and S in the fluids. The timing of serpentinization with respect to carbonatization is not known; it is possible that serpentinization and carbonatization represent different

metasomatic fronts of the same event. If this is the case it may be reasonable to postulate that Au liberated during serpentinization was deposited in talc-carbonate rocks in the Betts Big Pond area and as Au-veins in the northern part of the ultramafic belt.

ACKNOWLEDGEMENTS

The field work presented in this thesis was conducted as part of a Geological Survey of Canada (GSC) project on the Metallogeny of Newfoundland Ophiolites under the supervision of Dr. John W. Lydon. Dr. Lydon of the GSC is gratefully acknowledged for permission to use the data which forms the basis of this thesis and for the provision of whole rock chemical data and polished thin sections. Dr. Lydon is also thanked for numerous discussions about mineral deposits and general geology from which I have greatly benefitted.

Dr. Keiko Hattori is thanked for supervision and support. I wish to thank Don Harris (GSC) for assistance in identifying the fine grained sulphides in magnetite, Bruce Ballantyne (GSC) for introducing me to the Scanning Electron Microscope and providing numerous references relevant to this thesis, and Bob Delabio (GSC) for providing XRD analyses of serpentinite and talc-carbonate rocks. Greg Beischer (INCO Ltd) is thanked for providing drill logs from the Betts Big Pond area.

TABLE OF CONTENTS

CHAPTER FOUR - Au MINERALIZATION

CHAPTER FIVE - SUMMARY AND DISCUSSION

LIST OF FIGURES

LIST OF PLATES

LIST OF TABLES

CHAPTER 1

INTRODUCTION

1.1 Background

A number of Au vein deposits in Archean greenstone belts around the world are spatially associated with ultramafic rocks. These include deposits in Canada (e.g Boyle, 1979; Hodgson and MacGeehan, 1982; Fyon et al., 1983), deposits in Africa (e.g. Foster and Wilson, 1984; Viljoen, 1984, Fabiani, 1984), and deposits in Australia (e.g. Keays, 1984; 1987; Groves et al., 1984; Groves and Phillips, 1987). Au deposits hosted by Upper Proterozoic ultramafic rocks in northern Africa has been described by Buisson and Leblanc (1986; 1987). The association of Au deposits with ultramafic rocks has been described for Cenozoic Cordilleran deposits such as those in the Motherlode and Allegheny Districts, California (e.g. Knopf, 1929; Coveny, 1981; Bohlke, 1989). This association has prompted a number of people to propose genetic models for Au mineralization involving ultramafic rocks (e.g. Ferguson and Ganet, 1932; Boyle, 1961; Pyke, 1976; Keays, 1984; Groves et al., 1987; Buisson and Leblanc, 1987).

Although the deposits differ in detail, characteristics common to all include that they are associated with major faults or related splays and are associated with carbonate alteration. Tuach et al. (1988) recognized Au mineralization in

varied geological settings in Newfoundland. Among these is the occurrence of Au mineralization associated with altered ultramafic rocks in major fault zones. The two primary examples of this setting are the Gander River Ultrabasic Belt (GRUB-Line) (Blackwood, 1982) and the Baie Verte Line (Williams and St. Julien, 1982) (Figure 1.1).

Most Au vein occurrences of the Baie Verte Peninsula are hosted by or are directly spatially associated with deformed and carbonatized ophiolitic ultramafic rocks (Figure 1.2 and Table 1.1). Gower et al. (1990) have applied a model, similar to the "listwaenite" model (Buisson and Leblanc, 1986; 1987), to Au mineralization at Deer Cove. This model implies a direct link between ultramafic rocks, thrusting, carbonatization, and Au mineralization.

An area of the Betts Cove Ophiolite Complex (herein referred to as the Betts Big Pond area) contains a variety of altered ultramafic rocks whose contact relationships are particularly well exposed. These rocks and contact relationships include: layered peridotite cut by serpentinite shear zones; serpentinite containing carbonate veins and veinlets; talc-carbonate-serpentine assemblages; and talc-carbonate assemblages. During the 1987 field season, INCO Exploration and Technical Services Ltd. (INCO) outlined a broad Au geochemical anomaly in glacial till centred on talc-carbonate rocks in the Betts Big Pond area. Subsequent exploratory

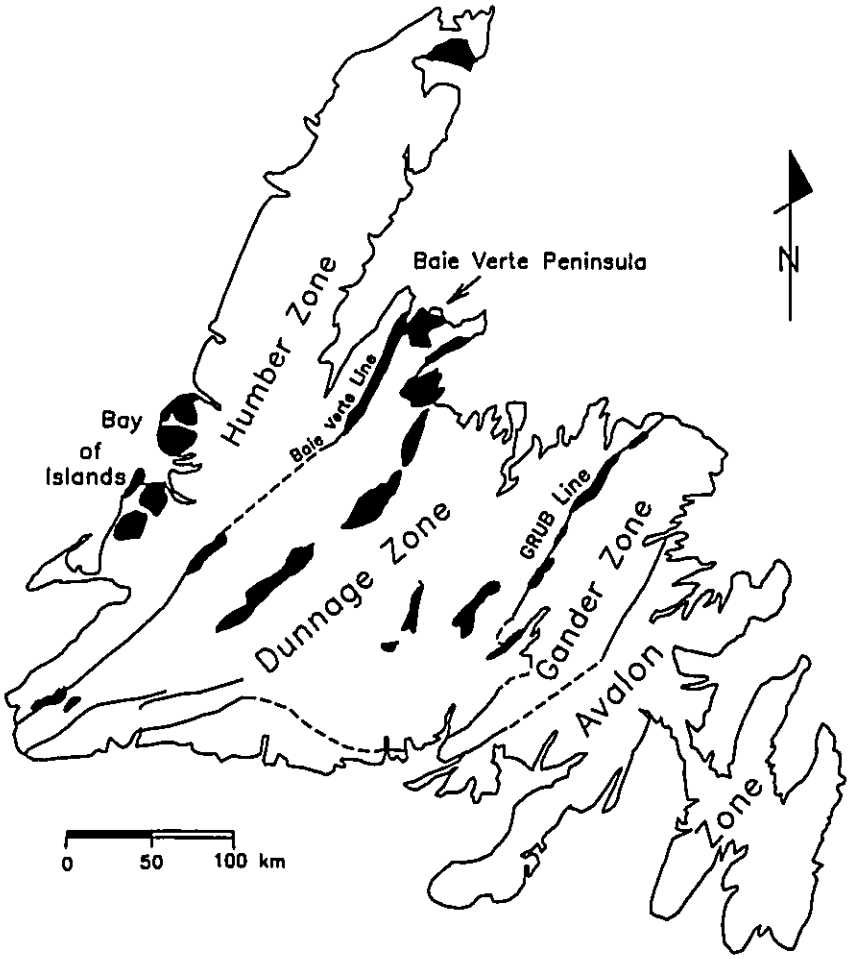

Figure 1.1. Tectonic-stratigraphic divisions of Newfoundland, location of the Baie Verte and GRUB Lines (from Williams et al., 1988) and ophiolite complexes (black) (modified from Fyffe and Swinden, 1991).

Table 1-1. Some characteristics of Au mineralization on the Baie Verte Peninsula

Prospect	Setting/Characteristics	Spatial association with ultramafic rocks
Deer Cove	- shear zone hosted quartz vein in ophiolitic mafic volcanic and volcaniclastic rocks[1]	- host rocks form hanging wall of thrust fault the footwall being occupied by serpentine, talc, carbonate, quartz altered ultramafic rocks[1]
Dorset Showing	- shear zone hosted quartz veins in mafic and tuffaceous rocks[2]	- serpentine and talc altered ultramafic rocks occur as faulted slivers on the property[2]
Stog'er Tight	- gold occurs disseminated and and in microveinlets in albitized and pyritic ophiolitic gabbro[3]	- host rocks located in hanging wall of major thrust fault the foot wall of which is characterized by the discontinuous occurrence of serpentine, talc, carbonate, quartz altered ultramafic bodies[4]
Long Pond	- quartz stockwork hosted by quartz-carbonate altered ultramafic rocks in fault zone with Silurian pyroclastic rocks[5]	- ultramafic hosted
Tom Showing	- quartz vein hosted by Silurian felsic pyroclastic rocks[5]	- located in same fault zone as Long Pond Showing which imbricates ultramafic rocks and felsic volcanic/sedimentary rocks
Arrowhead Pond	- quartz veins hosted by talc-carbonate-quartz altered ultramafic rocks within regionally altered talc-carbonate ultramafic rocks[5]	- ultramafic hosted

References: 1. Gower et al. (1990); 2. MacDougall and MacInnis (1990); 3. Huard (1990); 4. Hibbard (1983); 5. Al (1990).

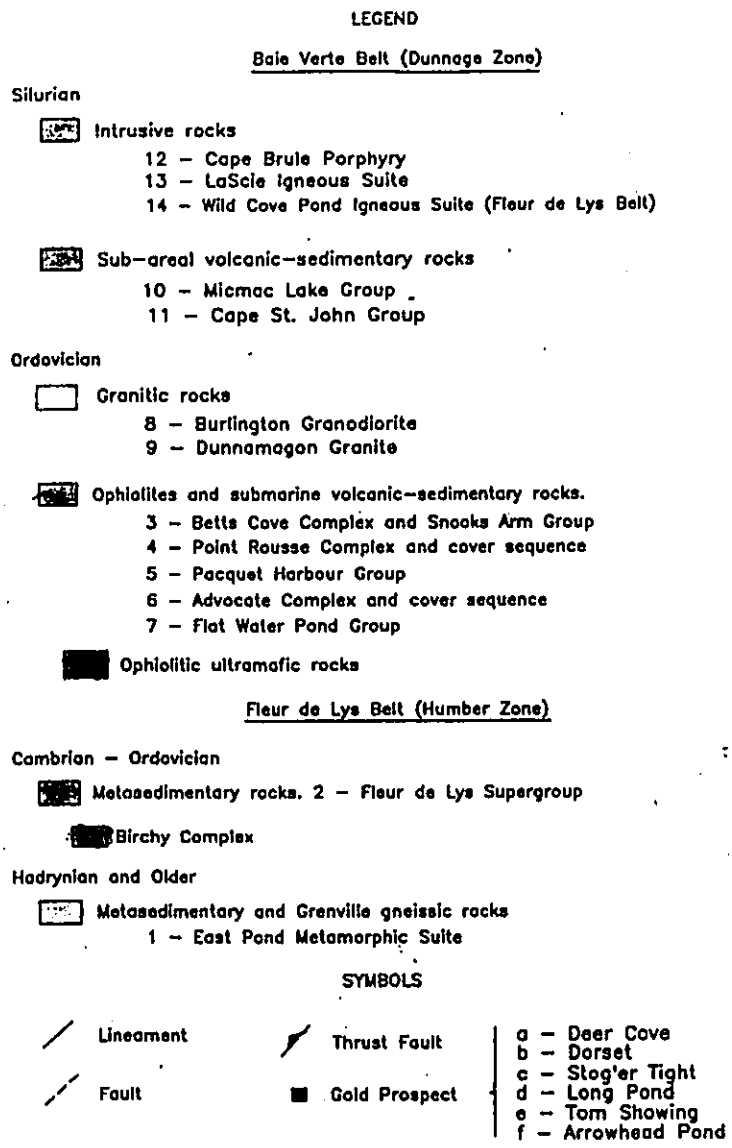

Figure 1.2. Geology of the Baie Verte Peninsula modified after Hibbard (1983). Lineaments from Scanning Airborne Radar Images from the Centre for Remote Sensing, Dept. of Energy Mines and Resources, Canada. Unpublished map Courtesy of the Geological Survey of Canada.

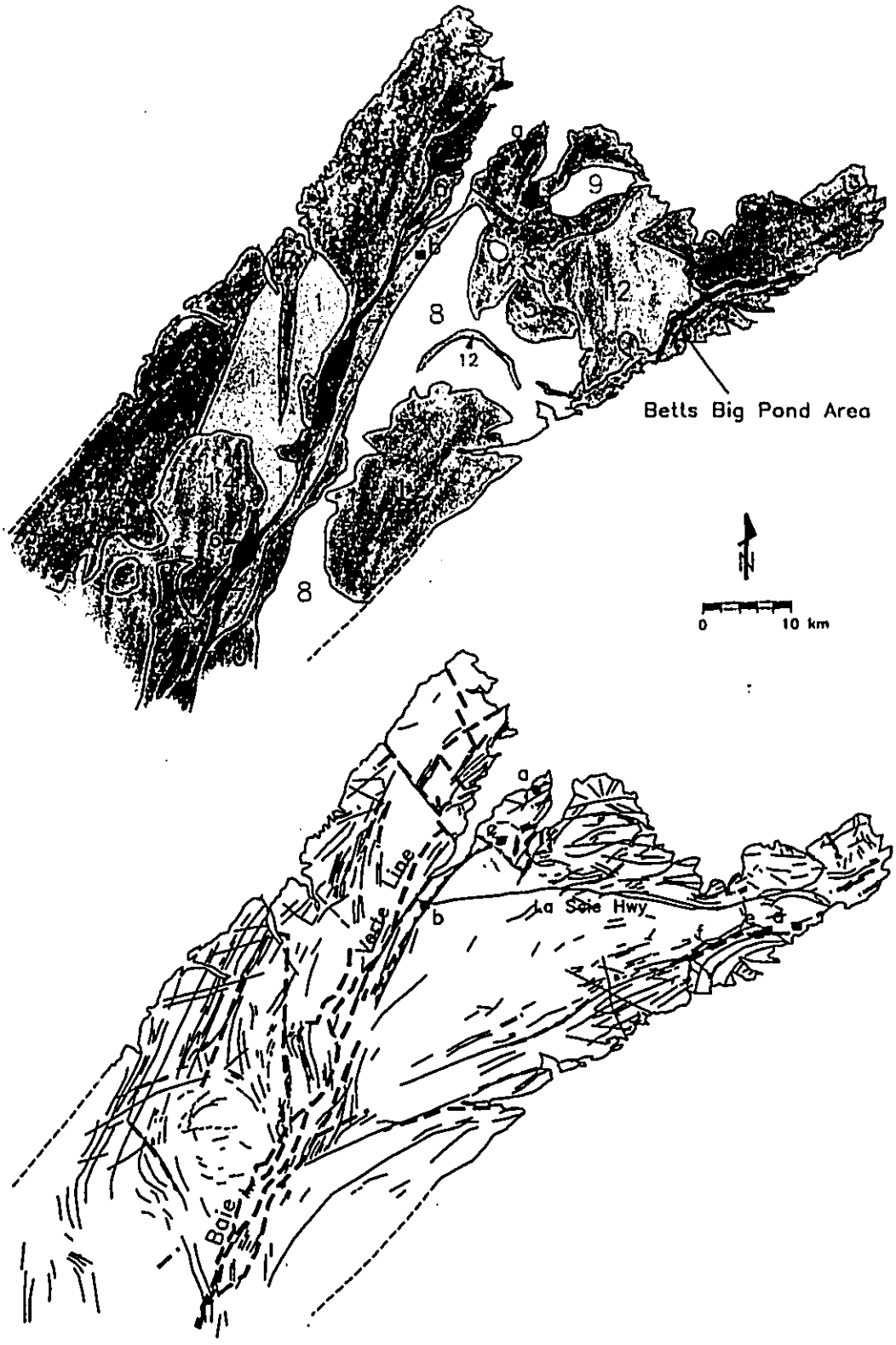
Betts Big Pond Area
0
10 km
Baie Verte Line
La Scie Hwy

drilling by INCO Ltd. indicated that talc-carbonate rocks in the Betts Big Pond area contained up to several hundred ppb Au over 10-15 metre widths (Bell and Beischer, 1991).

1.2 Purpose

Because most Au occurrences on the Baie Verte Peninsula are spatially associated with ultramafic rocks, the purpose of this study is to investigate possible genetic relationships between Au concentrations and ultramafic rocks. The Betts Big Pond area was chosen as a study area because a complete continuum of ultramafic rocks, from relatively unaltered peridotite to talc-carbonate rock, is exposed. This exposure allows an investigation of the geochemistry of gold as a function of progressive alteration of ultramafic rocks. Thus, the main components of this study are:

1) to map the ultramafic rock types exposed in the Betts Big Pond area.

2) to determine the Au content in all of the ultramafic rock types in the Betts Big Pond area.

3) to evaluate the effects of serpentinization and carbonatization of the ultramafic rocks on the distribution of Au.

4) to determine the relationship between Au enrichment in talc-carbonate in the Betts Big Pond area with talc-carbonate hosted Au vein mineralization at Arrowhead Pond (Figure 1.2 and

Table 1.1) in the northern part of the Betts Cove Complex.

1.3 Methods

Field mapping and outcrop sampling were carried out during a three week period in the summer of 1988 by the author and Dr. John W. Lydon of the Geological Survey of Canada as part of a Geological Survey of Canada project on the geology and metallogeny of Newfoundland ophiolites. Mapping and sampling utilized a 1:12,000 (approximately) air photo base. This was supplemented with detailed 1:100 grid mapping and sampling in some contact areas.

One hundred eighty six samples were analyzed for Au and seventy six of these were analyzed for major and selected trace elements. All samples were slabbed for hand sample petrography. Fourteen standard thin sections and sixty two polished thin sections were examined. Twelve polished thin sections (12 samples) were examined with the scanning electron microscope. Mineral compositions were determined from polished thin sections of six samples with the electron microprobe. The mineralogy of thirty two whole rock powders was determined with the X-ray diffractometer. Eighteen doubly polished thick sections of vein quartz were examined for fluid inclusion study. C and O isotopic compositions of magnesite were determined from three samples.

Analytical procedures are reported in Appendix I and

analytical data is reported in Appendix II.

1.4 Geology of the Baie Verte Peninsula

1.41 Tectonic setting

Newfoundland is located in the Appalachian structural province of Canada. Williams (1964) was the first to divide the Newfoundland Appalachians into litho-tectonic zones which group geotectonic environments and metamorphic and deformational histories. The scheme of division most commonly referred to today for the Canadian Appalachians is that of Williams (1979) which distinguishes the Humber, Dunnage, Gander, Avalon, and Meguma zones.

The Baie Verte Peninsula spans the Humber and Dunnage Zones in north central Newfoundland (Figure 1.1). The Humber Zone is the Appalachian miogeocline. It consists of a sequence of Eocambrian to Ordovician carbonate and clastic sedimentary rocks above crystalline Grenville basement. The Humber Zone contains allochthons consisting of rift and continental slope facies sedimentary rocks and ophiolite suites (e.g. Williams, 1979). The Dunnage Zone is defined largely by its ophiolite suites, island arc and back-arc basin volcanic and volcaniclastic rocks.

The contact between these two zones, traceable the entire length of the Canadian Appalachians, is refered to as the Baie

Verte-Brompton Line (Williams and St. Julien, 1982). The Baie Verte - Brompton Line is a narrow, steeply dipping structural zone marked by the discontinuous occurrence of ophiolitic rocks. It separates multideformed metaclastic rocks of the Humber Zone in the west from olistostromes and volcanic rocks of the Dunnage Zone to the east. It is interpreted to have originated as the Ordovician continent-ocean interface that has been accentuated during subsequent deformations (Williams and St. Julien, 1982). The Baie Verte-Brompton Line on the Baie Verte Peninsula is referred to as the Baie Verte Line (Hibbard, 1983).

1.42 General geology

The Humber and Dunnage Zones on the Baie Verte Peninsula are termed the Fleur de Lys and Baie Verte Belts respectively (Hibbard, 1983). The Fleur de Lys Belt consists dominantly of metaclastic rocks of continental derivation. These rocks are variably deformed and metamorphosed from greenschist to upper amphibolite grades. In contrast, the ophiolitic and volcanic-sedimentary sequences of the Baie Verte Belt typically consist of lower greenschist to sub-greenschist grade rocks (Figures 1.2a and 1.2b).

1.421 Fleur de Lys Belt

The Fleur de Lys Belt is divided into three suites of rocks: the East Pond Metamorphic Suite, the Fleur de Lys Supergroup, and the Wild Cove Igneous Suite. The East Pond Metamorphic Suite consists of gneisses, schists, and metaconglomerate. These rocks are interpreted as Late Proterozoic rift facies sedimentary rocks and underlying Grenvillian basement rocks (Williams and Stevens, 1969; deWit, 1974; Hibbard, 1983).

The East Pond Metamorphic Suite is overlain by the Fleur de Lys Supergoup. The contact is largely a wide ductile shear zone (Piasecki, 1988). The Fleur de Lys Supergroup is composed dominantly of schists with interlayered amphibolite and minor marble. The metasedimentary component of the Fleur de Lys Supergoup is correlated with less deformed rocks elsewhere in western Newfoundland and is interpreted as Cambrian-Ordovician slope-rise sedimentary rocks (Neale and Nash, 1963; Williams and Stevens, 1974).

The Birchy Complex, part of the Fleur de Lys Supergroup, consists of amphibolite, metagabbro, and graphitic schist. Protoliths of the Birchy complex are interpreted as a dismembered ophiolite consisting of mafic volcanic and volcanclastic rocks, basaltic dykes, and gabbro (Bursnall, 1975; Williams, 1979). The Birchy Complex is, in part, depositionally conformable with continentally derived

metaclastic rocks of the Fleur de Lys Supergroup to the west (Kennedy, 1971; deWit, 1972; Kidd, 1974; Bursnall, 1975).

The East Pond Metamorphic Suite and the Fleur de Lys Supergoup are intruded by the Wild Cove Pond Igneous Suite. It consists of diorite, granodiorite, granite, monzonite, syenite, and gabbro. The Wild Cove Pond Igneous Suite is believed to be coeval with widespread subareal volcanism and related high level grantic rocks in western Newfoundland (Coyle and Strong, 1987) which have Early Silurian U/Pb zircon ages (Chandler et al., 1987; Whalen et al., 1987).

1.422 Baie Verte Belt

The Baie Verte Belt consists of ophiolite complexes, submarine volcanic-sedimentary sequences, granitic intrusive rocks, and subaerial volcanic-sedimentary sequences. The oldest rocks in the Baie Verte Belt are the ophiolite complexes. Although structurally deformed and geographically separated, the ophiolite complexes of the Baie Verte Belt are thought to represent a segment of a once continuous sheet of oceanic crust (Stevens et al., 1969; Church and Stevens, 1971). The ophiolite complexes include the Betts Cove Complex, Point Rousse Complex, Advocate Complex, and Pacquet Harbour Group. Their ages are constrained by a U/Pb zircon age of 489 ±3/2 Ma of gabbro from the Betts Cove Complex (Dunning and Krogh, 1985).

Submarine volcanic-sedimentary rocks occur as ophiolitic

cover sequences. The Snooks Arm Group conformably overlies the Betts Cove Complex. It consists of mafic volcanic and volcaniclastic rocks. The Snooks Arm Group is correlated with the Point Rousse Cover Sequence (Hibbard, 1983). These sequences are interpreted to have formed in an island arc environment (Kidd et al., 1978; Upadhyay, 1973; DeGrace et al., 1976; Hibbard, 1983).

The Advocate Cover Sequence, which overlies the Advocate Complex, and the Flat Water Pond Group occur in an elongate belt parallel with and adjacent to the Baie Verte Line. The Advocate Cover Sequence and Flatwater Pond Group are distinguished by the occurrence of coarse boulder conglomerates and olisostromes. They are interpreted to have been deposited upon orogenically disturbed crust (Williams and St. Julien, 1982).

The Burlington Granodiorite intrudes the Betts Cove Complex and the Pacquet Harbour Group. The Dunnamagon Granite intrudes the Fleur de Lys Supergroup and the Pacquet Harbour Group. U/Pb zircon ages of these plutons indicate their emplacement at 450-460 Ma (Hibbard, 1983; Dallmeyer and Hibbard, 1984).

Subareal volcanic-sedimentary sequences on the Baie Verte Peninsula include the Cape St. John Group and the Micmac Lake Group. These groups consist dominantly of felsic volcanic rocks, quartz rich clastic sedimentary rocks, and lesser mafic volcanic rocks and are correlated by Neale (1957), Neale et al.

(1975), and DeGrace et al. (1976). A U/Pb zircon age of 427 ±2 Ma has been obtained from the Cape St. John Group (Coyle, 1990).

The Cape Brule Porphyry intrudes the Betts Cove Complex, the Snooks Arm Group, and the Burlington Granodiorite. Contacts with the Cape St. John Group are both intrusive and gradational (Neale, 1957; DeGrace et al., 1976). Hibbard (1983) indicates that the Cape Brule Porphyry can be lithically and geochemically correlated with the Cape St. John Group. The LaScie Intrusive Suite intrudes the Cape St. John at the northeastern most part of the Baie Verte Peninsula. It consists of a cogenetic suite of gabbro, syenite, and granite. A U/Pb zircon age of 435 ±15 Ma (Mattinson, 1977) indicates that it is part of the widespread Early Silurian magmatic event that includes the Wild Cove Pond Igneous Suite, the Cape Brule Porphyry, the Cape St. John Group, and the Micmac Lake Group as well as units elswhere in western Newfoundland (e.g. Sprindale Group, Chandler et al., 1987; Topsails Igneous Complex, Whalen et al., 1987).

1.43 Origin of the Baie Verte Belt ophiolites

The origin of ophiolites in west and central Newfoundland (i.e. suprasubduction zone vs. mid ocean ridge ophiolites) has been and continues to be debated (e.g. Jenner et al., 1991). Palinspastic reconstructions, radiometric age data, and

geochemical signatures are consistent with a suprasubduction zone origin for the central Newfoundland ophiolites (Serri, 1981; Searle and Stevens, 1984; Sun and Nesbitt, 1978; Coish et al., 1982; Swinden et al., 1990; Fyffe and Swinden, 1991; Dunning et al., 1991; Jenner et al. 1990; Jenner et al., 1991).

Lavas of the Baie Verte Belt ophiolites, including those of the Betts Cove Complex, are boninitic (Gale, 1973; Norman and Strong, 1975; Coish and Church, 1979; Upadhyay, 1982; Hibbard, 1983). Boninitic lavas are distinguished from typical tholeiitic lavas by their higher MgO, Ni, and Cr, contents, higher MgO/FeO_t ratios and lower TiO_2 contents. Based on the analyses of gabbro, Serri (1981) classified ophiolites as high- and low-Ti types emphasizing that boninitic lavas typically occur in the low-Ti type ophiolites.

Boninitic lavas are derived from a depleted mantle source (Sun and Nesbitt, 1978, Cameron et al., 1979; Hickey and Frey, 1982). Low-Ti ophiolites are interpreted to represent magma derived from a depleted mantle wedge above subducting oceanic crust (Serri, 1981).

Serri (1981; and references therein) consider the Betts Cove and Point Rousse to be low-Ti type ophiolite complexes and indicate that the complexes were derived from boninitic parental magmas. Jenner et al. (1990) similarly deduced that the Betts Cove Complex formed in a suprasubduction zone environment.

1.44 Deformation and tectonic development

A number of structurally oriented studies on the Baie Verte Peninsula have focused largely on specific areas and/or rocks of similar age and origin such as the Flat Water Pond area (Kidd, 1974), the northern Fleur de Lys Belt (Bursnall, 1975), the northeastern Baie Verte Belt (DeGrace et al., 1976), the Point Rousse Complex (Norman and Strong, 1975). Some of these studies have defined several phases of deformation. However, regionally, deformation on the Baie Verte Peninsula may be resolved into three main phases (cf. Hibbard, 1983).

Deformation on the Baie Verte Peninsula has largely been centred on the Baie Verte Line (Hibbard, 1983). Most of the Baie Verte Line is formed by the contact of the Birchy Complex to the west with the Advocate Complex to the east (Figure 1.2a). The Birchy Complex contains ophiolitic melange, slide zones, and zones of garnet pyroxene amphibolite, the latter being analogous to the dynamothermal aureole at the Bay of Islands (Williams and Smyth, 1973; Bursnall, 1975; Williams and St. Julien, 1982). This, and the observation that the Birchy Complex is conformable with continentally derived clastic sedimentary rocks of the Fleur de Lys Supergroup and has been deformed and metamorphosed with those rocks indicates that this area records the early disruption of the continental margin and transport of ophiolites from east to west (Williams et al., 1977; Williams and St. Julien, 1982; Hibbard, 1983).

D_2 structures in the Baie Verte Line and parallel fault zones immediately to the east (Figure 1.2b) record west over east reverse movement, a sense opposite to that during D_1 (Bursnall, 1975; Hibbard, 1983; Piasecki, 1988). The north-northeast structural trend that characterizes the Fleur de Lys Belt is interpreted to be largely a D_2 fabric. The latest phase of deformation recognized in the Baie Verte Line (D_3) records sinistral strike slip motion (Goodwin and Williams, 1990).

The northern part of the Baie Verte Belt (north of the LaScie Highway on figure 1.2) is characterized by a zone of penetratively deformed amphibolite grade metamorphic rocks (DeGrace et al., 1976; Hibbard, 1983). The metamorphic rocks are interpreted to have been uplifted about south verging east-west trending structures (D_3, indicated by overprinting of D_2; DeGrace et al., 1976) (Figure 1.2b). Sinistral strike slip along the north-northeast trending Baie Verte Line is interpreted to be temporally related to the south verging, east-west trending structures that characterize the northern part of the Baie Verte Belt being due to the northward movement of the Baie Verte Belt relative to the Fleur de Lys belt.

These three phases of tectonism are associated with coeval magmatism and/or metamorphism. Following Dunning et al. (1990) and Colman-Sadd et al. (1990) the orogenic events are referred to as, from oldest to youngest, the Taconic (D_1), Salinic (D_2), and Acadian (D_3) Orogenies. They are summarized in figure 1.3.

1.45 Timing of Au mineralization

Au vein mineralization was emplaced at Deer Cove (Figure 1.2) at ca. 395 Ma ($^{40}Ar/^{39}Ar$ age of vein sericite) during the later stages of easterly directed thrust and reverse faulting (D_2) during the Salinic Orogeny (Lydon et al. 1990). The relative timing of Au emplacement at Stog'er Tight (Figure 1.2), determined by Kirkwood and Dube (1991) on the basis of a structural analysis, is consistent with the timing of Au emplacement at Deer Cove determined by Lydon et al. (1990).

$^{40}Ar/^{39}Ar$ age spectra from the Long Pond and Tom Showing in the northern part of the Betts Cove Complex and adjacent Cape St. John Group (Figure 1.2 and Table 1.1) are highly disturbed and constrain the timing of vein formation to the period 395 - 427 Ma, during the Salinic Orogeny (D_2) (Lydon et al., 1990).

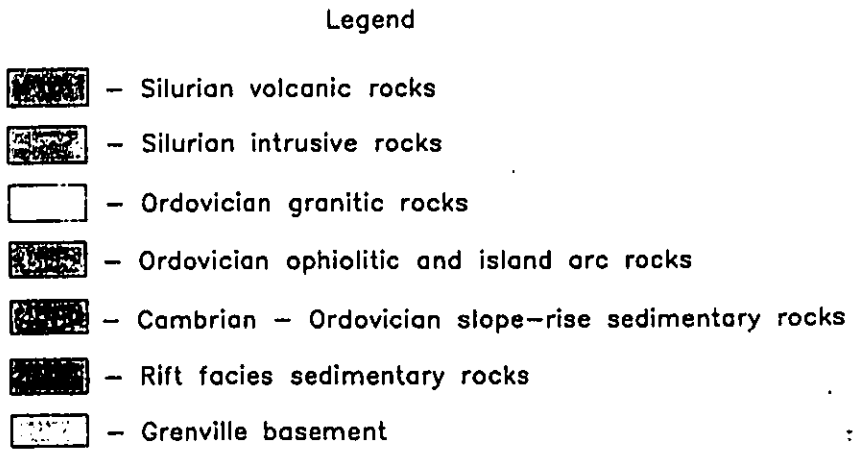

Figure 1.3. Orogenic development of the Baie Verte Peninsula. Synthesized from a number of studies as follows. Radiometric age data: Hibbard (1983), Hibbard and Dallmeyer (1984), Pringle (1978), Bell and Blenkinsop (1977), Dunning and Krogh (1985), Lydon et al. (1990), Coyle (1990). Structural/geological studies: Neale (1957), Williams and Stevens (1969), Church and Stevens (1971), Church and Riccio (1974), Bursnall (1975), Neale et al. (1975), Kidd et al. (1978), Williams and St. Julien (1982), Hibbard (1983), DeGrace et al. (1976), Piasecki (1988), Jamieson and Vernon (1987), Jamieson (1990), Al (1990), Goodwin and Williams (1990). Regional studies: Williams (1979), Swinden and Thorpe (1984), Swinden and Fyffe (1991), Dunning et al. (1990), Dunning et al. (1991), Colman-Sadd et al. (1990). Diagram modified after Lydon et al. (1990).

370 – 340 Ma →

- southward uplift and post metamorphic cooling in the northeast (D3)
- strike–slip displacement along NE–SW trending structures

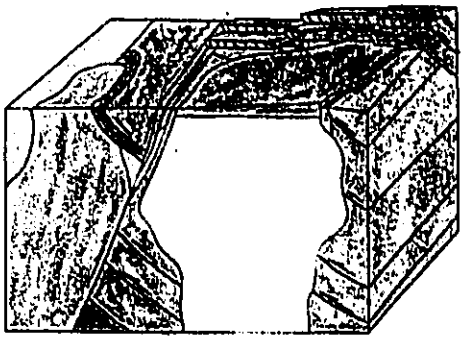

← Acadian →

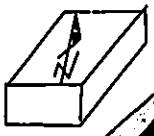

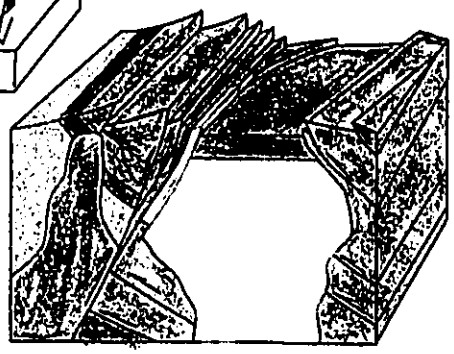

← 420 – 390 Ma

- continued post metamorphic cooling of the Fleur de Lys Belt and prograde metamorphism in the Baie Verte Belt
- reverse faulting adjacent to the Baie Verte Line

440 – 420 Ma →

- eastward uplift of the Fleur de Lys Belt and retrograde metamorphism (regional D2)
- emplacement of Silurian magmatic suite
- prograde metamorphism in the Baie Verte Belt

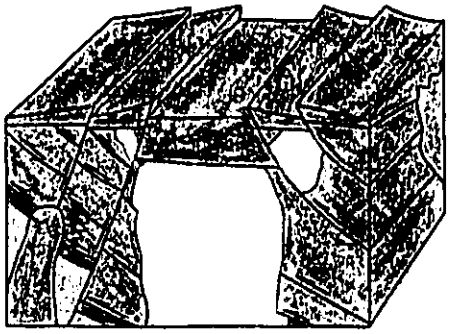

← Salinic →

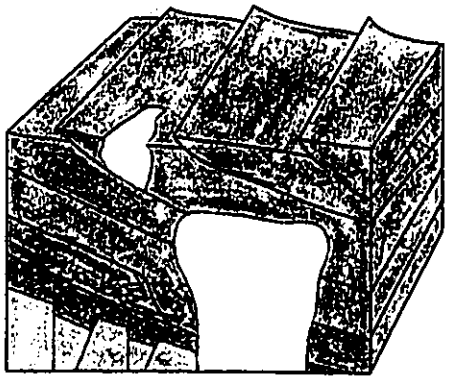

← 460 – 440 Ma

- westward obduction and imbrication of continental margin rocks and ophiolitic/arc rocks (regional D1)
- deposition of olistostromes
- prograde – peak metamorphism
- intrusion of granodiorite (460 Ma)
- intrusion of granite (ca. 450 Ma)

← Taconic →

CHAPTER 2

GEOLOGY AND MINERALOGY

2.1 Geology of the Betts Cove Complex and adjacent units

2.11 Lithostratigraphy

The Betts Cove Complex lies on the eastern side of the Baie Verte Peninsula. It is in contact with the Cape St. John Group and Cape Brule Porphyry to the north and west, the Snooks Arm Group to the south and east, and the Burlington Granodiorite to the south (Figures 1.2 and 2.1).

The Betts Cove Complex is the most complete and intact ophiolite on the Baie Verte Peninsula. It contains all of the essential ophiolite members (Anonymous, 1972) with the exception of the tectonite member (Upadhyay, 1973). At the stratigraphic base of the Betts Cove Complex are cumulate dunite, wehrlite, pyroxenite, harzburgite and lherzolite (Upadhyay, 1973). The gabbroic member of the Betts Cove Complex is zoned. The lower zone, transitional with the ultramafic member, is characterized by interlayered pyroxenite and gabbro with isolated lensoid pods of ultramafic rocks. This zone grades into the upper zone that consists of gabbro to leucogabbro (Upadhyay, 1973). The sheeted dyke member consists dominantly of diabase dykes with some picritic, ultramafic, and

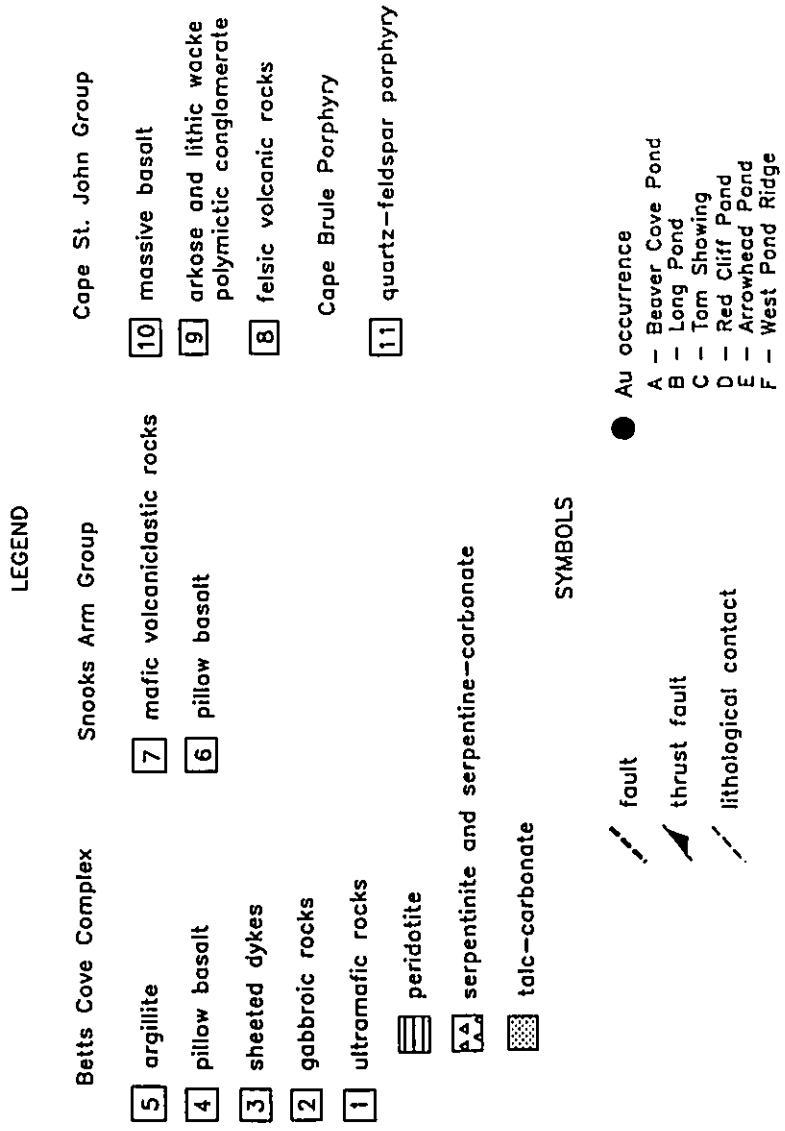

Figure 2.1. Geology of the Betts Cove Complex from Burtons Pond to Beaver Cove Pond. Geology of the part of the map north of the Betts Big Pond area simplified after DeGrace et al. (1976) and Al (1990). Geology south of the Betts Big Pond map area after DeGrace et al. (1976). Geology of the Betts Big Pond area simplified from figure 2.3. Au occurrences from Bell and Biescher (1991) and Al (1990). The Betts Cove Complex - Cape St. John Group (BCC - CSJG) fault zone includes those faults within and bounding the ultramafic member of the Betts Cove Complex.

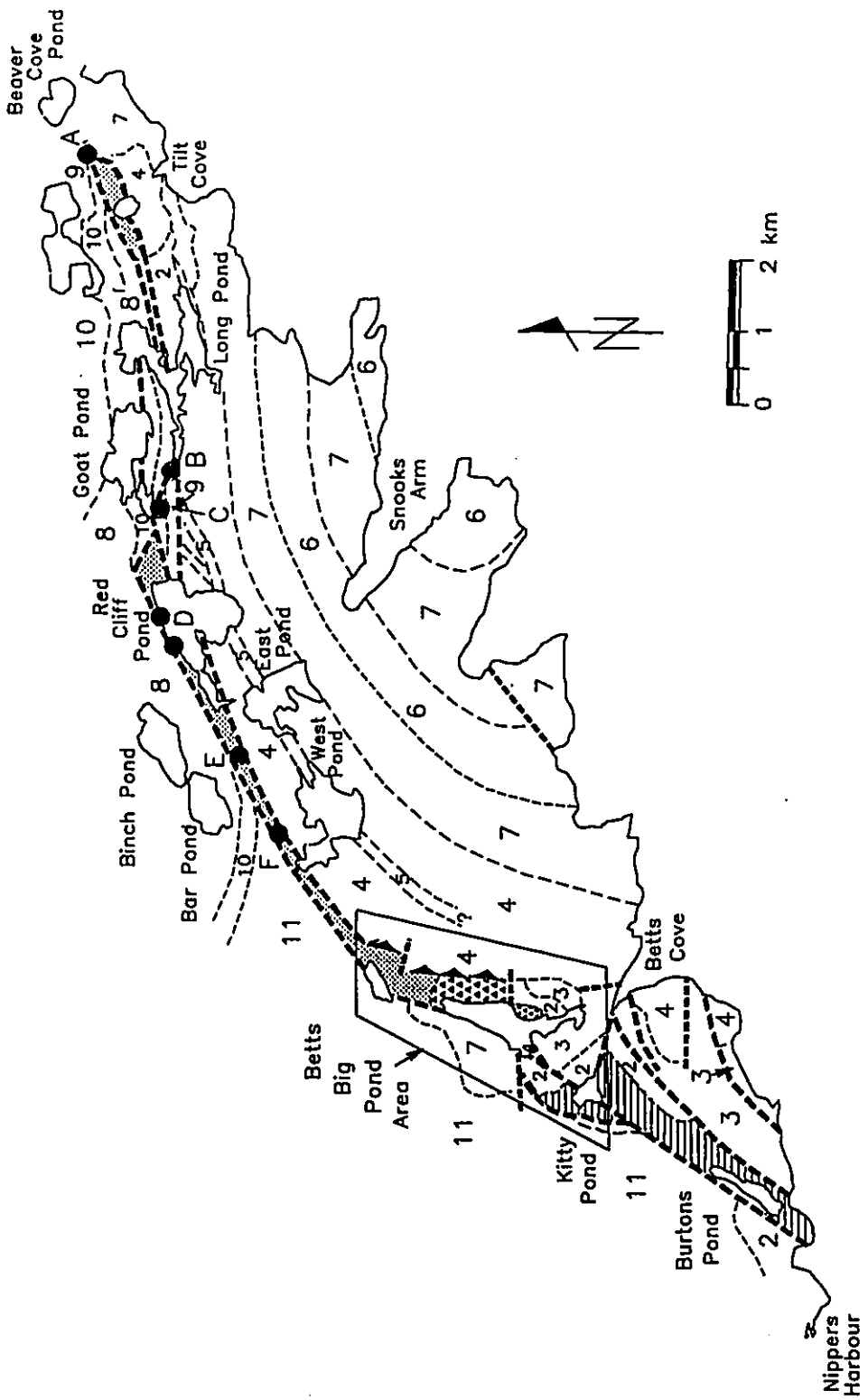
Beaver Cove Pond
Tilt Cove
Long Pond
Goat Pond
Red Cliff Pond
Snooks Arm
East Pond
West Pond
Binch Pond
Bar Pond
Betts Big Pond Area
Betts Cove
Kitty Pond
Burtons Pond
Nippers Harbour
A
B
C
D
E
F
N
0 1 2 km

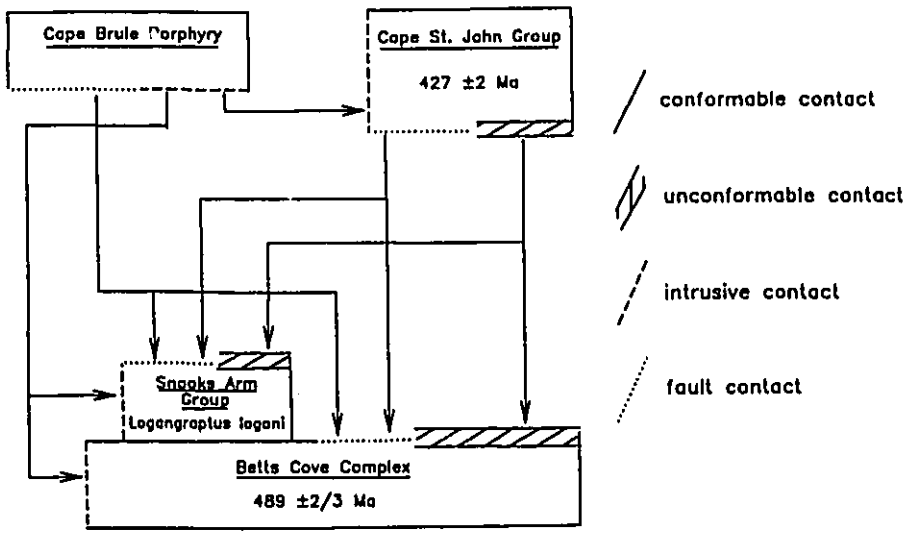

Figure 2.2. Summary of contact relationships of the Betts Cove Complex and adjacent units. Arrows indicate units in contact (types of contacts indicated in legend to the right of the diagram). Modified after Hibbard (1983). Cape St. John Group U/Pb zircon age from Coyle (1990), Betts Cove Complex U/Pb zircon age from Dunning and Krogh (1985), Snooks Arm Group fossil age reported in Hibbard (1983).

felsic dykes. They contain screens of gabbroic and ultramafic rocks (Upadhyay, 1973). Argillite beds occur in the pillow lava member (Upadhyay, 1973). Contact relationships of the Betts Cove Complex with adjacent units have been desribed in chapter 1 and are summarized in figure 2.2

2.12 Structure

The ultramafic member of the Betts Cove Complex makes a major structural dislocation between the Cape St. John Group and Cape Brule Porphyry to the north and west with the Betts Cove Complex and Snooks Arm Group to the south and east (BCC-CSJG fault zone) (Figure 2.1).

The structural geology of the eastern side of the Baie Verte Peninsula has been examined by Neale (1957), Upadhyay (1973), Church and Riccio (1974), DeGrace et al. (1976), Hibbard (1983), and Al (1990). Structural investigations during the course of this study include mapping in the Betts Big Pond area and reconnaissance traverses across the northern part of the BCC-CSJG fault zone (Figures 2.1 and 2.3).

Deformation affecting the eastern side of the Baie Verte Peninsula may be resolved into three main phases (D_1, D_2, and D_3) consistent with regional deformations during the Taconic, Salinic, and Acadian Orogenies respectively (Figure 1.3)

D_1. To the southeast of the BCC-CSJG fault zone, the Betts Cove Complex and Snooks Arm Group occupy the steeply dipping to

overturned northern limb of a regional syncline (Neale, 1957). In the Betts Big Pond area, D_1 structures are dominantly westerly vergent thrust faults (Figure 2.3). These include the eastern contact of the ultramafic member where it is overthrust dominantly by pillow lava; a thrust fault in the southern part of the map area where upper zone gabbro and sheeted dykes are thrust over ultramafic rocks; and a "knob" of basalt thrust over ultramafic rocks north of Betts Big Pond (Figure 2.2). The thrust geometry of the eastern fault contact was determined from rotated basalt clasts in serpentinite which form melange at the base of the thrust.

Hibbard (1983), on the basis of relatively undeformed porphyry dykes intruding strongly deformed Betts Cove Complex rocks, indicates that deformation in the Betts Cove Complex and Snooks Arm Group largely predates deposition of the Cape St. John Group. The observations that the Cape St. John Group unconformably overlies: 1) gabbro and sheeted dykes of the Betts Cove Complex in the Nippers Harbour area (DeGrace et al., 1976); 2) sheeted dykes and pillow lavas in the Long Pond area (Al, 1990); 3) members of the Snooks Arm Group in the Beaver Cove area (Neale et al, 1975; DeGrace et al., 1976); and 4) ultramafic rocks in the Tilt Cove area (Al, 1990) indicates that the Ordovician rocks were significantly disturbed prior to deposition of the Silurian rocks.

D_2. DeGrace et al. (1976) indicate that the BCC-CSJG fault zone is largely a dip slip fault with the south side upthrown.

Al (1990) indicates that the fault that bounds the ultramafic member to the northwest and forms the contact with the Cape St. John Group and Cape Brule Porphyry records the movement of the Betts Cove Complex and Snooks Arm Group up and over the Cape St. John Group. In the Betts Big Pond area, this fault is largely unexposed, being underwater for approximately 60 % of its length (Figure 2.3). However, its steep east-southeast dip is evident at the northern most part of the Betts Big Pond map area (indicated by steeply southeast dipping foliation in northern most part of figure 2.3) and has been delineated in the northern part of the map area through exploratory drilling by INCO Ltd (drill hole location indicated on figure 2.3). Where this fault emerges from Betts Big Pond in the southern part of the map area (Figure 2.3) it truncates the D_1 thrust fault and dips steeply to the east-southeast. South of Kitty Pond, this fault forms a distinct lineament on the air photo where it merges with the arcuate fault to the west, which also forms a prominant air photo lineament and has been mapped by DeGrace et al., (1976) (Figure 2.1).

To the northeast of the BCC-CSJG fault zone, the Cape St. John Group forms a major syncline defined by tight upright to overturned folds with axial planar schistosity. The orientation of the folds is reflected by the gently northeast plunging fold axes and variably northwest dipping axial planes (DeGrace et al., 1976).

D_3. In the northern part of the Cape St. John Group, the

northeast trending structures (D_2) are overprinted by south verging recumbent folds and thrust faults with associated north dipping schistosity (note the east-west structural trend in the northeastern part of the Baie Verte Peninsula in figure 1.2) (DeGrace et al., 1976; Hibbard, 1983). The penetrative aspect of this east-west trending deformation decreases from the north southward to where Hibbard (1983) defined a southern limit of polydeformation that approximately coincides with the LaScie Highway (figure 1.2). Similarly, the metamorphic grade decreases from amphibolite in the northern most Cape St. John Group to lower to sub-greenschist south of the limit of polydeformation (Hibbard, 1983).

In the area between Red Cliff Pond and Beaver Cove Pond, the trend of the BCC-CSJG fault zone has been rotated to east-west (Figure 2.1). In this area, rocks of the Cape St. John Group are structurally imbricated with rocks of the Betts Cove Complex and Snooks Arm Group. Al (1990) mapped east trending north dipping faults in the Red Cliff Pond - Long Pond area. In the Beaver Cove Pond area (Figure 2.1) two phases of deformation are recognized (Lavigne, 1988). The early phase of deformation includes tight folding of the Cape St. John Group and Betts Cove Complex about a northeast trending fold axis (D_2). The second deformation is moderately to steeply north dipping fault planes with north plunging lineations defined by elongated clasts in the Cape St. John Group (D_3).

Hibbard (1983), Dallmeyer and Hibbard (1984), and Lydon et

al. (1990) report Ar/Ar age spectra from the northern part of the Baie Verte Peninsula that range from 370 Ma (hornblende) to 340 Ma (biotite). The ages are from all lithologies exposed in the northern part of the Baie Verte Peninsula including the Cape St. John Group. These authors interpret these spectra as post metamorphic cooling ages during southerly vergent uplift of amphibolite grade metamorphosed rocks. Lydon et al. (1990) report Ar/Ar ages from Au vein muscovite from the BCC-CSJG fault zone at Long Pond and the Tom Showing (Figures 1.2 and 2.1). The spectra indicate initial sericite formation at 395 Ma or before, during D_2, and resetting at 350 Ma or later related to D_3 (Lydon et al., 1990).

2.13 Distribution of ultramafic rocks

The ultramafic member of the Betts Cove Complex consists dominantly of relatively fresh layered ultramafic rocks, talc-carbonate rocks, and lesser amounts of serpentine-carbonate rocks. The ultramafic member forms an almost continuous belt from Burtons Pond in the south to Beaver Cove Pond in the north (Figure 2.1). From just north of Betts Big Pond to Beaver Cove Pond, the ultramafic belt has an average width of approximately 150 metres and the dominant rock type is talc-carbonate rocks. Serpentine-carbonate rocks and serpentinite occur locally. From Kitty Pond southwards to Burtons Pond, the ultramafic rocks are dominantly layered, partially serpentinized peridotite.

2.2 Ultramafic rocks in the Betts Big Pond area

2.21 Description

The Betts Big Pond map area straddles the ultramafic member of the Betts Cove Complex (Figure 2.1 and Figure 2.3). It extends from north of Betts Big Pond southward to Kitty Pond, encompassing the transition from strongly altered ultramafic rocks (talc-carbonate rocks) that dominate in the northern part of the Betts Cove Complex to relatively fresh peridotite that characterizes the southern part of the Betts Cove Complex (Figures 2.1 and 2.2).

Five ultramafic map units are recognized in the Betts Big Pond map area: 1) layered ultramafic rocks consisting of variably serpentinized peridotites, 2) serpentinite, 3) green weathering serpentine-carbonate rocks, 4) red weathering serpentine-carbonate rocks, and 5) talc-carbonate rocks (Figure 2.3). The carbonate-bearing rocks represent the progressive carbonatization of serpentinite. They are characterized by variable ratios of serpentine, talc, and carbonate minerals and textures include carbonate veins in serpentinite (green weathering serpentine-carbonate rock unit) to massive red weathering serpentine-carbonate rocks and talc-carbonate rocks. These rock units will be more simply referred to as serpentine-carbonate, and talc-carbonate reflecting their dominant mineralogical components, with distinction, where applicable,

Legend

Silurian

Cape Brule Porphyry

[6] – quartz–feldspar porphyry

Ordovician

Snooks Arm Group

[5] – mafic volcanic and volcaniclastic rocks

Betts Cove Complex

[4] – pillow lava

[3] – sheeted diabase dikes and gabbro

[2] – pyroxenite and gabbro (layered in part)

[1] – layered ultramafic rocks

[1d] – talc–carbonate

[1c] – red serpentine–carbonate

[1b] – green serpentine–carbonate

[1a] – serpentinite

Symbols

– thrust fault; defined, approximate

– fault; defined, approximate

– lithological contact; defined, approximate

– metasomatic contact; defined, approximate

– foliation; dip unknown, with dip

– magmatic layering

45 – ddh (INCO 1987)

Figure 2.3. Geology of the Betts Big Pond area.

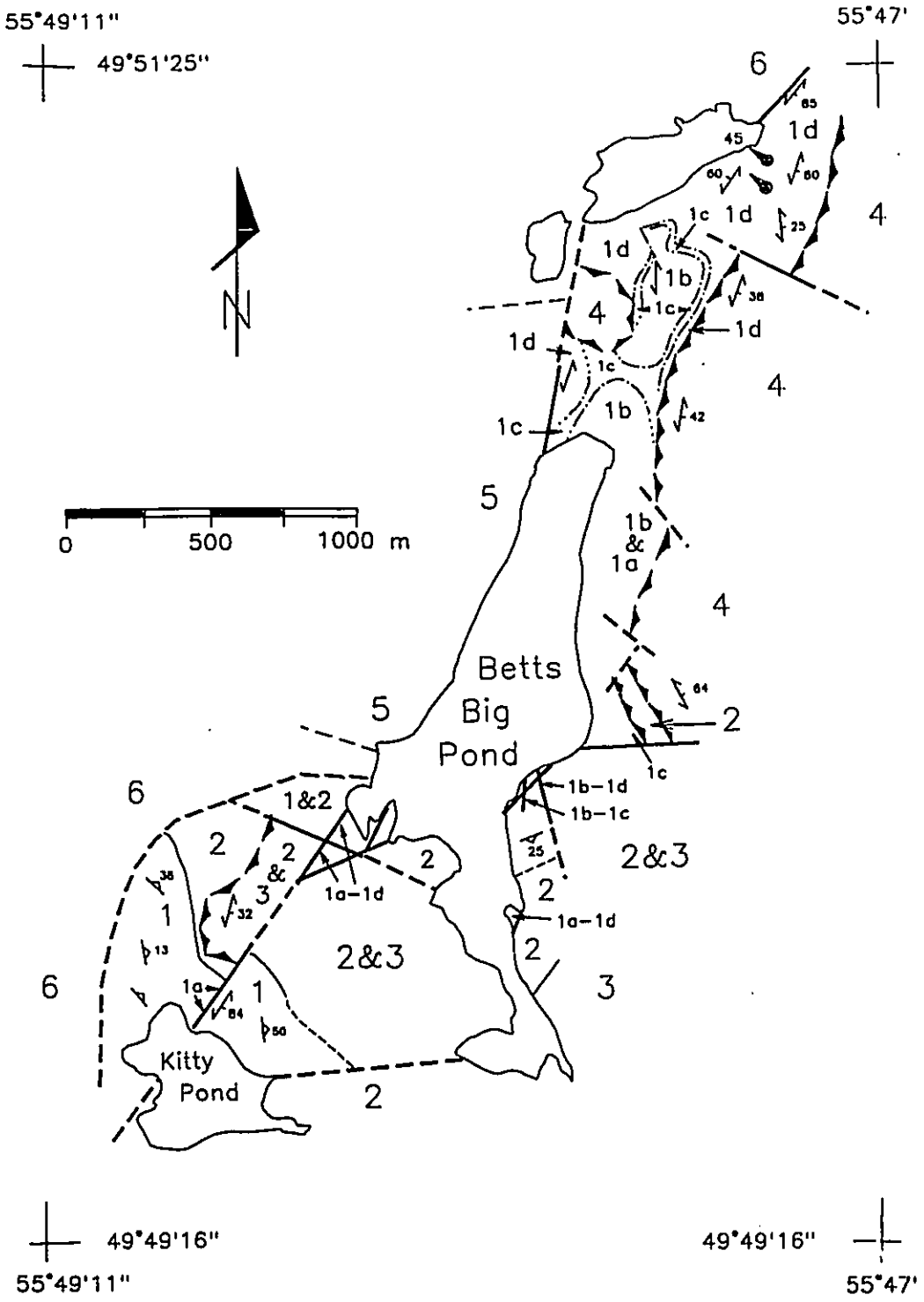
55°49'11"
49°51'25"
55°47'
N
0
500
1000 m
Betts
Big
Pond
Kitty
Pond
1d
1b
1c
1a
1b–1d
1b–1c
1a–1d
1&2
2&3
49°49'16"
55°49'11"
49°49'16"
55°47'

between red and green serpentine-carbonate.

1) The layered ultramafic rocks consist dominantly of layers of dunite, harzburgite, orthopyroxenite, websterite, and wehrlite (classification after Streckeisen, 1979; Plate 2.1). The thickness of the layers range from < 1 cm to > 1 m. Dunite has a typically smooth outcrop surface. It weathers black to yellowish brown; depending on the proportion of serpentine. Dunite weathers recessively compared to the pyroxene bearing rocks. Harzburgite is characteristically knobby and reddish in outcrop reflecting the preferential weathering of olivine and the relatively coarse grained orthopyroxene. Where orthopyroxene is the dominant mineral, the rock is a grey-brown colour. Where clinopyroxene is dominant, which is the least common, the rocks weather a green-grey colour.

2) Serpentinite, which contains minor but ubiquitous magnetite is black to green. It most commonly contains a penetrative foliation.

3) Where serpentinite contains veins and veinlets of carbonate, it forms the green weathering serpentine-carbonate unit. Carbonate veins are rarely >2 cm wide. They have a random orientation and are variably deformed.

4) The red serpentine-carbonate unit is similar to the green weathering unit. The former is significantly harder and consists of relatively massive serpentine-carbonate with carbonate veins.

5) Talc-carbonate consists dominantly of talc and

carbonate. It is brownish red or dark grey and possesses a penetrative foliation. The talc-carbonate unit locally exhibits carbonate rich zones within an outcrop.

2.22 Distribution

The overall distribution of the ultramafic rocks in the Betts Big Pond area is of the least altered layered peridotite in the south and most altered talc-carbonate rocks in the north. The layered ultramafic rocks are exposed around Kitty Pond in the southern part of the map area and to a lesser extent on the south-eastern side of Betts Big Pond (Figure 2.2). Faults transgress the ultramafic rocks and form the contacts with mafic ophiolitic rocks. The fault/shear zones are occupied dominantly by serpentinite (Plate 2.2). The distribution of minerals and textures in the shear/fault zones have a typical shear zone geometry with the most strongly cleaved and intensely serpentinized rocks occurring in the center and less deformed and altered rocks occurring at the margins.

Serpentine-carbonate and talc-carbonate occur locally in the fault zones in the southern part of the map area. Quartz veins occur in the fault zones and are restricted to areas of carbonate alteration.

The D_1 thrust fault that forms the eastern contact of the ultramafic rocks with basalt (Figure 2.3) is characterized by

Plate 2.1. Layered ultramafic rocks in the southern part of the Betts Big Pond map area between Betts Big Pond and Kitty Pond.

Plate 2.2. Serpentinite shear zone in layered ultramafic rocks in the southern part map area near Kitty Pond. Photo was taken facing approximately WNW. Note the steep SE dip of the shear zone.

melange consisting of serpentinite with blocks of basalt (Plate 2.3). Carbonatization occurs locally in the melange. Specifically, the ultramafic rocks consist of red weathering serpentine-carbonate in the area where gabbro forms a thrust slice between basalt and ultramafic rocks on the eastern side of Betts Big Pond (Figure 2.3). Traced northwards, the melange is dominantly serpentinite with minor carbonate veining. In the northern part of the map area, the proportion of serpentine-carbonate and talc-carbonate in the D_1 thrust fault increases as it forms the contact with the talc-carbonate unit.

In the northern part of the map area no primary layering was observed during this study. However, Upadhyay (1973) noted magmatic layering immediately north of Betts Big Pond. An elongate pod shaped lens of chromitite with a maximum thickness of .35 m and minimum length of 1.2 m occurs in serpentinite north of Betts Big Pond. The chromitite lens is enclosed in a zone of serpentinite that is characterized by the occurrence of diffuse lenses and veins of almost massive magnetite.

In the northern part of the Betts Big Pond map area, a complete continuum from serpentinite to talc-carbonate is recognized. Most serpentinite in the northern part of the map area contains carbonate forming the green serpentine carbonate unit (Plate 2.4). At the contact between the areally more extensive green weathering serpentine-carbonate and talc-carbonate map units occurs the red-weathering serpentine carbonate unit. The red weathering serpentine-carbonate forms

Plate 2.3. Serpentinite melange at the thrust fault contact between hangingwall basalt and footwall serpentinite (east side of Betts Big Pond). Note the blocks of basalt in the strongly cleaved serpentinite (below note book).

Plate 2.4. Cut slab of green weathering serpentine-carbonate. Note the variably resorbed fragments of serpentinite in magnesite. Sample NT-0036.


cm

Plate 2.5. Contact of red weathering serpentine-carbonate and talc-carbonate in northern part of the Betts Big Pond map area. Talc-carbonate forms a rind on red serpentine-carbonate in the upper right of the photo. Red serpentine-carbonate occurs as isolated zones within the talc-carbonate.

Plate 2.6. Lithons of talc-carbonate (weathering in relief) in carbonate rich talc-carbonate (weathering recessively) indicating the progressive carbonatization of talc-carbonate. Photo from talc-carbonate unit in the northern part of the Betts Big Pond map area.

angular to rounded blocks of variable size (≈1m^3 to 5 cm^3) in talc carbonate (Plate 2.5).

Talc-carbonate commonly forms a rind on the surface and in fractures of the red weathering serpentine-carbonate blocks indicating the conversion of serpentine-carbonate to talc-carbonate (Plate 2.5). Zones of deformation consisting of talc-carbonate lithons in a matrix of talc-carbonate with a higher abundance of carbonate are recognized (Plate 2.6).

In the northern most part of the map area, D_2 is characterized by talc-carbonate adjacent to carbonatized and sericitized quartz-feldspar porphyry. There is some structural intercalation of talc-carbonate and porphyry in this region.

2.23 Mineralogy and petrography

2.231 layered ultramafic rocks

The layered ultramafic rocks consist of various proportions of forsterite, orthopyroxene, and clinopyroxene. The silicate minerals form a cumulus texture. Metallic minerals include magnetite, chromite, pyrrhotite, pentlandite, and chalcopyrite. In addition, a small (< 5 μm) unidentified Fe-Ni-S-As mineral was found using the scanning electron microscope (SEM). The sulphide and oxide minerals occur disseminated along grain boundaries and within silicate minerals. No particular mineralogical or textural siting for the sulphides was

identified (Plate 2.7).

Magnetite forms euhedral grains that range in size from 20 to 50 μm. Chromite is also euhedral but larger (average $\approx$ 100 μm) than magnetite. Sulphide grains are of various size up to 100 μm. Magnetite and sulphide occasionally occur in contact, though pentlandite and pyrrhotite occasionally occur enclosed in magnetite.

The layered ultramafic rocks contain a variable amount of secondary hydrous minerals while preserving the primary cumulus texture. These include antigorite, lizardite, and chlorite. The most common is antigorite which forms pseudomorphs after olivine and orthopyroxene. These assemblages contain a variable amount of secondary magnetite, which in contrast to euhedral primary magnetite, is anhedral and intergrown with antigorite. Chlorite is a very minor component. It was identified on grain boundaries and along cleavage traces of pyroxene. The amount and distribution of lizardite is unknown due to difficulty in optically distinguishing it from antigorite. It was recognized only locally as finer grains with slightly higher birefringence than antigorite. It was positively identified in serpentinite with the X-ray diffractometer (XRD).

2.232 serpentinite

Serpentinite consists dominantly of antigorite with a lesser amount of magnetite and and minor to trace amounts of

Plate 2.7. Electron back scatter (EBS) image of magnetite, chalcopyrite, and pentlandite and olivine (dark) in dunite. Note the euhedral magnetite and the relatively uncorroded sulphide. Sample NT-0424.

Plate 2.8. EBS image of serpentinite. Magnetite forms a euhedral mass (compare with primary magnetite in plate 2.7). Subhedral to euhedral mineral (marked FAY) consists of Fe and Si (determined with EDS). Sample NT-0426.

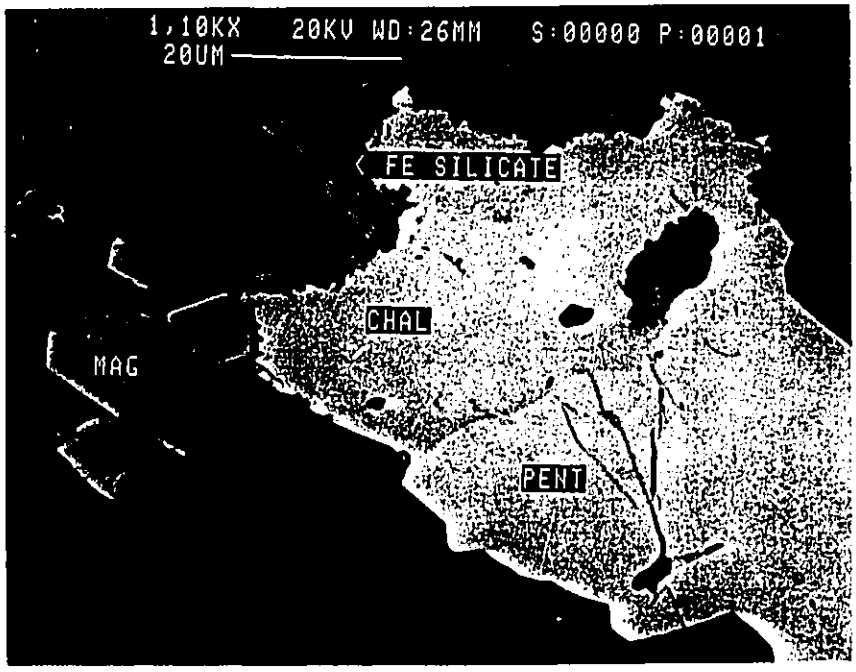
1,10KX 20KV WD:26MM S:00000 P:00001
20UM
FE SILICATE
CHAL
MAG
PENT

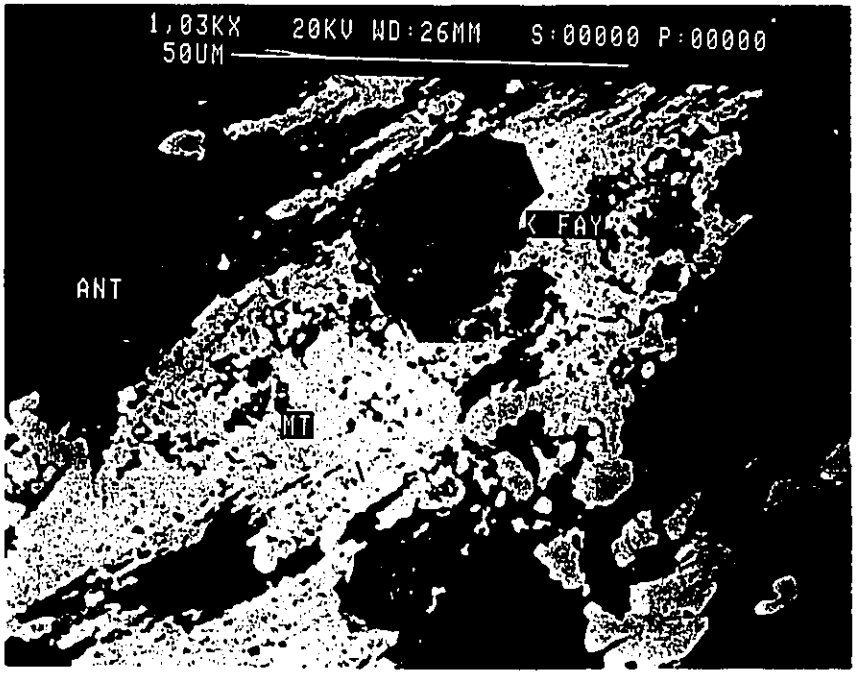
1,03KX 20KV WD:26MM S:00000 P:00000
50UM
FAY
ANT
MT

chrysotile, lizardite, chlorite, garnierite, brucite, and possibly fayalite or greenalite. Metallic minerals in serpentinite include magnetite and chromite. Sulphide minerals are scarce.

Excluding chromite and possibly euhedral magnetite, no primary igneous minerals or textures are present in serpentinite. Secondary magnetite in serpentinite forms anhedral masses intergrown with antigorite. A very minor amount of brucite was recognized as part of this assemblage in one of 14 thin sections. Brucite was not detected in nine XRD analyses of serpentinite. In one case, euhedral to subhedral (orthorhombic ?) crystals were identified with magnetite and antigorite. The Energy Dispersion Spectrometer (EDS) attached to the SEM indicates that they contain Si and Fe and are thus interpreted to be either a fayalite or a greenalite pseudomorph of forsterite or orthopyroxene (Plate 2.8). The amount of lizardite is unknown but is ubiquitous as determined with the XRD. In one section, a thin vein (< .1 cm) of chrysotile cut the antigorite-magnetite assemblage.

Chromite in serpentinite is rimmed by magnetite. Sulphide is rare and very fine grained making identification by optical techniques difficult. Identified sulphide minerals using the SEM are pentlandite, pyrrhotite, and chalcopyrite. However, they are very strongly corroded. Pentlandite forms a mixture with garnierite (Plates 2.9 - 2.11). There are rare occurrences of very fined grained (< 10 μm) yellow (in plane polarized

Plate 2.9. EBS image of partially resorbed pentlandite in serpentinite. Dark grey mineral that rims the grain and occurs within the grain (left side) is garnierite. Sample NT-0301.

Plate 2.10. EBS image of euhedral magnetite in serpentinite. Grain attached to magnetite is interpreted to be resorbed pentlandite/pyrrhotite based on EDS (indicated on the grain). Note pentlandite in magnetite. Sample NT-0430.

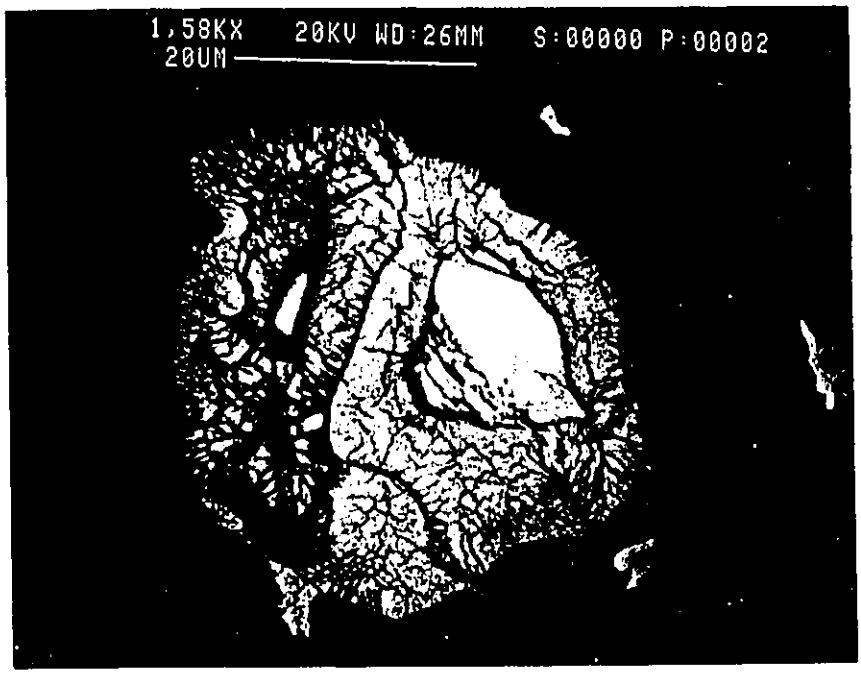
1,58KX 20KV WD:26MM S:00000 P:00002
20UM

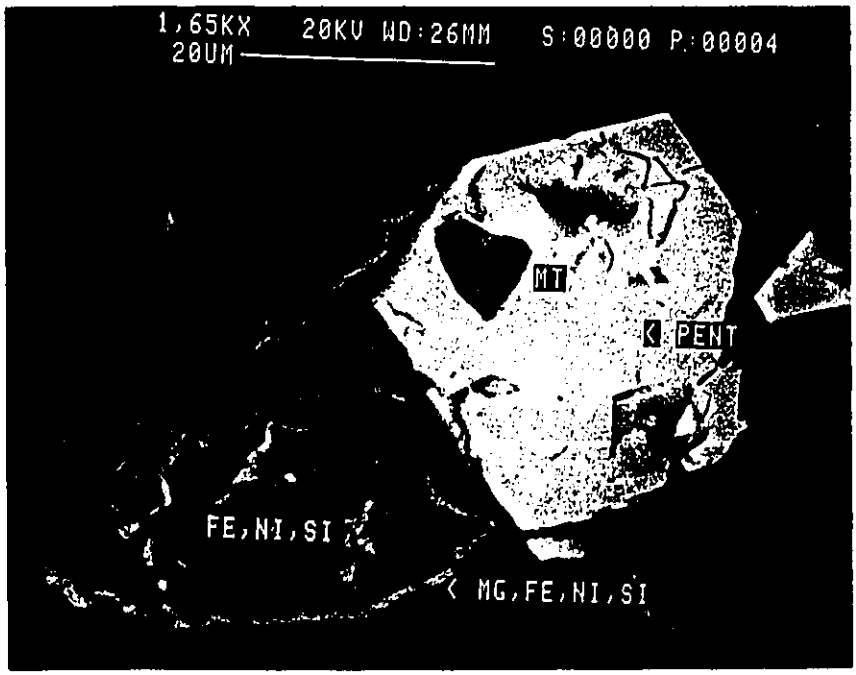
1,65KX 20KV WD:26MM S:00000 P:00004
20UM
MT
K PENT
FE,NI,SI
MG,FE,NI,SI

Plate 2.11. EBS image of euhedral magnetite (white) in serpentinite. EDS from the resorbed grain adjacent to magnetite consists of Ni-Fe-S-As. Sample NT-0426.

Plate 2.12. Photomicrograph. Reflected light. Massive magnetite (grey) hosting sulphide grains (light). Dark areas are antigorite. Sample NT-0327.

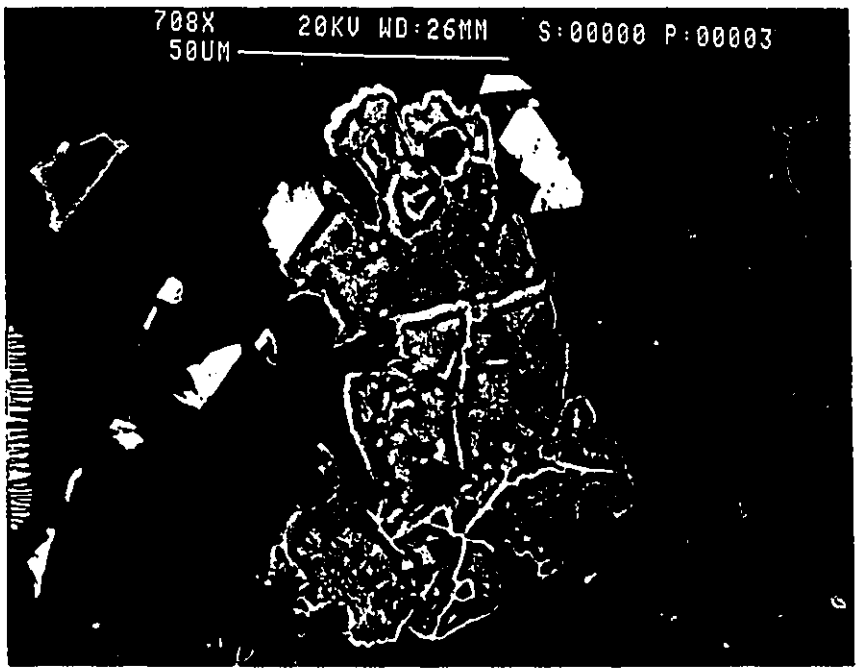
708X
50UM
20KV WD:26MM
S:00000 P:00003

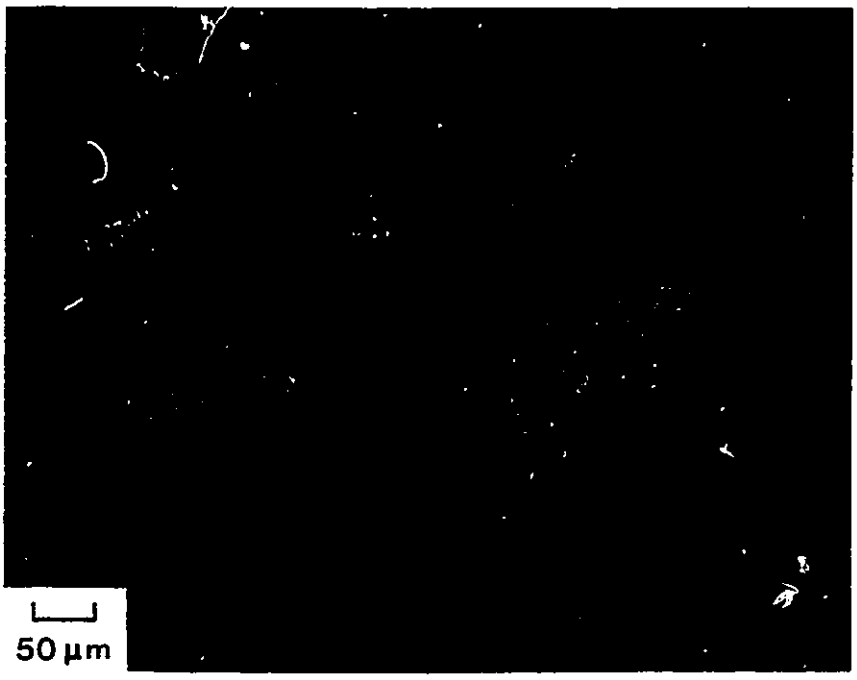
50 µm

reflected light) grains that appear to have sharp grain boundaries. Their small sizes preclude positive identification. However, the EDS indicates that they are Fe-sulphides and therefore interpreted to be either pyrrhotite and/or pyrite. Euhedral pyrite occurs in serpentinite in the northern part of the Betts Cove Complex near Red Cliff Pond.

Massive magnetite bearing serpentinite occurs adjacent to a lens of primary chromitite in the northern part of the map area. The chromitite forms a cumulus texture with euhedral chromite with interstitial silicate minerals. Magnetite replaces chromite along grain boundaries and fractures. The silicate minerals consists of antigorite and chlorite; chlorite occurs exclusively in contact with chromite. The massive magnetite contains relict chromite grains and numerous inclusions of evenly disseminated fine sulphide < 25 μm (Plate 2.12). The sulphides consist of, in order of decreasing abundance, pyrrhotite, chalcopyrite, pentlandite, bornite, and pyrite.

2.233 serpentine-carbonate rocks

The green weathering serpentine-carbonate unit consists of serpentinite, as described above, with magnesite veins and veinlets. The veins are variably oriented and deformed. They commonly contain fragments of serpentinite that are either angular or are partially corroded. The distribution of talc in

the green weathering unit is erratic. It is identified in some samples but not in all. Where identified, it is a volumetrically minor component and invariably occurs as a narrow zone at the magnesite vein - serpentinite contacts.

Sulphides in the serpentine-magnesite unit are similar to those in serpentinite. No sulphide minerals are recognized in contact with carbonate. Where magnetite and magnesite occur together, the magnetite is embayed and corroded. Similarly, chromite is strongly corroded when in contact with magnesite.

The red weathering serpentine-carbonate is mineralogically similar to the green weathering unit. However, it contains a greater abundance of magnesite which occurs as a fine grained magnesite-serpentine assemblage and a greater number of magnesite veins and veinlets. Also, discrete 'patches' of magnesite, interpreted as dismembered veins and veinlets, occur with greater frequency in the red weathering unit. Talc occurs as isolated grains or grain aggregates disseminated in the fine grained serpentine-magnesite and, as in the green weathering unit, at the contact of magnesite veins. Talc crystals have no preferred orientation. The mineral proportions and distribution makes the red weathering unit more competent in contrast to the adjacent talc-carbonate and green weathering serpentine-carbonate units. The red weathering of this unit is due to the weathering of the higher abundances and Fe contents of magnesite (mineral compositions described in the next chapter) and finegrained occurrence with the silicate minerals (in

contrast to the dominantly vein occurrence in the green serpentine-carbonate unit).

2.234 talc-carbonate rocks

The talc-carbonate unit is composed almost exclusively of talc and magnesite. Trace amounts of antigorite were found in samples adjacent to the serpentine-carbonate units. Quartz was not detected in thin sections or in XRD analyses. Trace amounts of chlorite occur in talc-carbonate. Metallic minerals include magnetite, hematite, chromite, chalcopyrite, and pyrite.

Talc and magnesite form a fine grained assemblage in which the modal abundance of talc is approximately equal to or less than that of magnesite. This fine grained assemblage hosts larger subhedral magnesite crystals and anhedral aggregates of magnesite. Where the proportion of magnesite increases, the rock forms a texture akin to a grain supported conglomerate in which large magnesite grains and grain aggregates are set in a matrix of fine grained talc-magnesite. The larger magnesite grains commonly contain inclusions of talc.

Chromite is strongly corroded and replaced by either a mixture of talc-magnesite or magnesite (Plate 2.13). In contrast to serpentinite where magnetite forms anhedral masses, magnetite in talc-carbonate occurs as disseminated anhedral grains (Plate 2.14). It is strongly corroded and commonly occurs as skeletal inclusions in magnesite but also locally

occurs as grains with relatively regular shapes.

Hematite occurs in trace amounts in some talc-carbonate samples. The abundance of magnetite is greater than that of hematite. Hematite occurs as a replacement of magnetite and as very irregular grains in magnesite (Plates 2.15 and 2.16). INCO (confidential drill logs) reports the occurrence of disseminated pyrite in drill cores of talc-carbonate. Chalcopyrite is rimmed by magnetite which is replaced by hematite (Plate 2.17).

Plate 2.13. Photomicrograph. Reflected light. Strongly resorbed chromite grains (center of the photograph) replaced by talc-carbonate. Note that magnetite approximately defines the original euhedral chromite crystals. Sample NT-0015.

Plate 2.14. Photomicrograph. Reflected light. Irregularly shaped and strongly embayed magnetite grains (white) in magnesite (center of photo). Sample NT-0218.

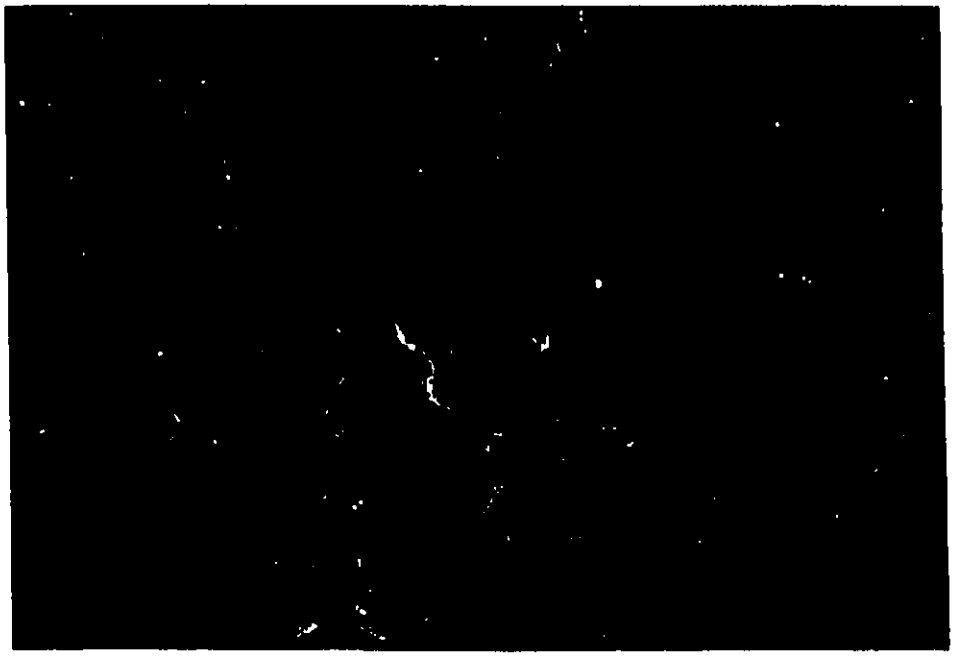

Plate 2.15. Photomicrograph. Reflected light. Hematite (white) and magnetite (duller white) in talc-carbonate. Sample NT-0016.

Plate 2.16. EBS image of hematite, magnetite, and chromite in magnesite. Sample NT-0016.

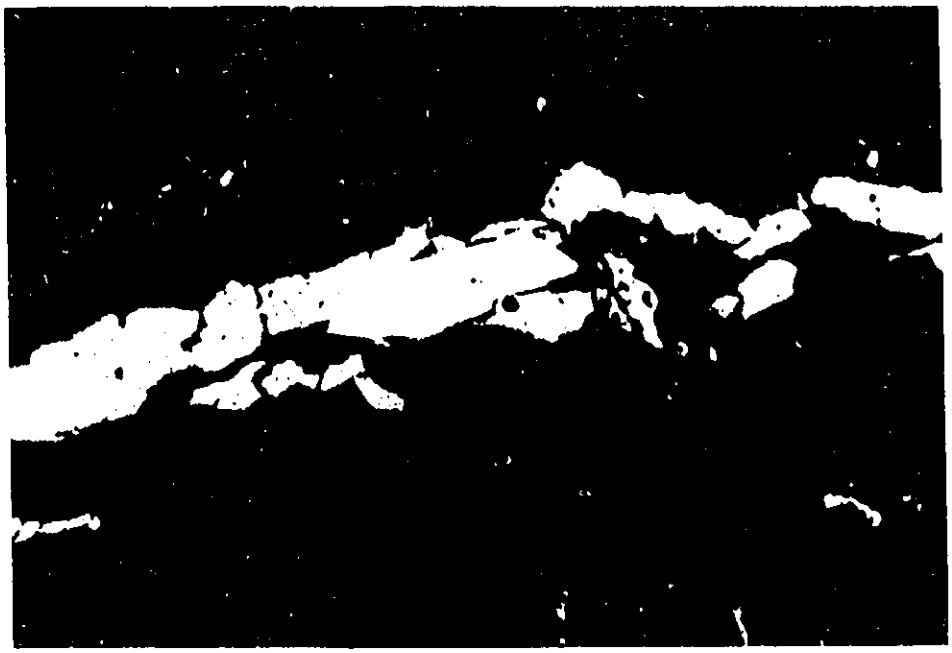

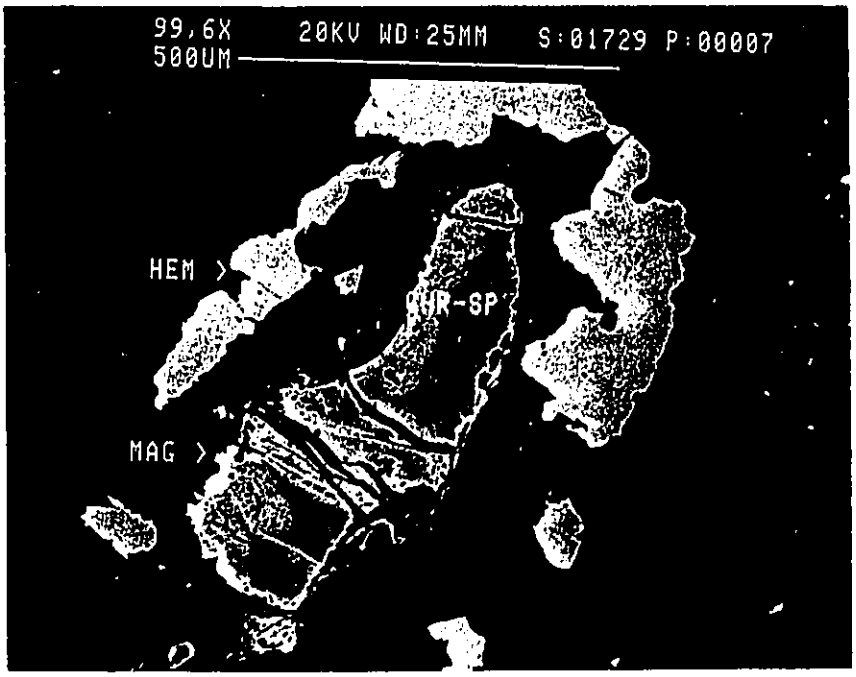
99,6X 20KV WD:25MM S:01729 P:00007
500UM
HEM >
MAG >

Plate 2.17. EBS image of chalcopyrite replaced by magnetite which is partially replaced by hematite. Talc-carbonate map unit. Sample NT-0228.

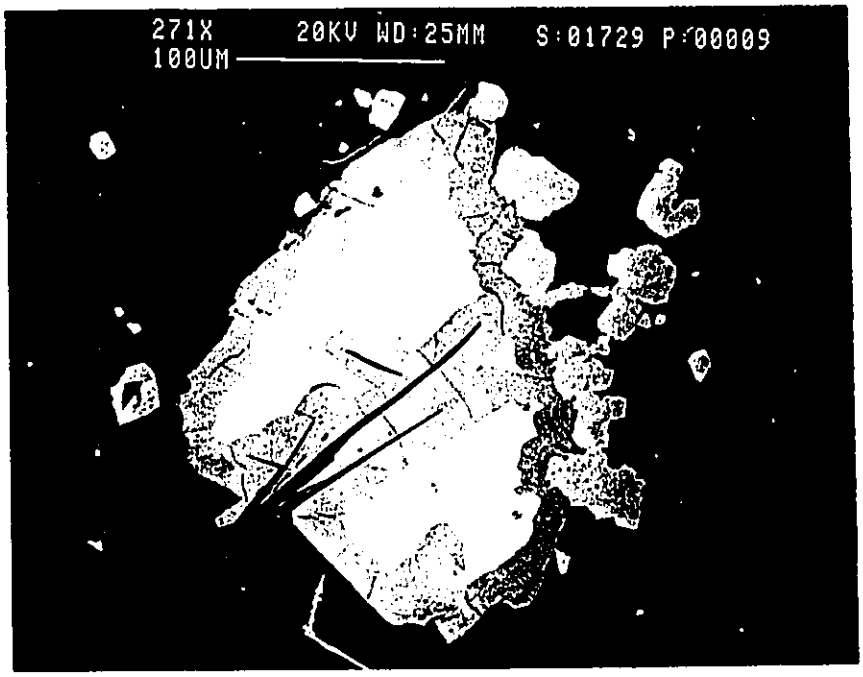
271X 20KV WD:25MM S:01729 P:00009
100UM

CHAPTER 3

GEOCHEMISTRY

3.1 Whole rock geochemistry

Seventy six samples of ultramafic rocks from the Betts Big Pond area were analyzed for major and selected trace element concentrations. Average chemical compositions for the ultramafic rock units are reported in table 3.1. The complete data set is tabulated in Appendix II.

The layered ultramafic rocks from the Betts Big Pond area are plotted with some olivine, orthopyroxene, and clinopyroxene compositions in figure 3.1a. Note that they form a compositional trend from dominantly dunite and harzburgite to wehrlite, lherzolite, and websterite. The metasomatized rocks form a field distinct from that of the layered ultramafic rocks in figure 3.1b.

The most apparent chemical trends in the metasomatized rocks are the addition of H_2O to serpentinite and the addition of CO_2 to serpentine-carbonate and talc-carbonate (Figure 3.2). The trend of the CO_2 bearing rocks emanates from serpentinite which indicates the progressive carbonatization of serpentinite. Also, between 10 and 15 wt % CO_2, the total volatile contents (CO_2+H_2O) decreases with increasing CO_2 contents indicating a loss of H_2O greater than when CO_2 contents are < 10 wt % and > 15 wt %.

Table 3.1. Average chemical composition of the ultramafic map units (Figure 2.3)

	Method	Unit	DL	1	2	3	4	5	6
SiO2	XRF	%	0.01	40.19	39.53	38.69	34.28	34.05	24.30
Al2O3	XRF	%	0.01	0.77	0.57	0.21	0.22	0.24	0.48
TiO2	XRF	%	0.01	0.01	0.02	0.02	0.02	0.02	0.02
MgO	XRF	%	0.01	37.10	37.62	38.68	37.42	35.42	35.00
CaO	XRF	%	0.01	0.78	0.10	0.22	0.25	0.19	0.15
Na2O	XRF	%	0.01	0.03	0.02	0.02	0.03	0.02	0.03
K2O	XRF	%	0.01	0.01	0.01	0.01	0.01	0.01	<.01
Fe2O3	XRF	%	0.01	9.11	8.37	6.64	6.80	6.97	7.63
MnO	XRF	%	0.01	0.13	0.09	0.12	0.14	0.13	0.06
P2O5	XRF	%	0.01	<.01	0.01	0.01	0.01	0.01	0.01
CO2	wet	%	0.01	<.01	0.01	4.33	13.25	18.42	31.43
H2OP	wet	%	0.01	10.65	12.00	10.53	6.28	2.93	1.10
S	XRF	%	0.01	0.01	0.01	0.01	0.01	<.01	<.01
Total		%		98.71	98.48	99.49	98.71	98.40	100.21
Co	DCP	ppm	1	97	90	82	82	77	72
Ni	DCP	ppm	1	1400	1700	2000	2000	2000	2100
Cu	DCP	ppm	.5	2	1	<.5	<.5	<.5	<.5
Zn	DCP	ppm	.5	30	25	24	20	22	24
Mo	DCP	ppm	1	<1	<1	<1	<1	<1	<1
Cd	DCP	ppm	1	<1	<1	1	1	<1	<1
Pb	DCP	ppm	2	3	<2	11	3	2	2
Y	XRF	ppm	2	5	6	6	7	5	5
Zr	XRF	ppm	3	8	13	12	11	13	22
Nb	XRF	ppm	10	<10	<10	10	<10	<10	<10
Ba	XRF	ppm	10	<10	24	18	18	11	52
Cr	DCP	ppm	2	2500	1800	1600	1700	1600	1700
Sr	XRF	ppm	2	2	<2	7	6	3	6
Rb	XRF	ppm	2	4	9	15	13	9	6
As	XRF	ppm	3	<3	23	22	8	14	<3
Tl	DCP	ppm	2	<2	<2	<2	<2	<2	<2
Ag	DCP	ppm	.5	<.5	<.5	<.5	<.5	<.5	<.5
Pt	FADCP	ppb	10	<10	<10	<10	<10	<10	<10
Pd	FADCP	ppb	2	3	5	11	<2	2	3
Se	GFAA	ppm	.1	<.1	<.1	<.1	<.1	<.1	<.1

1- Layered peridotite (n=8). 2- Serpentinite (n=11). 3- Green serpentine-carbonate rocks (n=15).
4- Red serpentine-carbonate rocks (n=17). 5 - Talc-carbonate rocks (n=24). 6- Carbonate rich talc-carbonate (n=1).
DL = detection limit. Significant figures for Cr and Ni = 2.

3.1a

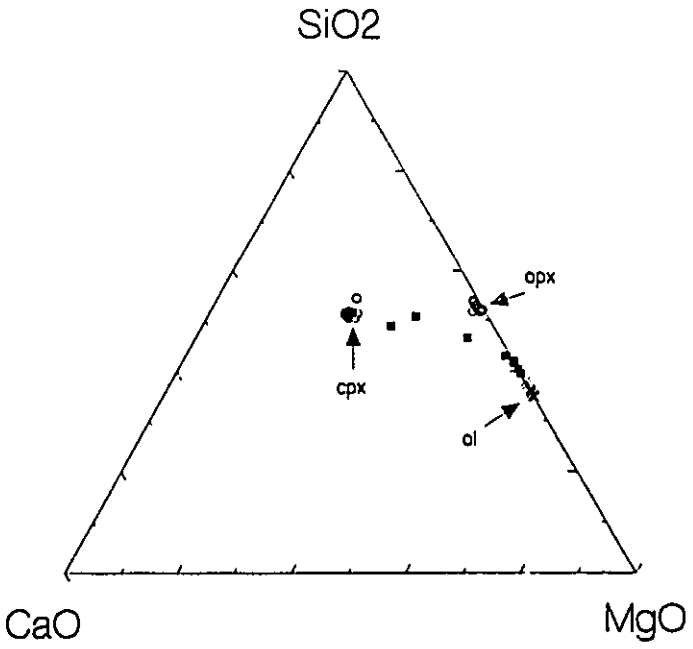

3.1b

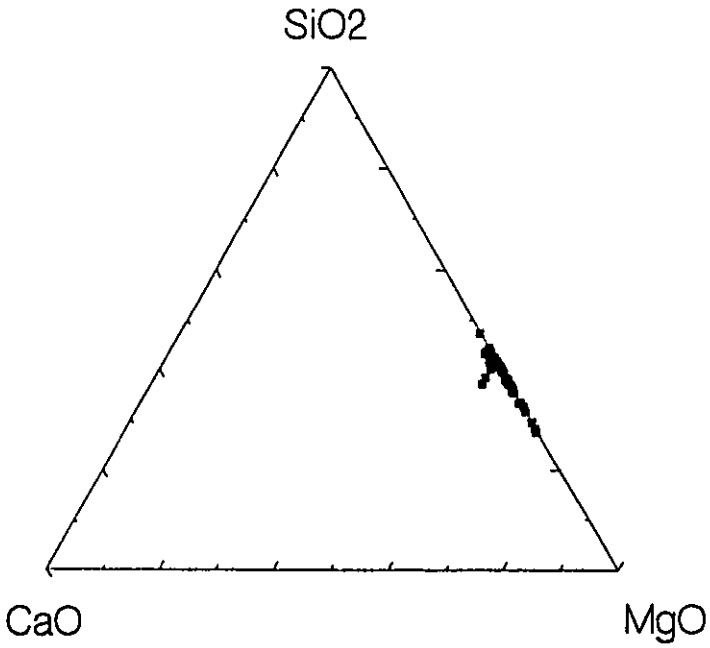

Figure 3.1. SiO_2-MgO-CaO (mole fractions) ternary plots of ultramafic rocks from the Betts Big Pond area. a) Layered ultramafic rocks from the Betts Big Pond area (squares). Mineral data from the Bay of Islands Ophiolite Complex, courtesy of the Geological Survey of Canada (unpublished data). Abbreviations: ol - olivine, opx - orthopyroxene, cpx - clinopyroxene. b) All metasomatized rocks from the Betts Big Pond area.

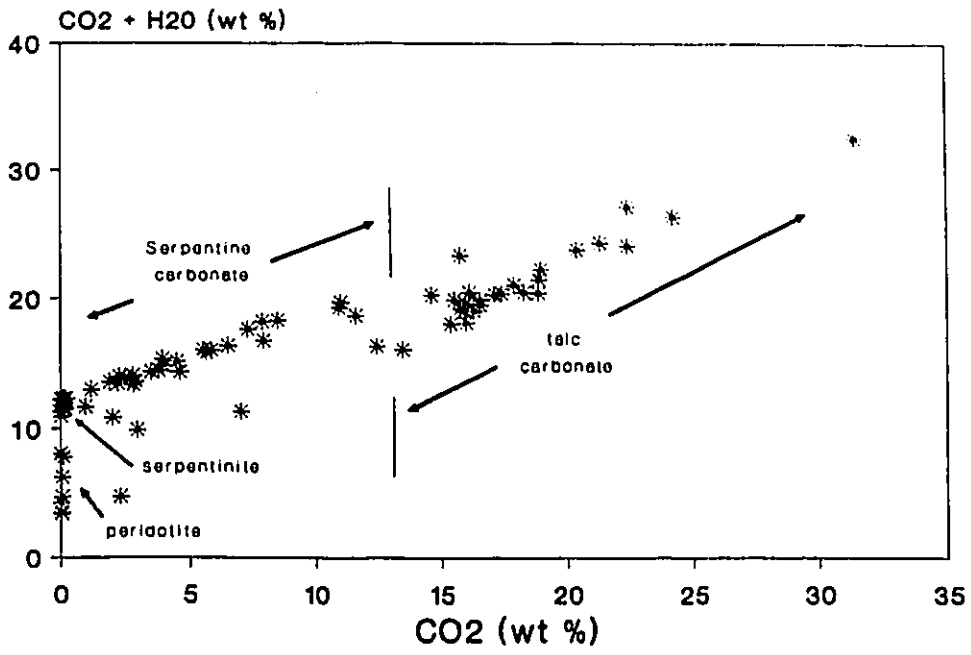

Figure 3.2. CO_2 vs. CO_2+H_2O plot of all ultramafic rock analyses from the Betts Big Pond area. The change in the trend of data points from serpentine-carbonate to talc-carbonate largely reflects the addition of SiO_2 to talc-carbonate relative to serpentine-carbonate (discussed in section 3.4)

3.2 Mineral compositions

The samples analyzed, some mineralogical and whole rock geochemical characteristics, and the minerals analyzed are indicated in table 3.1. In addition, sample NT-228 which contains 1300 ppb Au was chosen to determine if there are any anomalous mineral compositions associated with Au mineralization. The results are tabulated as average mineral compositions in tables 3.2, 3.3, and 3.4. The complete data set is contained in Appendix II.

Table 3.2. Summary of minerals analyzed and some sample characteristics

Sample	Wt %		Rock Type	Minerals* Probed				
	H_2O	CO_2		Srp	Mgs	Mag	Chr	Tlc
NT-053	11.7	.9	serpentinite with carb. veinlets	x	x	x		
NT-054	10.3	7.9	serp-carb	x	x	x	x	
NT-055	9.8	8.4	serp-carb	x	x	x		
NT-228	3.2	15.9	talc-carb		x	x		x
NT-027	3.0	21.3	talc-carb		x	x		x
NT-224	2.1	24.2	talc-carb		x			x

* mineral abbreviations from Kretz (1983)

3.21 Carbonate

The average carbonate composition in serpentine-carbonate is magnesite whereas the average carbonate composition in talc-carbonate is breunnerite (i.e. breunnerite = ferroan magnesite, > 5 wt % FeO; classification from Deer et al., 1962) (Table 3.3 and Figure 3.3). There is little variation in the average magnesite composition in the serpentine-magnesite rocks and the three samples have a similar range of Mg/(Mg+Fe) (Figure 3.3). The breunnerite in talc-carbonate differs from magnesite in serpentine-carbonate. 1) The former has a lower average Mg/(Mg+Fe) than the latter (Figure 3.3) and 2) Breunnerite has a lower average MnO content (average MnO in talc-carbonate =

.16 wt %, average MnO in serpentine-carbonate = .71 wt %; Table 3.3). Although the average carbonate composition is similar in the talc-carbonate samples, they show a trend where increasing Fe content increases with whole rock CO_2 content (Figure 3.3 and Table 3.3).

3.22 Serpentine and talc

The compositions of serpentine and talc remain relatively constant among samples (Table 3.4). In samples NT-054 and NT-055, a number of analyses yield compositions and anhydrous totals intermediate between those of serpentine and talc (Figure 3.4) and are interpreted to reflect fine grained mixtures of serpentine and talc. During sample preparation an effort was made to isolate lizardite for analysis. However, the fine grained size and intimate intergrowth with antigorite precludes confidant determinations of lizardite. However, the variability of Al_2O_3 in serpentine probably reflects the presence of aluminous lizardite.

3.23 Magnetite and chromite

Little variation exists in the magnetite composition among samples (Table 3.5). The only exception is high Cr_2O_3 concentration in one sample which reflect the origin of magnetite as a chromite replacement. One chromite composition

was determined. It is compared with chromite determinations from the Betts Cove Complex reported by Coish and Church (1979).

Table 3.3. Average compositions of magnesite (wt %)

	NT-053	NT-054	NT-055	NT-228	NT-027	NT-224
CaO	0.28	0.19	0.20	0.35	0.10	0.28
MgO	45.40	44.63	45.14	44.23	44.06	43.16
MnO	0.74	0.77	0.62	0.08	0.14	0.26
FeO	2.76	2.59	2.38	5.33	5.38	6.69
BaO	0.04	0.02	0.04	0.04	0.03	0.02
SrO	0.01	0.01	0.01	0.02	0.01	0.00
	49.23	48.21	48.84	50.05	49.72	50.41

Table 3.4. Average compositions of serpentine and talc (wt %)

	NT-053	NT-054	NT-055	NT-228	NT-027	NT-224
SiO2	43.12	42.86	42.68	62.25	61.81	62.79
Al2O3	0.40	0.41	0.46	0.11	0.09	0.11
FeO	4.33	4.02	4.23	1.46	2.32	1.8
MnO	0.02	0.04	0.04	0.01	0.03	0.02
MgO	37.51	37.6	37.57	30.37	29.40	29.44
Cr2O3	0.11	0.27	0.40	0.06	0.05	0.05
NiO	0.23	0.26	0.26	0.33	0.43	0.57
CaO	0.06	0.03	0.03	0.01	0.02	0.03
Na2O	0.05	0.00	0.00	0.00	0.00	0.00
K2O	0.04	0.01	0.01	0.02	0.01	0.01
Total	85.87	85.5	85.73	94.62	94.16	94.82

Table 3.5. Average compositions of magnetite and chromite (wt %)

	NT-053	NT-054	NT-055	NT-228	NT-027	NT-224	Chr-Avg
Al2O3	0.04	0.03	0.02	0.03	0.02	14.87	10.05
Cr2O3	0.26	0.04	1.31	0.67	0.21	51.58	55.88
Fe2O3	67.93	66.68	65.42	66.75	67.01	.00	5.43
V2O3	0.00	0.05	0.08	0.10	0.16	.33	N/R
TiO2	0.03	0.04	0.04	0.05	0.04	.04	.02
FeO	30.10	29.45	29.62	29.79	29.76	16.94	14.94
MgO	0.02	0.09	0.09	0.11	0.10	7.52	12.30
MnO	0.06	0.02	0.00	0.05	0.03	.21	.79
ZnO	0.10	0.04	0.00	0.03	0.08	.21	N/R
NiO	0.51	0.49	0.42	0.45	0.40	.06	N/R
	99.05	96.84	97.00	98.03	97.81	91.76	100.03

Chr-avg is average of chromite compositions reported by Coish and Church (1979). N/R - not reported

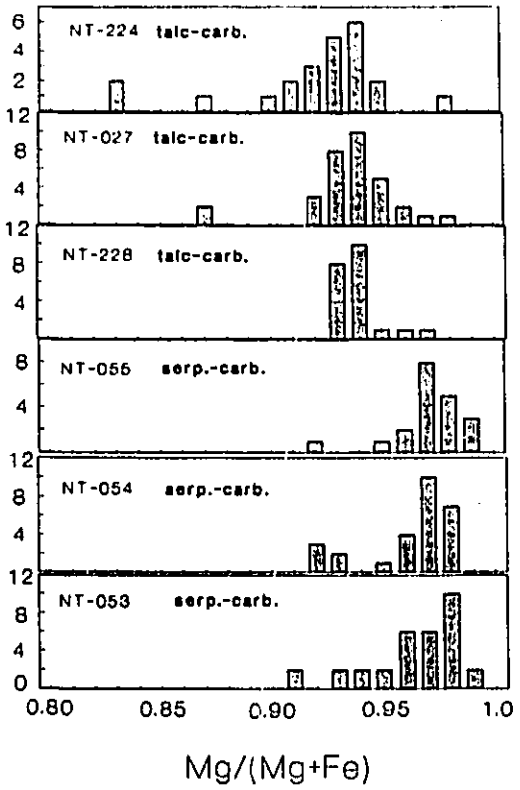

Figure 3.3. Histogram of MgO/(MgO+FeO(t)) (wt. %) in carbonate. Each point represents a grain determination. Samples indicated in table 3.2.

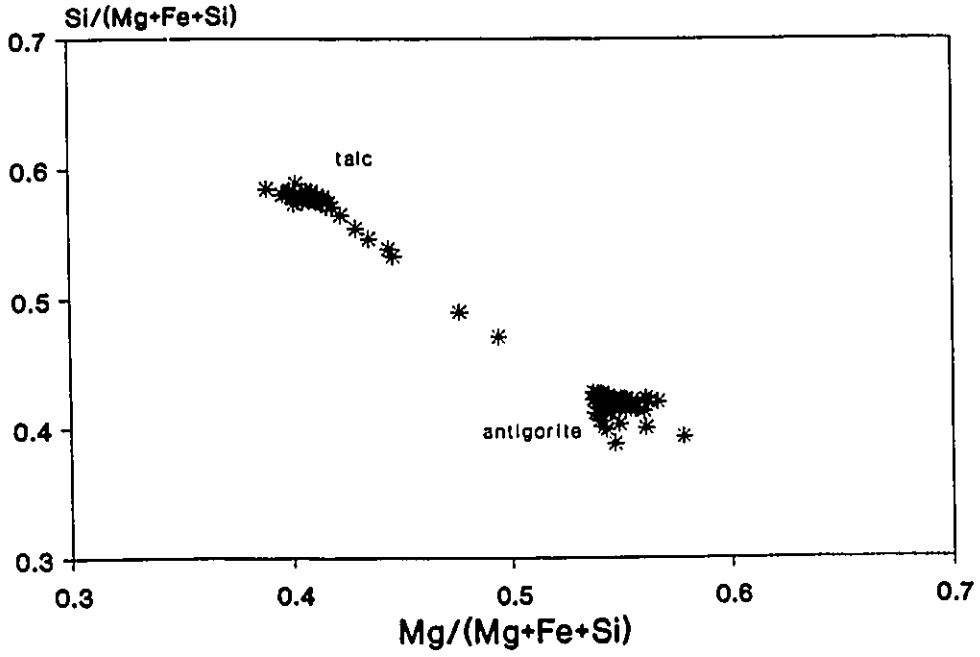

Figure 3.4. Si/(Mg+Fe+Si) vs Mg/(Mg+Fe+Si) plot of serpentine and talc.

3.3 Normative mineralogy

The fine grain size, irregular grain shapes, and replacement textures make the accurate determination of mineral modes by optical methods difficult. As an alternative, the mineralogical composition of the metasomatized rocks were calculated using the whole rock and mineral chemical data. The general method used is that outlined by Thompson (1982), Brimhall et al. (1984), and others and is outlined in Appendix III. The method involves solving the equation:

$$Ax \approx b$$

where A is a coefficient matrix, in this study consisting of moles oxide/mole mineral (mineral data), b is a vector matrix consisting of moles oxide/100 g rock (whole rock data), and x, the desired solution vector matrix, consists of moles mineral/100 g rock.

The results of the calculations are plotted versus whole rock CO_2 content in figure 3.5 and illustrate the mineralogical changes in the rock with progressive metasomatism. Serpentinite (at 0 wt % CO_2) consists of 80-95 mole % serpentine (Figure 3.5a) and 5-20 mole % magnetite with the exception of two magnetite rich samples (Figure 3.5b).

The molar abundances of serpentine, magnesite, talc, and magnetite with increasing whole rock CO_2 content are described in terms of the abundances with 0 -16 wt % whole rock CO_2 and those with greater than 16 wt % CO_2. Magnesite (Figure 3.5c)

3.5a

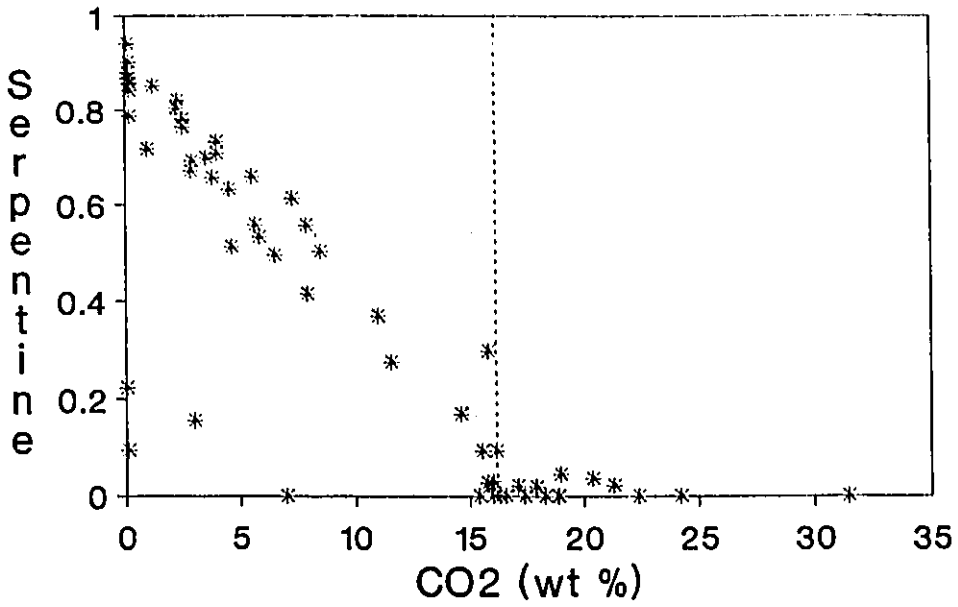

3.5b

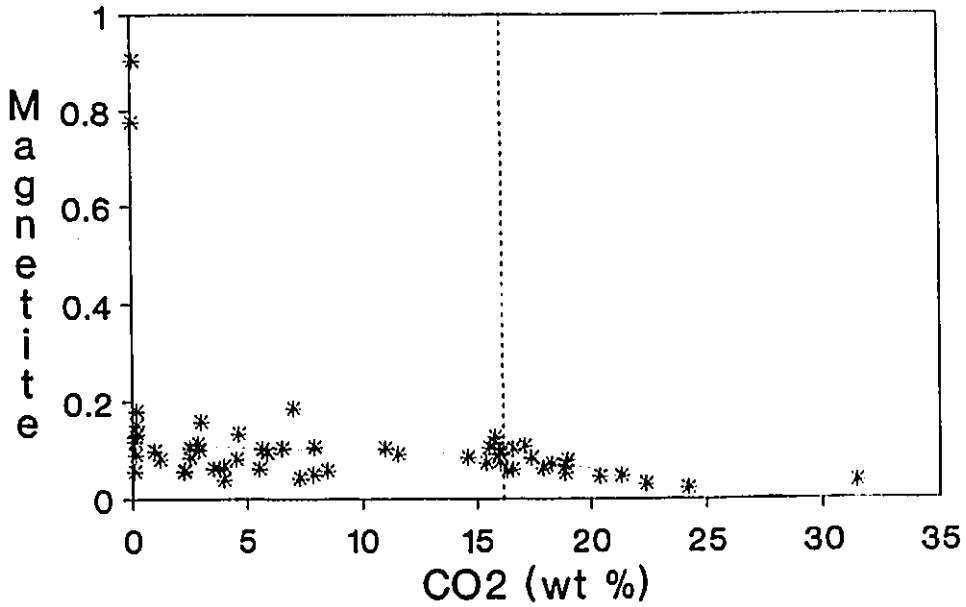

Figure 3.5. Plots of normative minerals in the metasomatized rocks vs. whole rock CO_2 content. Y axis is mole fraction mineral.

3.5c

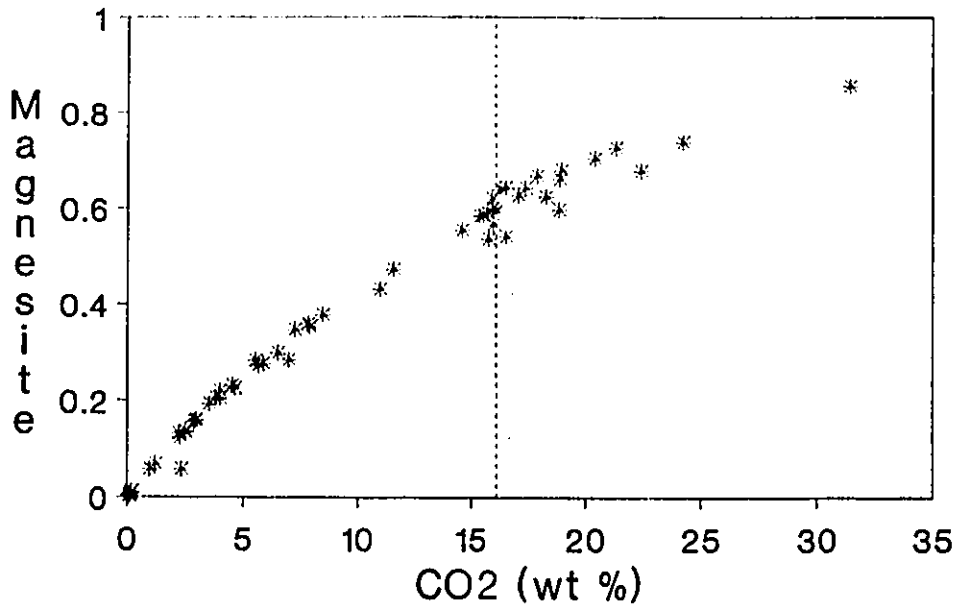
Magnesite
1
0.8
0.6
0.4
0.2
0
0
5
10
15
20
25
30
35
CO2 (wt %)

3.5d

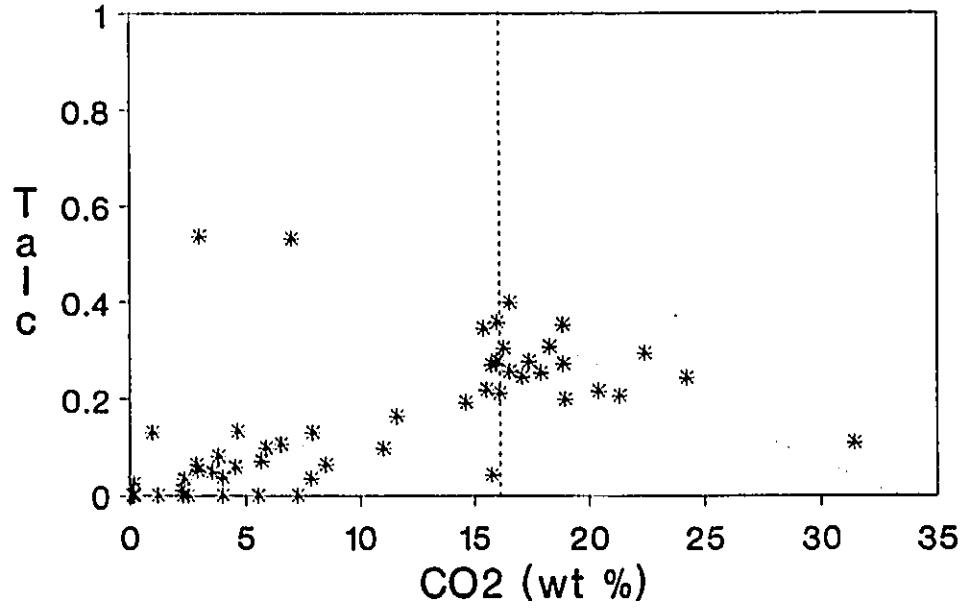
Talc
1
0.8
0.6
0.4
0.2
0
0
5
10
15
20
25
30
35
CO2 (wt %)

increases from nil in serpentinite to approximately 60 mole % of the rocks at whole rock CO_2 contents of approximately 16 wt %. There is sympathetic decrease in serpentine content from 80 to 95 mole % in serpentinite to approximately 10 mole % at 16 wt % CO_2. Samples with the same (or very similar) whole rock CO_2 contents have serpentine contents that may vary up to 15 mole %.

There is a general increase in the molar abundance of talc (Figure 3.5d) from 0 to 16 wt % CO_2 and, as in serpentine contents, considerable variation exists between samples with similar CO_2 contents. A number of samples, up to approximately 7.5 wt % CO_2, do not contain talc.

At approximately 16 wt % CO_2, serpentine is almost completely eliminated. At approximately 16 wt % CO_2, there is an increase in the molar abundance of talc and this increase is above the trend of talc increase from 0 to just below 16 wt % CO_2. The talc content reaches a maximum at approximately 16 wt % CO_2. In rocks containing higher CO_2 contents, the molar abundance of talc consistently decreases. The molar abundance of magnetite remains relatively constant between 0 and 16 wt % CO_2 beyond which there is a consistent decrease in the molar abundance of magnetite.

Brucite was a normative mineral in two of the calculations in which its concentration is < 1 mole %. Chlorite was not included in the calculations because attempts to determine its composition were not successful. It was not included with an

ideal composition because of the variable Al_2O_3 content of serpentine and doing so would probably overestimate the mole fraction of chlorite present. Also, since Al_2O_3 is generally less than 0.3 wt %, inclusion of it in the calculations would not materially affect the results.

3.4 Metasomatic gains and losses

Gains and losses of oxides and elements are evaluated using the equation of Gresens (1967) as derived by Grant (1986). The procedure for calculation is outlined in Appendix III. The first step in the procedure is determination of an immobile element against which the remaining elements and oxides can be compared.

It is indicated that high-field-strength elements (HFSE: Ti, Zr,Y, Nb, Ta, Hf) are least susceptible to movement during various metasomatic or metamorphic processes (e.g. Pearce, 1975; Wood et al., 1979; Saunders et al., 1980; Kerrich and Fyfe 1981; Shervais, 1982; Lydon and Galley, 1986). A number of studies have indicated that in carbonate alteration zones associated with gold mineralization, the cations in carbonate minerals are derived from the host rock and the carbonate from the hydrothermal fluid (e.g. Kerrich and Fyfe, 1981; Fyon et al., 1983). Bohlke (1989) described alteration assemblages in ultramafic rocks at Allegheny, California identical to those at Betts Big Pond and has quantitatively shown that Mg^{2+} has been

conserved. If the same process is applicable to the Betts Big Pond area, the conversion of Mg-anhydrous silicates to Mg-hydrous silicates and Mg-carbonates suggests, at least qualitatively, that Mg^{2+} has been derived from the protolith during metasomatism in the Betts Big Pond area.

That Mg^{2+} has remained immobile in the Betts Big Pond area is indicated in the ternary plots of MgO-Zr-Y-Co (Figure 3.6). Since it is unlikely that these elements would be gained or lost in the same relative proportions during serpentinization and carbonatization, the relatively tight clusters of data points in figure 3.6 indicate that they remained essentially immobile (cf. Lydon and Galley, 1986). Of these elements, MgO is chosen as the basis for comparison because it is a major rock forming component and as such the ratio of [MgO in unaltered rocks]/[MgO altered rocks] will more closely monitor total mass changes. Because MgO has a range of values in the original ultramafic rocks (Figure 3.1), it is necessary to compare the MgO in the altered rocks to the magmatic range of MgO values in the layered rocks to distinguish the effects of metasomatism from original magmatic variation.

The elements are classified into three categories (Table 3.6): 1) those with a definable change in concentration during metasomatism, 2) those with no defineable change in concentration during metasomatism, and 3) those that cannot be assessed because they have concentrations below or near detection limits in the layered rocks and the metasomatic rocks

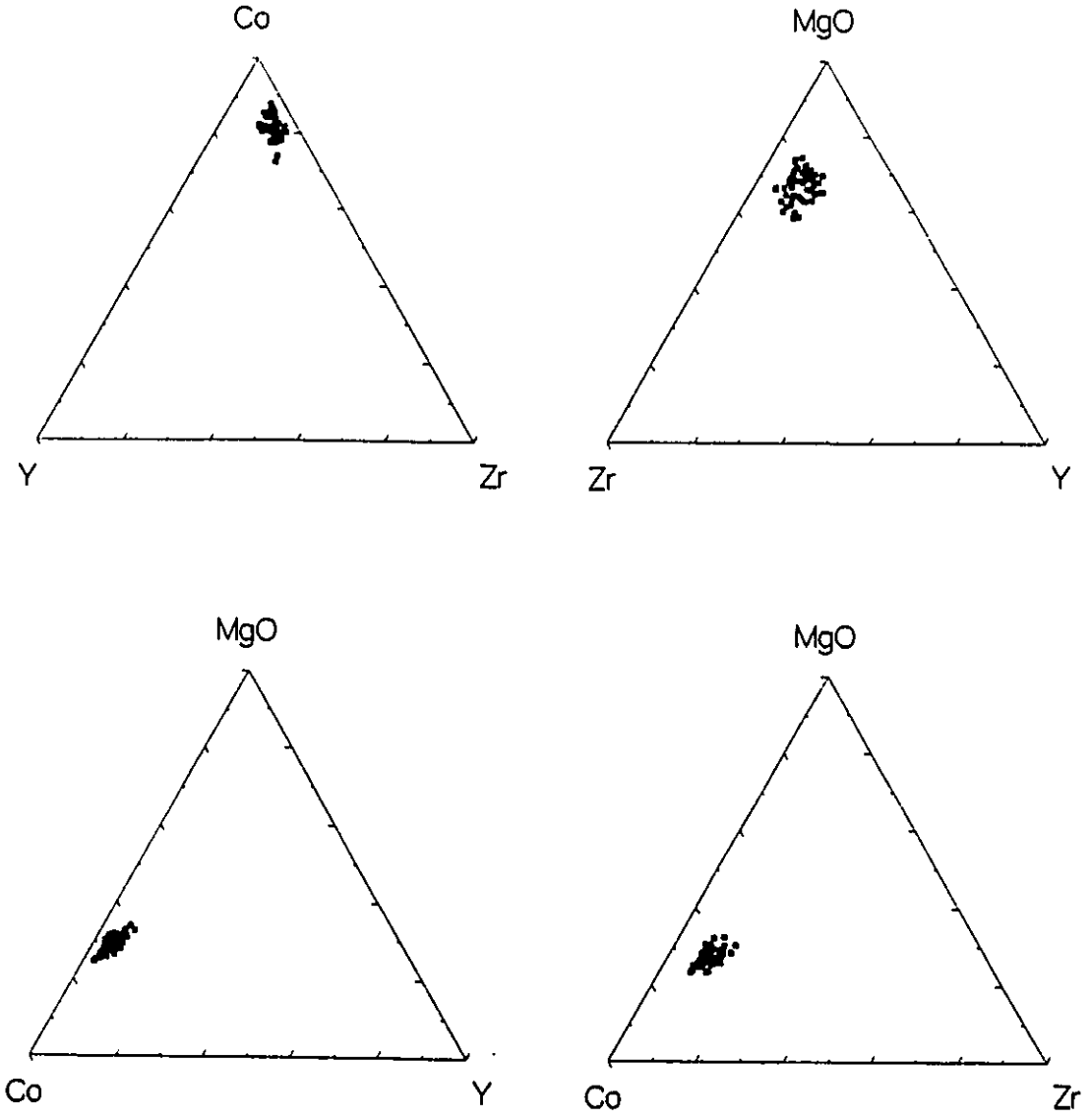

Figure 3.6. MgO-Co-Zr-Y ternary plots of all ultramafic rocks from the Betts Big Pond area. Mole fractions.

(Table 3.1). Those elements whose behavior during metasomatism can be determined have either been added to the rock, lost to the rock, or have a net zero flux during serpentinization and carbonatization. (Table 3.7 and Figure 3.7)

SiO_2. The immobility of SiO_2 during serpentinization is indicated by the cluster of data (at 0 wt % CO_2) around 0 change $mSiO_2$ (Figure 3.7a). The distribution of SiO_2 with increasing whole rock CO_2 wt % shows three distinct trends. The first trend is characterized by a consistent loss of SiO_2 from 0 to 16-17 wt % CO_2. The second trend is indicated where there is a sharp increase in $mSiO_2$ at approximately 16 wt % CO_2. The third trend shows a similar loss in SiO_2 as the first trend, from a maximum at approximately 16 wt % CO_2 to a minimum in the sample with the highest whole rock CO_2 content (Figure 3.7a).

Note that the first trend of SiO_2 loss from 0 to approximately 16 wt % CO_2 corresponds with serpentine decreasing from 80 to 95 mole % of the rock (serpentinite) to approximately 10 mole % of the rock (Figure 3.5a), magnesite increasing from zero to approximately 60 mole % of the rock (Figure 3.5c), and a modest increase in talc from zero to approximately 20 % of the rock (Figure 3.5d). The second trend, characterized by a steep increase in $mSiO_2$ from the end of the first trend to the start of the third at approximately 16 wt % CO_2 (Figure 3.7a) corresponds with the marked increase in the molar abundance of talc (Figure 3.5d). The decrease in SiO_2 with increasing whole rock CO_2 content (third trend) from a

maximum at approximately 16 wt % CO_2 corresponds to a decrease in the molar abundance of talc and increase in magnesite (Figure 3.5d).

Al_2O_3. In serpentinite (i.e. 0 wt % CO_2), Al_2O_3 is distributed sub-equally above and below the zero change line (Figure 3.7b). In a magnetite-serpentine assemblage, Al_2O_3 will dominantly occur in serpentine. The distribution of Al_2O_3 in serpentinite is interpreted to reflect the variability in the serpentine/magnetite ratios (Figures 3.5a and 3.5b) and therefore suggests that Al_2O_3 has not changed during serpentinization.

The effect of carbonatization on Al_2O_3 content is unclear as no trend exists with increasing CO_2 and could be interpreted as the carbonatization of rocks whose Al_2O_3 content, inherited from serpentinization, was below the zero change line. However, carbonatization involves increasing the proportion of minerals that do not accommodate Al^{3+} (i.e. increasing magnesite and talc and decreasing serpentine; compare Al_2O_3 contents in serpentine and talc, table 3.4). Therefore, the observation that some data points lie below the magmatic range, defined by the concentration of Al_2O_3 in the layered rocks, suggest that Al_2O_3 is largely conserved but may be lost from some samples during carbonatization.

Total Fe expressed as FeO. That FeO is generally conserved during serpentinization is indicated by the cluster of data (at 0 wt % CO_2; Figure 3.7c) about the zero change line. The

occurrence of magnetite rich zones within the serpentinite may be indicative of a local redistribution of Fe.

The general distribution of data points within the magmatic range indicates that FeO has not been added to or lost from the rock during carbonatization. However, the data points below the magmatic range indicate a possible small amount of loss. The general conservation of FeO is also suggested by the observation that the decreasing modal abundance of magnetite (Figure 3.5b) and the decrease in FeO content in talc from that in serpentine (Table 3.4) corresponds to an increase in the FeO content of the carbonates (decrease in the ratio Mg/(Mg+Fe) in figure 3.3).

H_2O. There are two trends of H_2O loss from the rock with increasing whole rock CO_2 content (Figure 3.7d). The first extends from 0 to approximately 16 wt % CO_2. The second trend extends from approximately 16 wt % CO_2 to higher CO_2 contents. The slope of the first trend is steeper than that of the second trend. Also, there is sharp decrease in H_2O concentration from the high CO_2 end of the first trend to the low CO_2 end of the second trend. This sharp decrease in H_2O concentration corresponds to an elimination of serpentine from a value of approximately 20 mole % of the rock (Figure 3.5a).

Ni. The mobility of Ni during serpentiniztion is indicated by the dissolution of Ni-sulphides (Plates 2.9 - 2.11). The distribution of data points at 0 wt % CO_2 suggest that some serpentinite samples have lost Ni and others have gained it

(Figure 3.7e). The occurrence of garnierite and sporadically high NiO contents in antigorite (Table 3.4; Appendix II) suggest that Ni^{2+} originated from pentlandite and forsterite was concentrated in antigorite conserving the overall NiO abundance of the bulk rocks.

The distribution of NiO appears to be independent of whole rock CO_2 content. The data points mostly lie within the magmatic ranges.

Zn. Although there is significant variation in Zn concentration, almost all calculations fall within the limits defined by the abundances in the layered rocks (Figure 3.7f) suggesting that Zn is largely conserved during metasomatism.

Cr. The replacement of chromite by magnetite in serpentinite suggests at least a local mobility of Cr. However, the bulk rock data indicates that Cr is largely conserved during serpentinization (Figure 3.7g). The Cr_2O_3 concentrations of serpentine and magnetite are variable indicating that serpentine accommodated Cr^{3+} and the replacement of chromite by magnetite and it is therefore immobile at the scale of the hand samples.

A number of points fall outside the primary range and may indicate Cr mobilization during carbonatization. This is suggested by the dissolution of chromite in carbonate bearing assemblages and the observation that talc is consistently lower than serpentine in Cr_2O_3.

Table 3.6. Summary of the effects of metasomatism on the concentration of elements.

Defineable Trends	Undefineable Trends	Too Low
Si, Al, Fe, H_2O, CO_2, Ni, Zn, Cr, MgO, Y, Zr, Co	Ti, Ba, As, Ca, Mn	K, Na, P, S, Cu, Mo, Cd, Nb, Sr, Tl, Ag, Pt, Pd, Se, Pb, Rb

Too Low - elements reported at or near detection limit (Table 3.1)

Table 3.7. Summary of enrichments, losses, and conservation of those elements with defineable behaviors during metasomatism

	Enriched			Depleted			Immobile
	Str.	Mod.	Weak	Str.	Mod.	Weak	
Serp.	H_2O						Si, Al, Mg, Fe, Co, Y, Zr, Zn, Cr, Ca, Ni
Carb.	CO_2			Si, H_2O		Al, Fe Cr(?)	Mg, Co, Y, Zr, Fe(?), Zn, Cr(?), Ni

Serp=serpentinization; Carb=carbonatization

3.7a

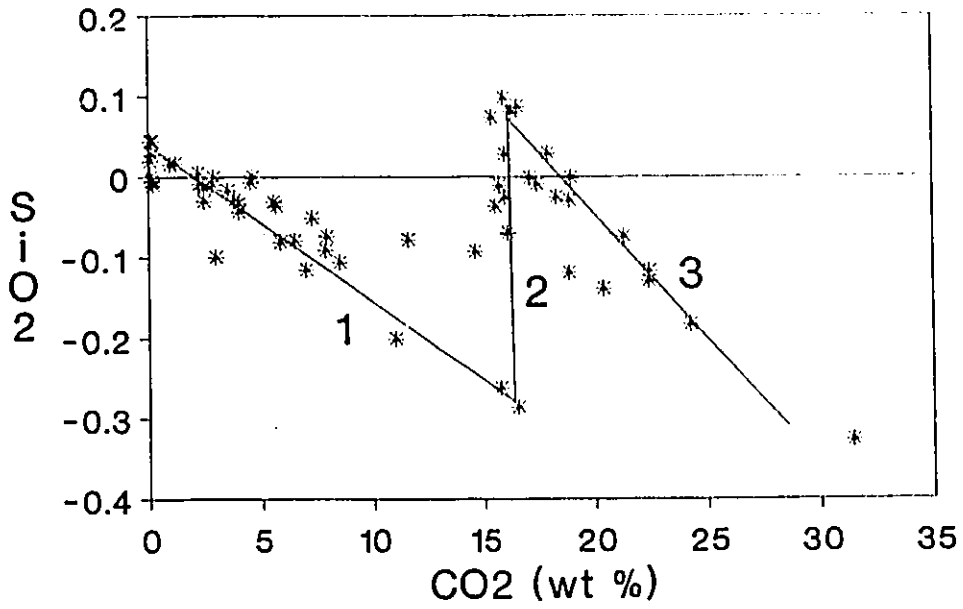

Figure 3.7. Plots of the change in concentration of components in moles (Y-axis) vs. whole rock CO_2 content (X-axis). Calculation of Y-axis values indicated in Appendix III. Dotted lines represent the range of values in the layered ultramafic rocks to which the metasomatized rocks are being compared. Data points that fall above the magmatic range indicate that component has been added to the rock, those that fall below the range have been lost from the rock, and those that fall within the range cannot be distinguished from original magmatic variation.

3.7b

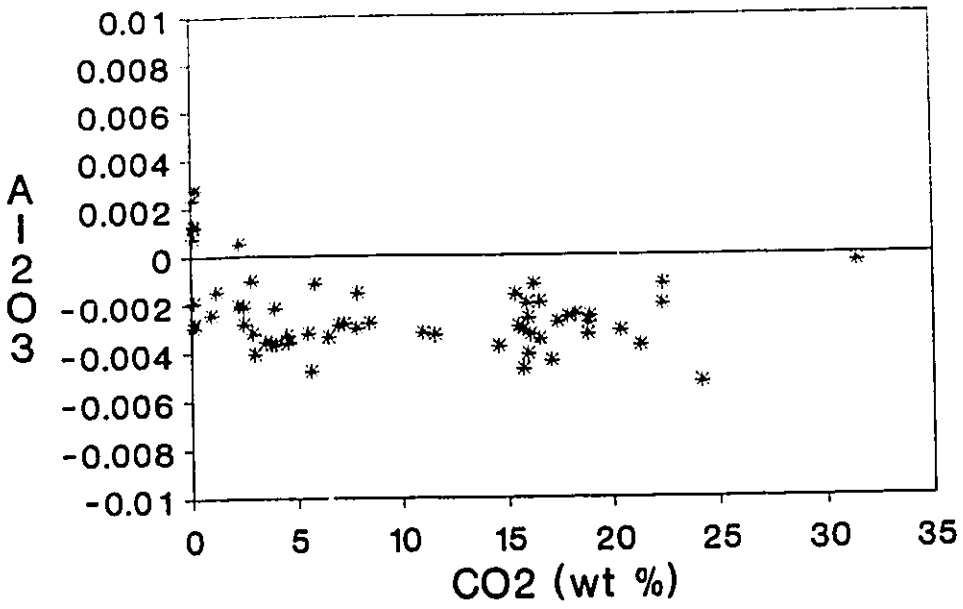
0.01
0.008
0.006
0.004
0.002
0
-0.002
-0.004
-0.006
-0.008
-0.01
Al2O3
0
5
10
15
20
25
30
35
CO2 (wt %)

3.7c

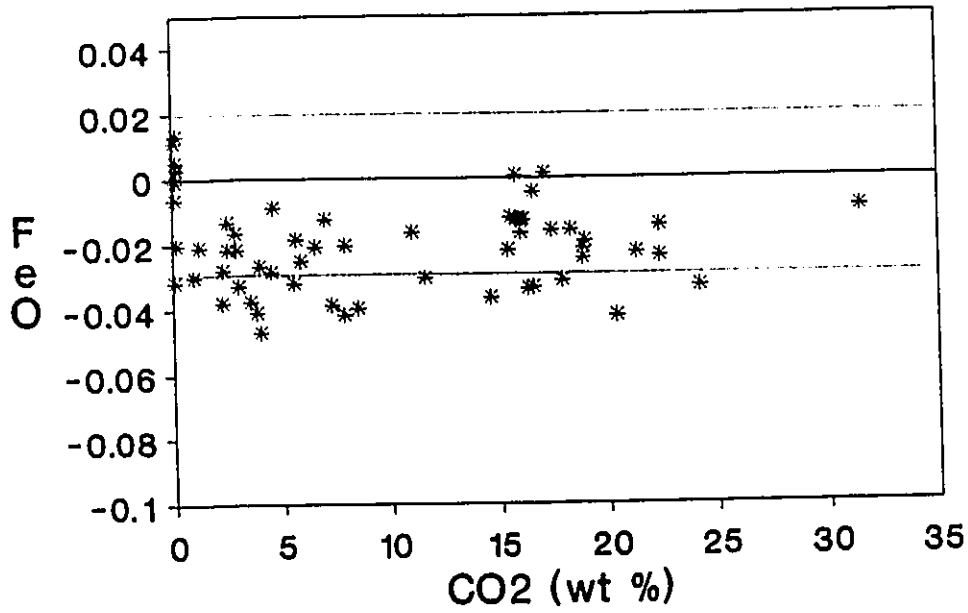
0.04
0.02
0
-0.02
-0.04
-0.06
-0.08
-0.1
FeO
0
5
10
15
20
25
30
35
CO2 (wt %)

3.7d

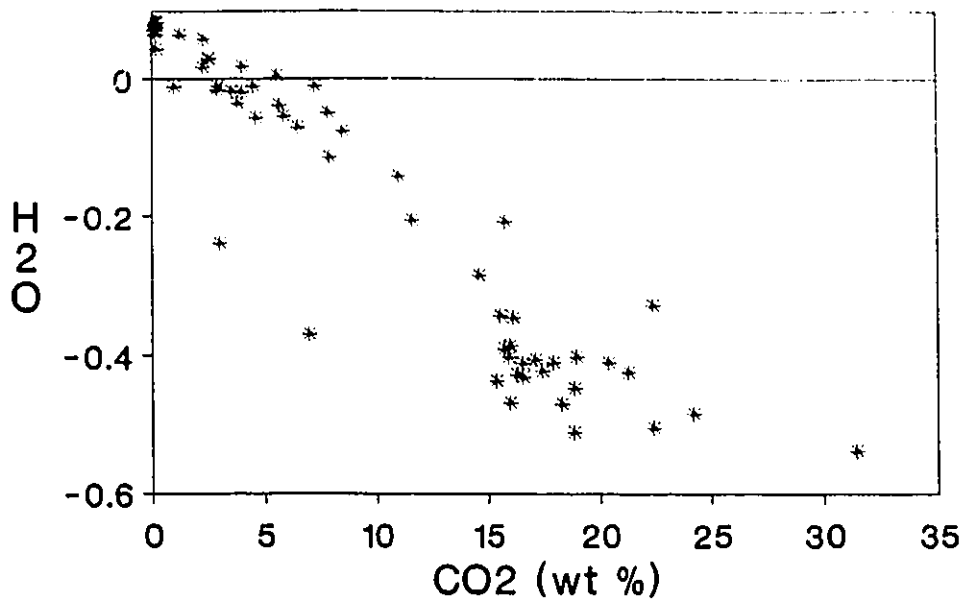
H
2
O
0
-0.2
-0.4
-0.6
0
5
10
15
20
25
30
35
CO2 (wt %)

3.7e

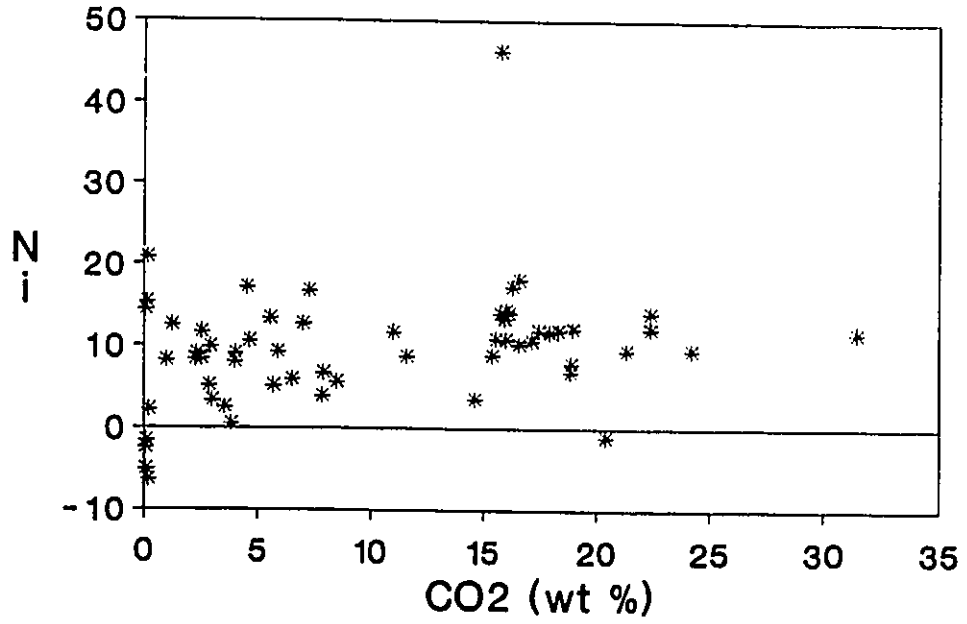
N
i
50
40
30
20
10
0
-10
0
5
10
15
20
25
30
35
CO2 (wt %)

3.7f

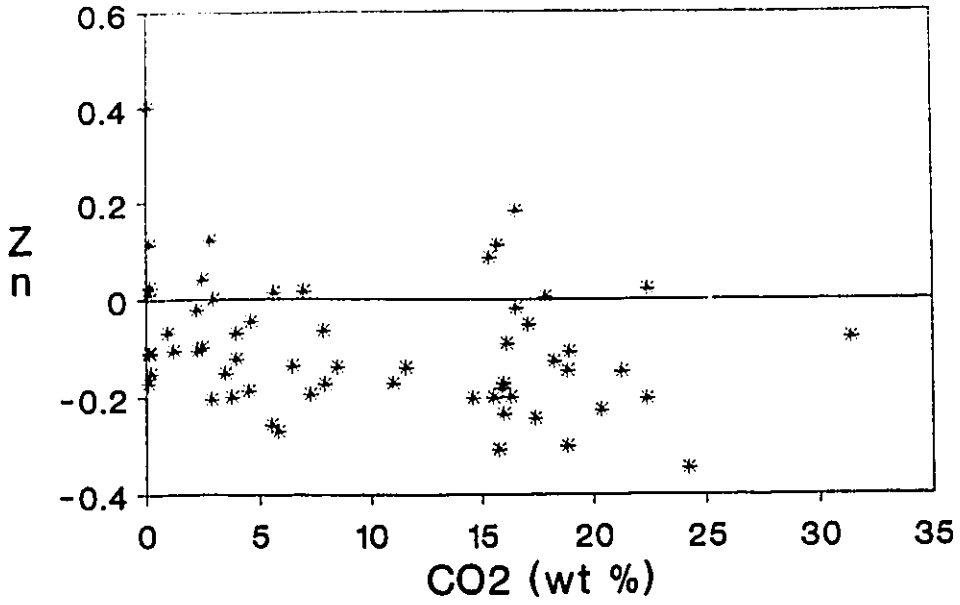
0.6
0.4
0.2
0
-0.2
-0.4
Zn
0
5
10
15
20
25
30
35
CO2 (wt %)

3.7g

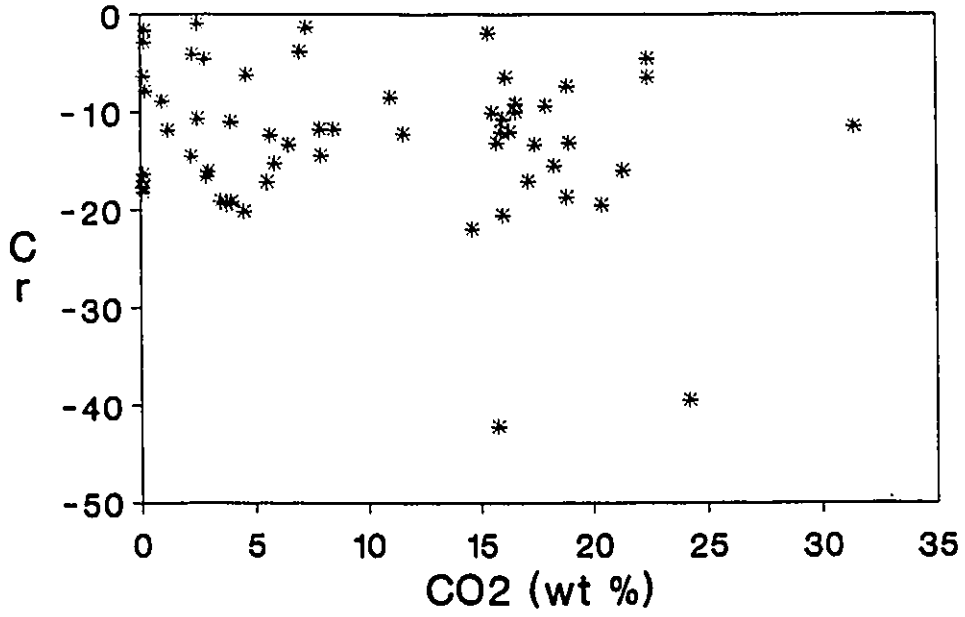
0
-10
-20
-30
-40
-50
Cr
0
5
10
15
20
25
30
35
CO2 (wt %)

CHAPTER 4

Au MINERALIZATION

4.1 Au mineralization in the Betts Big Pond area

4.11 Distribution

INCO Exploration and Technical Services Ltd (INCO) outlined a geochemical till anomaly, consisting of up to 35 ppm Au in heavy concentrates, centred on the ultramafic member of the Betts Cove Complex. The anomaly overlies talc-carbonate and extends from the northern part of the Betts Big Pond map area in the south to West Pond in the north (Figure 2.1). Subsequent exploration drilling by INCO revealed that talc-carbonate in the northern part of the Betts Big Pond map area contains "several hundered" ppb Au over 10-15 m thicknesses (Bell and Biescher, 1991).

Au analyses of outcrop samples during this study tested all ultramafic rock types in the Betts Big Pond area (Figures 4.1 and 4.2). Of the ten layered ultramafic rocks analyzed, nine had concentrations of Au below detection limit (1 ppb) and one contained 4 ppb Au (Figure 4.1). Twenty of 23 serpentinite samples yielded values below detection limit and one had a concentration of 10 ppb Au. The two samples in the 11-50 ppb range (Figure 4.1) contain 22 and 26 ppb Au, respectively. These samples are of magnetite rich serpentinite which occur

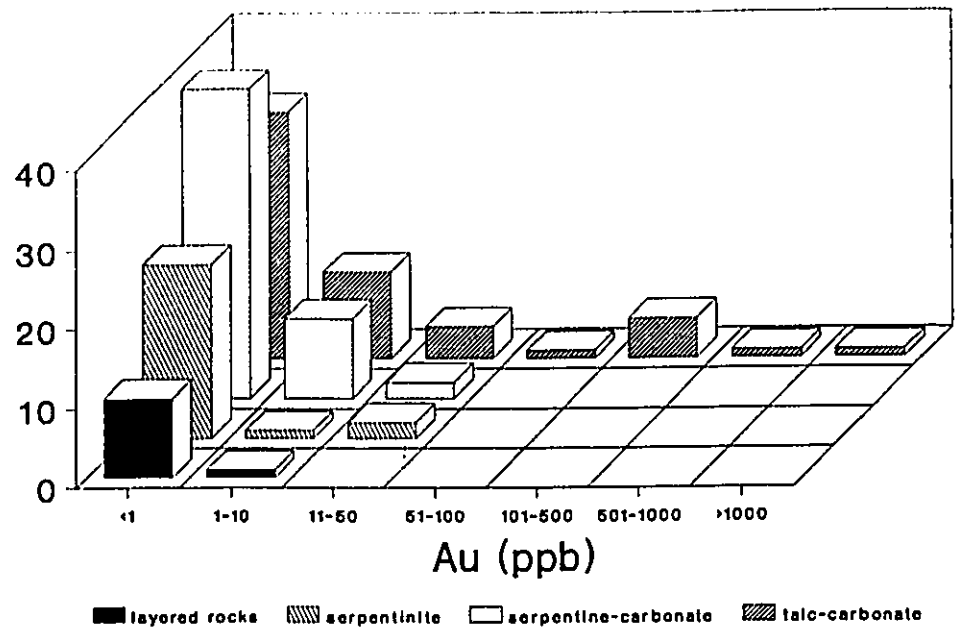

Figure 4.1. Distribution of Au by ultramafic rock type in the Betts Big Pond area.

adjacent to a chromite lens in the green serpentine-carbonate unit north of Betts Big Pond (Figure 4.2). Of the fifty one serpentine-carbonate samples thirty nine returned Au values less than detection limit. Those samples which had detectable Au abundances contained 7 ±5 ppb (average and standard deviation). Of the 53 talc-carbonate samples, 30 were below detection limit. The average of those samples that contain detectable Au is 150 ±302 ppb. The talc-carbonate samples containing > 100 ppb Au are located in a zone in the northern most part of the map area (Figure 4.2). This zone overlies the inclined drill holes of INCO Ltd. in which Au values of several hundred ppb were located.

Several quartz veins in fault zones in the southern part

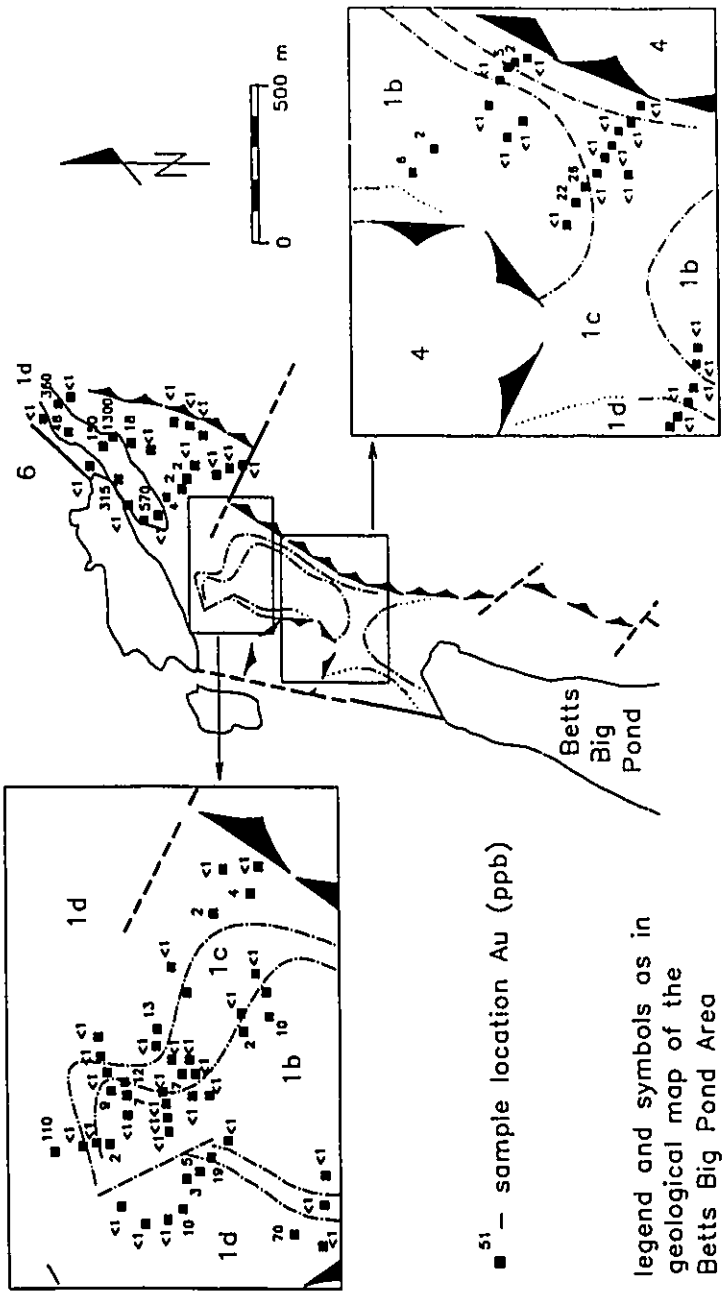

Figure 4.2. Map of the Betts Big Pond area indicating sample locations and Au values.

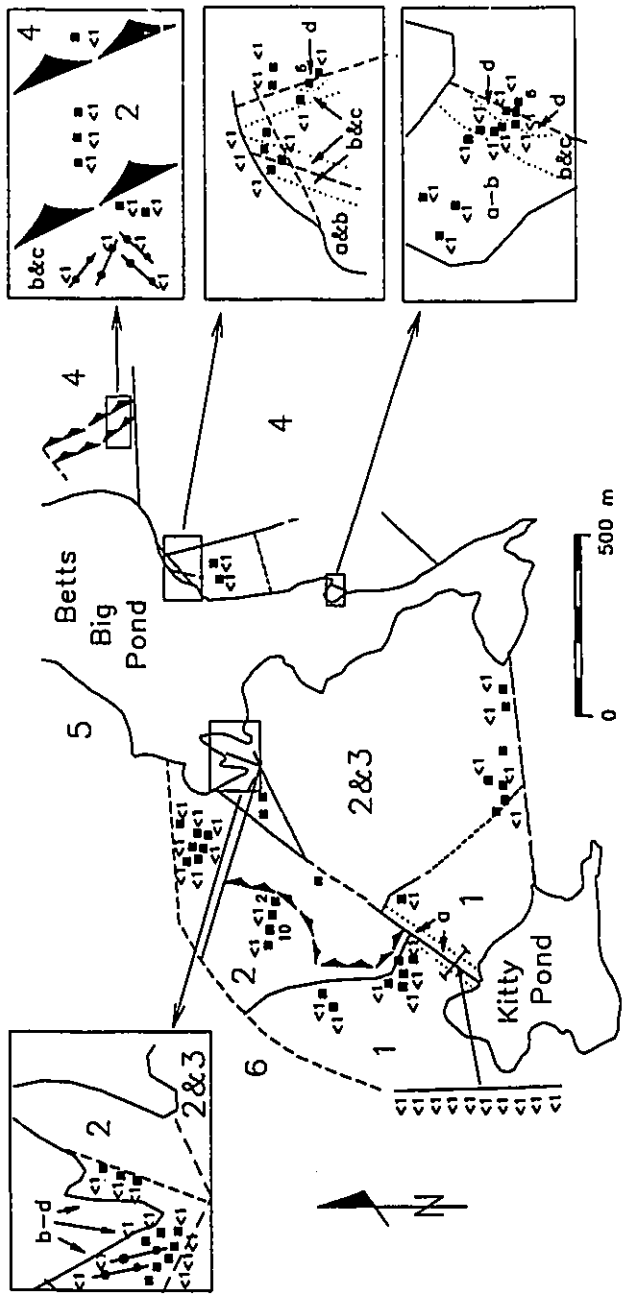
Betts
Big
Pond
Kitty
Pond
2&3
4
5
6
1
2
b&c
a&b
a–b
b–d
d
500 m
0
N

of the Betts Big Pond map area were analyzed for Au (Figure 4.2). All returned Au values less than detection limit.

4.12 Mineralogy

The Au-bearing talc-carbonate is virtually indistinguishable from talc-carbonate with undetected Au abundances (section 2.234). Exceptions include the occurrence of hematite, native gold, and possibly barite.

All of the Au-bearing samples contain specular hematite which is observed in either hand samples or in thin sections. This is in contrast to the talc-carbonate map unit in general in which hematite is not ubiquitous. Bell and Beischer (1991) recovered native gold from drill core in the Betts Big Pond area the majority of which are in the 10-75 μm range.

Heavy concentrates of Au bearing talc-carbonate samples were examined with the SEM. Barite grains (< 5 μm) were identified in two of the samples using the Energy Dispersion Spectrum. Due to its small grain size, the exact occurrence and distribution of barite remains unknown.

The magnetite-rich samples that contain 22 and 26 ppb Au consists of approximately 80 mole % magnetite and 20 mole % antigorite (Figure 3.5). The magnetite contains finely disseminated sulphides including pyrrhotite, chalcopyrite, pentlandite, pyrite, and bornite (Plate 3.12).

4.13 Geochemistry

The composition of Au bearing talc-carbonate is compared with unmineralized talc-carbonate in the isocon diagram (Grant, 1986) in figure 4.3. An isocon is a straight line connecting points of equal geochemical concentration (Gary et al., 1974 sited in Grant, 1986) and therefore is the solution to the equation:

$$C^A = (M^O/M^A)C^O \quad \text{(Grant, 1986)}$$

where C = concentration and M = mass and O and A denote original and altered rocks respectively. Taking Mg as immobile and the relation $M^O/M^A = C_{Mg}{}^A/C_{Mg}{}^O$ (Grant, 1986), the isocon is drawn from the origin through the point $C_{Mg}{}^A/C_{Mg}{}^O$. The slope of this line is very close to 1 as is expected due to the similar mineralogical compositions of the Au bearing and non-Au bearing talc-carbonate. The isocon diagram (Figure 4.3) illustrates that there is no chemical difference between Au bearing and non-Au bearing talc-carbonate.

The Au bearing magnetite rich serpentinites are compared to average serpentinite in the isocon diagram (Grant, 1986) in which the isocon is defined by the masses of equal volumes of magnetite rich serpentinite and average serpentinite (Figure 4.4). The masses of the average serpentinite and the two magnetite rich serpentinite samples were calculated using the specific gravities of magnetite and antigorite and the serpentine/magnetite ratios calculated in chapter 3. The

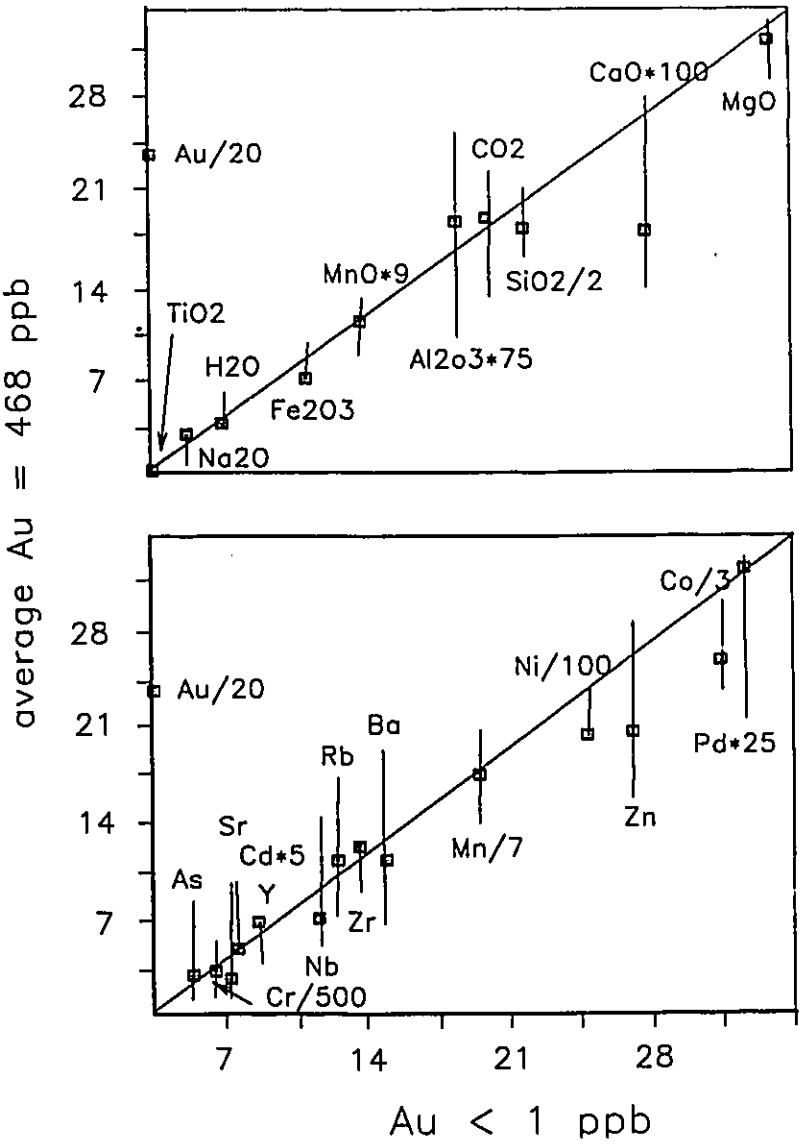

Figure 4.3. Isocon diagram comparing the composition of Au-bearing talc-carbonate (samples with Au > 100 ppb) with talc-carbonate samples containing Au < 1 ppb. Mass units. Vertical bars represent the range in talc-carbonate with Au < 1 ppb. Components that lie above the isocon have been added to the rock and those that lie below have been lost from the rock. Those components that lie on the isocon have been conserved.

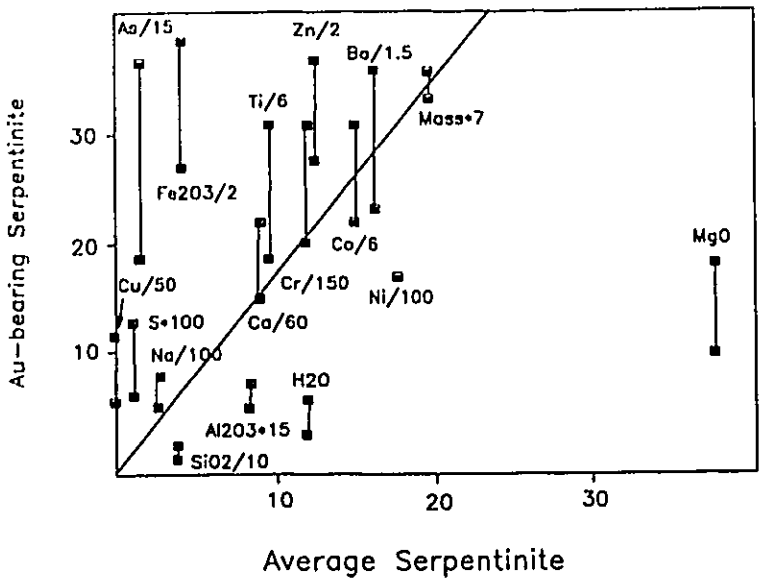

Figure 4.4. Isocon diagram comparing the composition of the two Au-bearing serpentinite samples with average serpentinite. Vertical line connects the two Au-bearing samples. Mass units. Components that lie above the isocon have been added to the rock and those that lie below have been lost from the rock. Those components that lie on the isocon have been conserved.

elements (SiO_2, Al_2O_3, H_2O, MgO, and Ni) below the isocon comprise serpentine and thus reflect the difference in the magnetite/serpentine ratios. Similarly, the higher Fe_2O_3 content reflects the higher proportion of magnetite.

Au, Cu, S, As, Zn are all enriched in the magnetite-rich serpentinite relative to average serpentinite (Figure 4.4). The enrichment of Cu, S, and in part Fe_2O_3 can be ascribed to the occurrence of Cu-Fe sulphides. The magnetite rich samples contain 54 and 71 ppm Zn. The average Zn content of serpentinite is 25 ppb. Magnetite contains ZnO ranging from

below detection limit to .3 wt % (Appendix II). Thus, the slight enrichment in Zn in the magnetite rich samples may be due to the high proportion of magnetite. The magnetite rich samples contain 276 and 528 ppm As and the average serpentinite contains 23 ppm As (Table 3.1 and Appendix II). The enrichment of As (by an order of magnitude) is greater than the difference in serpentine/magnetite among typical serpentinite and the magnetite rich rocks (Figure 3.5). For this reason, As is interpreted to have been added to the magnetite rich-serpentinites. Thus, the Au anomalies are most closely associated with anomalous concentrations of Cu, S, and As.

The remainder of the elements plotted in figure 4.4 occur as trace concentrations in serpentine and magnetite. Their distribution on or very close to the isocon indicates neither significant addition to or loss from the magnetite rich serpentinites. Similarly, those elements below detection limit in serpentinite are below detection limit in the magnetite rich serpentinite samples.

4.2 Talc-carbonate hosted Au-vein mineralization

4.21 Introduction

A number of Au vein occurrences in the northern part of the Betts Cove Complex (Figure 2.1) have been investigated by Al (1990) and Bell and Beischer (1991). They occur either

within the ultramafic member of the Betts Cove Complex or in rocks in direct fault contact with the ultramafic member. Also, magnetite rich serpentinite samples (with or without minor carbonate) from the northern Betts Cove Complex have returned Au values as high as 5400 ppb. These occur at Beaver Cove Pond (Lavigne, 1988) and at Red Cliff Pond (Al, 1988) (Figure 2.1).

Au veins hosted by talc-carbonate occur approximately 2 and 3 km north of the Betts Big Pond map area at the West Pond Ridge and Arrowhead Pond Showings (Figure 2.1). These showings were investigated in detail by Al (1990) who illustrated that little geological or geochemical difference exists between the showings. For purposes of comparison with the Betts Big Pond area, 16 samples were collected from the Arrowhead Pond Showing for chemical analyses. These include one vein sample, ten samples from the alteration halo enclosing the veins, and five samples of talc-carbonate.

4.22 Geology

The faults that bound the ultramafic member of the Betts Cove Complex and comprise the BCC-CSJG fault zone in the Betts Big Pond area extend northwards and bound talc-carbonate at Arrowhead Pond (Figures 2.1 and 2.3). The talc-carbonate at Arrowhead Pond is texturally and mineralogically similar to that in the Betts Big Pond area. The only exception is the occurrence of erratically distributed patches of talc-

carbonate+quartz, ranging in size from < 1 m x <1 m to < 10 m x < 10 m. Quartz bearing talc-carbonate is recognized in the field by a distinctive weathering surface in which quartz stands out in high relief.

Gold mineralization occurs as two parallel and undeformed veins. They have a maximum strike length of 5 m and maximum width of .4 m (Al, 1990). They are enclosed in halos of talc-carbonate-quartz.

4.23 Petrography and mineralogy

The auriferous veins have a massive to banded texture in which the bands are parallel to the vein walls (Al 1990). The alternating bands are quartz-rich and magnesite-rich. Talc occurs disseminated in the magnesite rich bands. Minor metallic minerals are chalcocite, bornite, pyrite, chalcopyrite, and magnetite. Chalcocite is replaced by bornite and bornite by magnetite (Al 1990). Au occurs as native gold associated with chalcocite and bornite and in quartz adjacent to chalcocite (Al, 1990).

Quartz occurs interstitial to magnesite in the alteration halo. Otherwise, the haloes are mineralogically similar to the regional talc-carbonate unit.

4.24 Geochemistry

Elements that are near or below detection limits in talc-carbonate of the Betts Big Pond area are similarly depleted in talc-carbonate in the Arrowhead Pond area (Table 4.1). Those elements which exhibit defineable trends in talc-carbonate have similar trends in talc-carbonate in the Arrowhead Pond area talc-carbonate (Figure 4.5).

The alteration halo is clearly distinguished from talc-carbonate by the presence of normative quartz (Figure 4.6a). The alteration halo is also distinguished from typical talc-carbonate by lower normative talc and slightly higher normative magnesite (Figures 4.6b and 4.6c) reflecting dilution by quartz. The normative magnetite abundance (Figure 4.6d) is similar between the alteration halo and talc-carbonate which are similar to the distribution of molar magnetite in the Betts Big Pond area talc-carbonate (Figure 3.5). Serpentine was not present in the normative calculations.

The CO_2 contents of the samples from the alteration halo at Arrowhead Pond are variable, ranging from approximately 18 wt % to 37 wt % (Figure 4.5). However, the CO_2 content in the alteration halo is similar to the range of CO_2 contents in talc-carbonate at Arrowhead Pond and at Betts Big Pond (Figure 4.5). The average H_2O content of the alteration halo is lower than talc-carbonate but is within the range of H_2O contents of talc-carbonate from the Betts Big Pond area. The high Cu

Table 4.1. Chemical compositions of peridotite and talc-carbonate from the Betts Big Pond area and talc-carbonate, alteration haloe, and Au-vein from the Arrowhead Pond area

	Method	unit	DL	1	2	3	4	5
SiO2	XRF	%	0.01	40.19	34.05	36.18	26.44	62.40
Al2O3	XRF	%	0.01	0.77	0.24	0.62	0.80	0.84
TiO2	XRF	%	0.01	0.01	0.02	0.02	0.03	0.01
MgO	XRF	%	0.01	37.10	35.42	34.38	32.45	15.70
CaO	XRF	%	0.01	0.78	0.19	0.56	0.20	0.65
Na2O	XRF	%	0.01	0.03	0.02	0.02	0.03	<.01
K2O	XRF	%	0.01	0.01	0.01	<.01	<.01	<.01
Fe2O3	XRF	%	0.01	9.11	6.97	7.09	7.43	2.84
MnO	XRF	%	0.01	0.13	0.13	0.07	0.08	0.14
P2O5	XRF	%	0.01	<.01	0.01	0.01	0.01	0.01
CO2	wet	%	0.01	<.01	18.42	17.40	31.24	16.68
H2OP	wet	%	0.01	10.65	2.93	2.65	1.19	0.50
S	XRF	%	0.01	0.01	<0.01	<0.01	<0.01	<0.01
Total		%		98.71	98.40	98.99	99.88	99.77
Co	DCP	ppm	1	98	77	88	80	30
Ni	DCP	ppm	1	1400	2000	2000	1900	630
Cu	DCP	ppm	.5	2	<.5	80	5	450
Zn	DCP	ppm	.5	30	22	31	32	12
Mo	DCP	ppm	1	<1	<1	<1	<1	<1
Cd	DCP	ppm	1	<1	<1	<1	<1	<1
Pb	DCP	ppm	2	3	2	3	3	<2
Y	XRF	ppm	2	5	4	5	<2	<2
Zr	XRF	ppm	3	8	13	21	22	19
Nb	XRF	ppm	10	<10	<10	12	<10	11
Ba	XRF	ppm	10	15	11	39	17	107
Cr	DCP	ppm	2	2500	1600	1700	1400	500
Sr	XRF	ppm	2	<2	3	11	10	11
Rb	XRF	ppm	2	4	9	5	7	5
As	XRF	ppm	3	<3	14	9	9	<3
Tl	DCP	ppm	2	<2	<2	<2	<2	<2
Ag	DCP	ppm	.5	<.5	<.5	<.5	<.5	7
Pt	FADCP	ppb	10	<10	<10	<10	<10	<10
Pd	FADCP	ppb	2	3	2	3	4	<2
Se	GFAA	ppm	.1	<.1	<.1	<.1	<.1	<.1

1- Layered peridotite (column 1, table 3.10, 2- Talc-carbonate (column 5, table 3.1), 3- Average talc-carbonate, Arrowhead Pond (n=5), 4- Average of alteration haloe samples, Arrowhead Pond (n=10), 5- Au-vein Arrowhead Pond (n=1).
Significant figures for Ni and Cr = 2. DL = detection limit.

4.5a

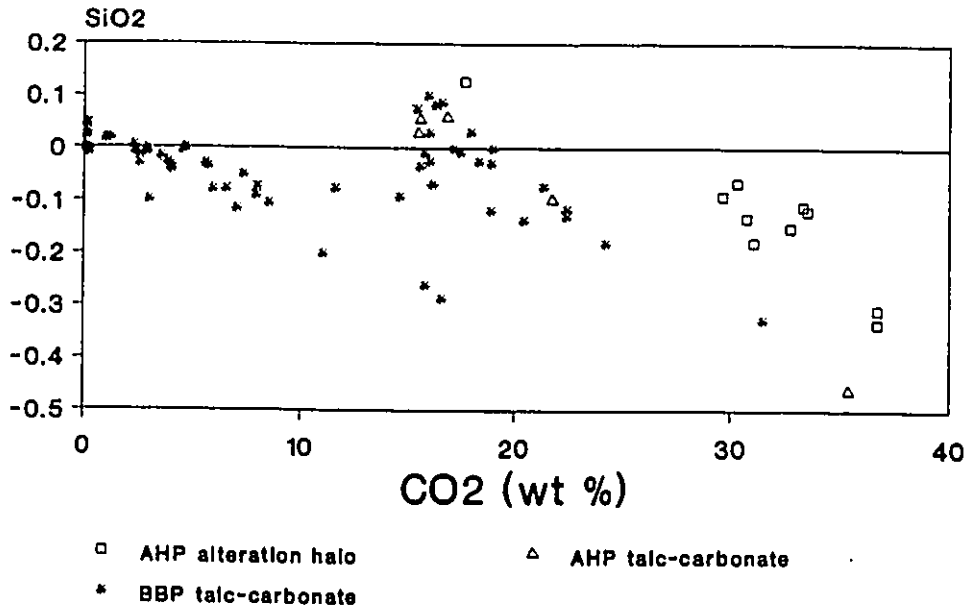

Figure 4.5. Plots of the change in concentration (solution to equation derived from Grant, 1986) vs. whole rock CO_2 content (as in figure 3.7). Layered ultramafic rocks from the Betts Big Pond are the least altered equivalents used in the comparison here. Results of calculations from the Betts Big Pond area are shown for comparison.

4.5b

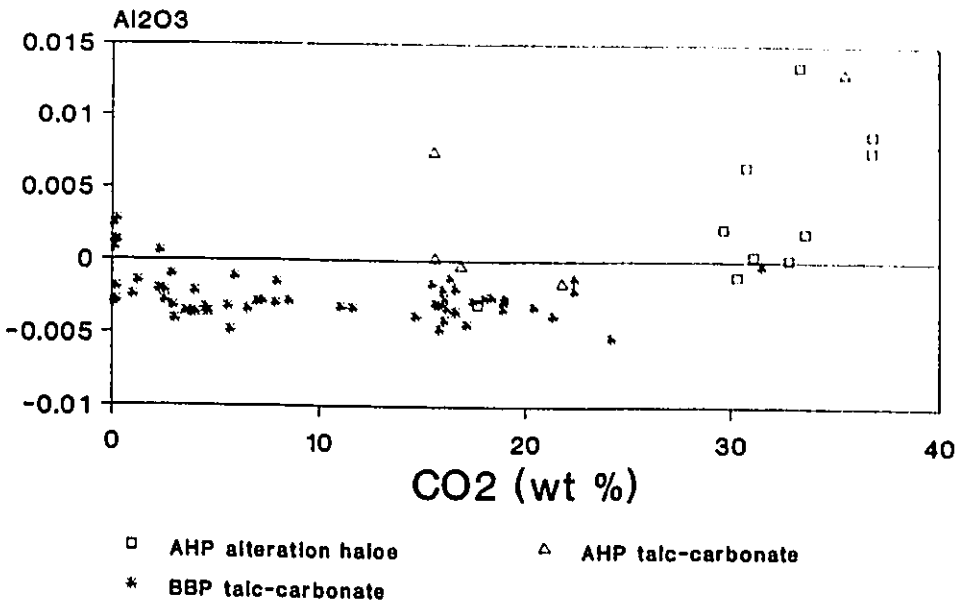
Al2O3
0.015
0.01
0.005
0
-0.005
-0.01
0
10
20
30
40
CO2 (wt %)
AHP alteration halos
AHP talc-carbonate
BBP talc-carbonate

4.5c

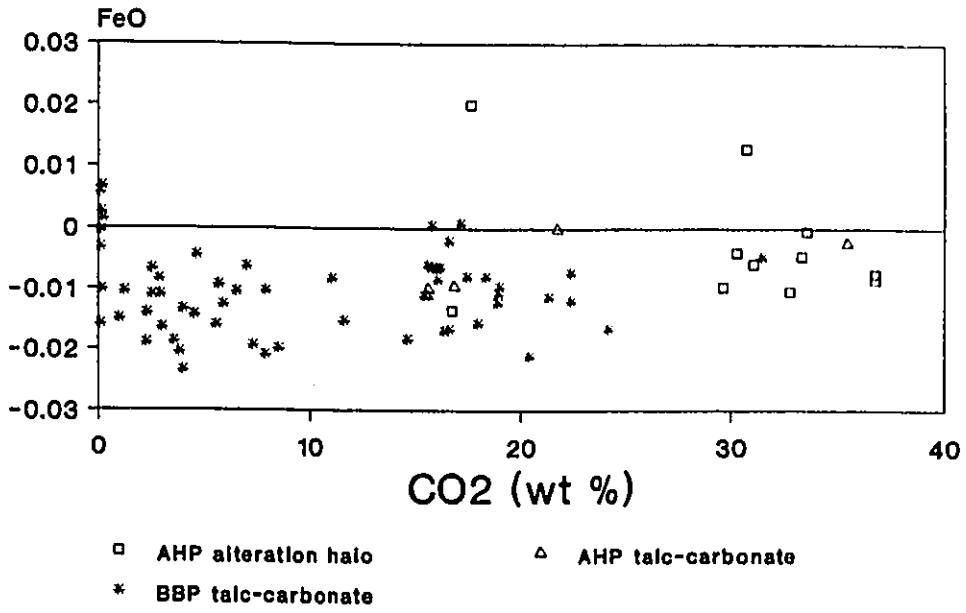
FeO
0.03
0.02
0.01
0
-0.01
-0.02
-0.03
0
10
20
30
40
CO2 (wt %)
AHP alteration halo
AHP talc-carbonate
BBP talc-carbonate

4.5d

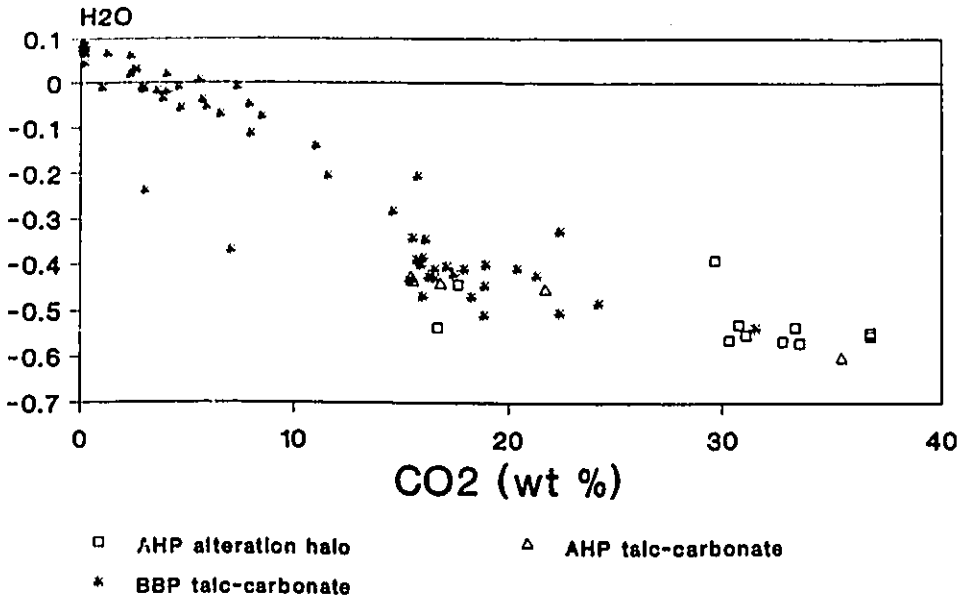
H2O
0.1
0
-0.1
-0.2
-0.3
-0.4
-0.5
-0.6
-0.7
0
10
20
30
40
CO2 (wt %)
AHP alteration halo
AHP talc-carbonate
BBP talc-carbonate

4.5e

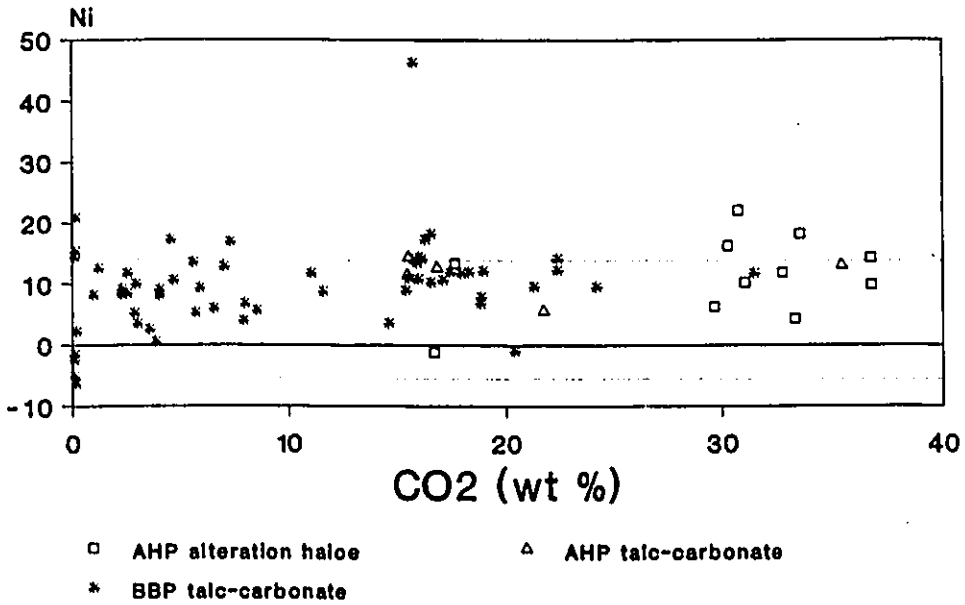
Ni
50
40
30
20
10
0
-10
0
10
20
30
40
CO2 (wt %)
AHP alteration haloe
AHP talc-carbonate
BBP talc-carbonate

4.5f

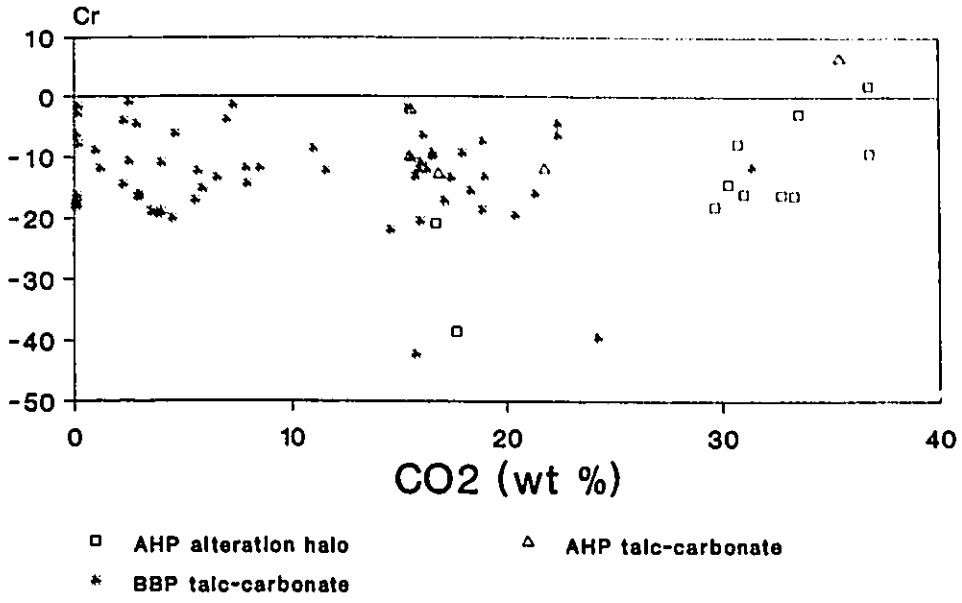
Cr
10
0
-10
-20
-30
-40
-50
0
10
20
30
40
CO2 (wt %)
AHP alteration halo
AHP talc-carbonate
BBP talc-carbonate

4.5g

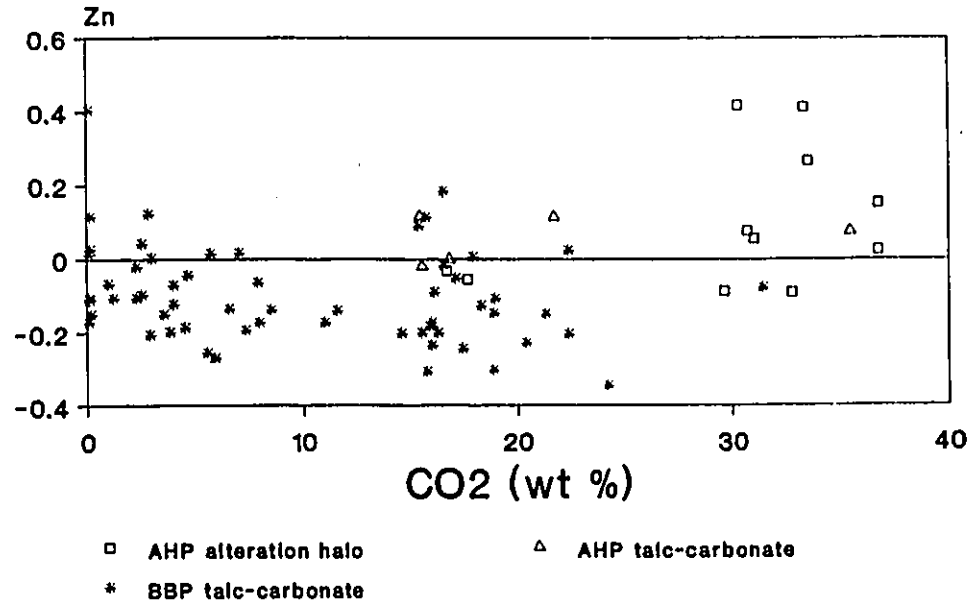
Zn
0.6
0.4
0.2
0
-0.2
-0.4
0
10
20
30
40
CO2 (wt %)
AHP alteration halo
AHP talc-carbonate
BBP talc-carbonate

4.6a

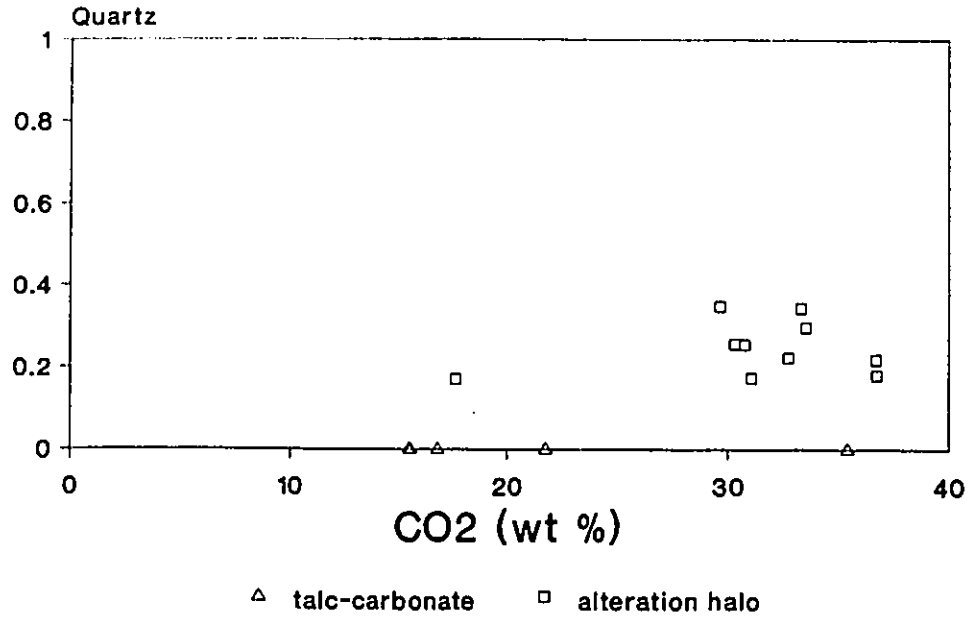

4.6b

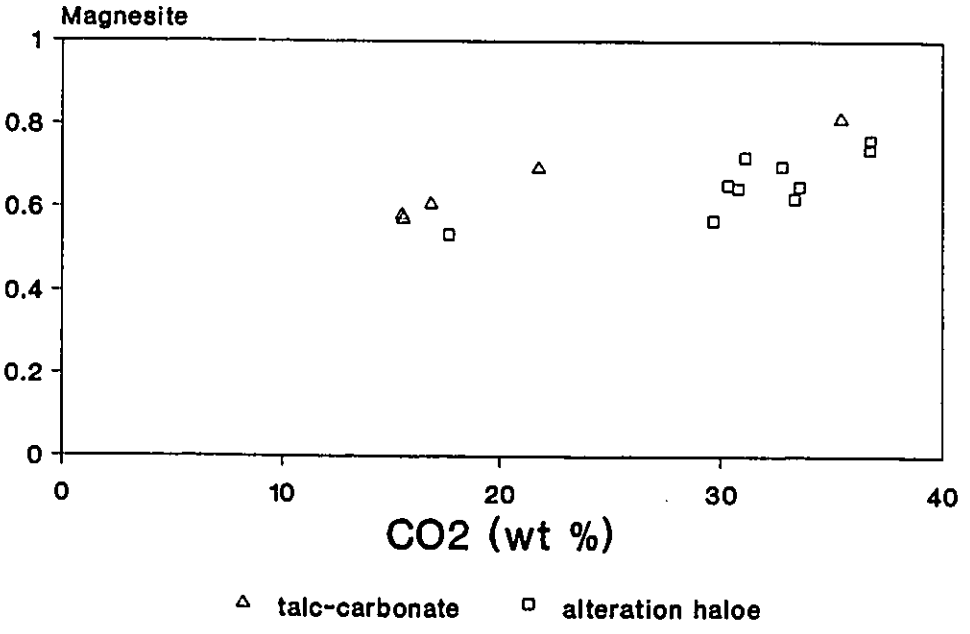

Figure 4.6. Plots of normative minerals vs. CO_2 from talc-carbonate and the alteration halo at the Arrowhead Pond showing

4.6c

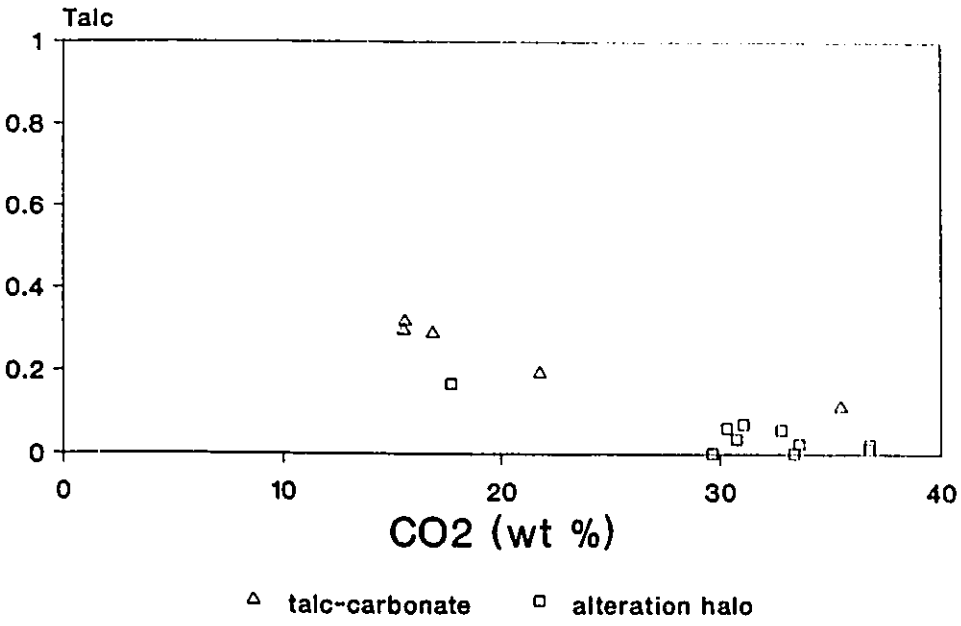
Talc
1
0.8
0.6
0.4
0.2
0
0
10
20
30
40
CO2 (wt %)
talc-carbonate
alteration halo

4.6d

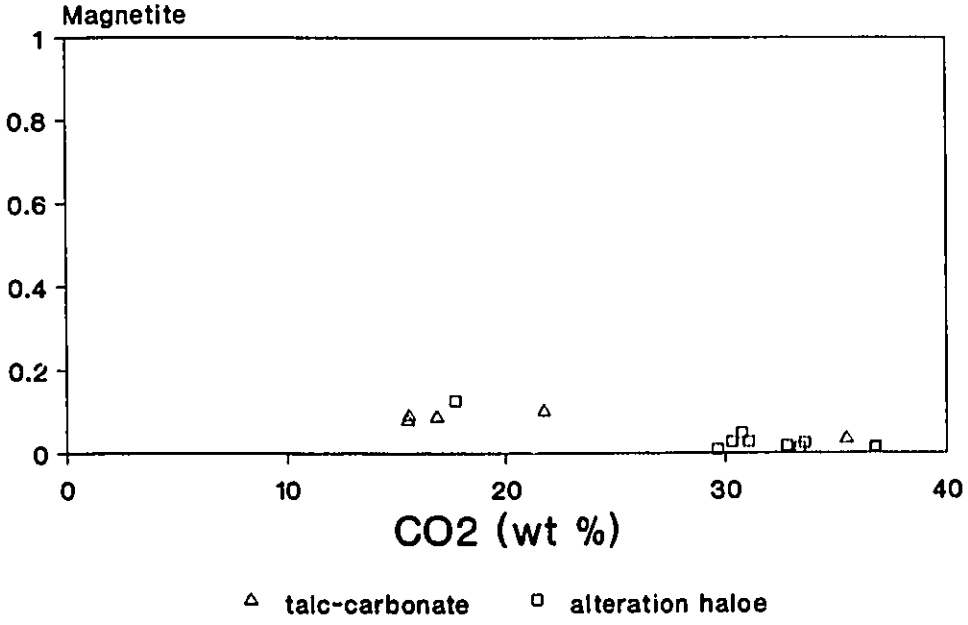
Magnetite
1
0.8
0.6
0.4
0.2
0
0
10
20
30
40
CO2 (wt %)
talc-carbonate
alteration haloe

content in talc-carbonate at Arrowhead Pond (relative to talc-carbonate at Betts Big Pond and the alteration halo at Arrowhead Pond) reflects one particularly anomalous sample (Appendix III). SiO_2 in the alteration halo at Arrowhead Pond is high relative to talc-carbonate at Arrowhead Pond and at Betts Big Pond (Figure 4.5a). Sporadic enrichments of Al_2O_3 (Figure 4.5b) may be due to the occurrence of minor amounts of chlorite reported by Al (1990). Fe_2O_3 in the alteration halo is largely similar to that in talc-carbonate with the exception of two samples which are slightly enriched (figure 4.5c). The decrease in H_2O with increasing CO_2 wt % is similar between talc-carbonate and the alteration halo (Figure 4.5d). Ni (Figure 4.5e) and Cr (Figure 4.5f) concentrations are similar between talc-carbonate and the alteration halo. Zn (Figure 4.5g) is similar in the talc-carbonate and alteration halo but shows an enrichment trend in the alteration halo. In summary, with the exception of SiO_2 enrichment, the alteration halo at Arrowhead Pond is chemically comparable to talc-carbonate at Arrowhead Pond and at Betts Big Pond.

Quantitative comparison between the concentration of elements in the vein and alteration halo at Arrowhead Pond is not possible because the conservation of Mg cannot be demonstrated and therefore not used to monitor mass changes. However, the chemical compositions of the vein and alteration halo are similar in as much as the major rock forming elements of the alteration halo are also major elements in the vein and

those elements with low concentrations in the alteration halo have similar low concentrations in the vein (Table 4.1). The composition of breunnerite from the Arrowhead Pond vein, the alteration halo, and Betts Big Pond talc-carbonate are similar (Table 4.2).

Al (1990) reported Au contents that range from > 10 ppm to 70 ppb from the Arrowhead Pond veins and indicated that the highest Au values were obtained from Cu-sulphide bearing samples. The vein sample in this study returned 360 ppb Au and 450 ppm Cu, supporting the Au-Cu association in the Arrowhead Pond veins. Au analyses of the alteration halo range from 8900 ppb to 1 ppb. All of the samples from the alteration halo returned Cu abundances less than detection limit with the exception of 42 ppm in one sample which contains 57 ppb Au.

Table 4.2. Average compositions of breunnerite from Arrowhead Pond and Betts Big Pond

	1	2	NT-228	NT-027	NT224
CaO	0.11	0.21	0.35	0.10	0.28
MgO	40.73	40.63	44.23	44.06	43.16
MnO	.05	.09	.08	.14	.26
FeO	6.68	6.79	5.33	5.38	6.69

1 - Average alteration halo (Al, 1990); 2 - Average vein (Al, 1990). Differences in analytical method and calculation of oxides used by Al (1990) and in this study preclude detailed comparison.

4.3 Fluid Inclusions

4.31 Introduction

Fluid inclusion studies were undertaken to determine the composition of vein forming fluids and to provide an independent estimate of the temperature and pressure of vein formation. Four veins from three locations in the ultramafic member of the Betts Cove Complex were examined: two from the Arrowhead Pond Showing, the Long Pond Showing, and a vein from the serpentine-carbonate shear zone in the southern part of the Betts Big Pond map area between Betts Big Pond and Kitty Pond (Figure 2.3).

Fluid inclusions are classified on the basis of their origin and composition following Roedder (1984). The composition of the fluid inclusions were qualitatively determined through observation of phases at room temperature and phase changes during heating and freezing. Quantitative fluid compositions were calculated using the computer program FLINCOR (Brown, 1989). The equipment used and procedures followed are described in Appendix III.

4.32 Fluid inclusion compositions

Three compositional types of fluid inclusions are recognized in the veins from the ultramafic member of the Betts

Cove Complex: 1) H_2O-NaCl inclusions, 2) H_2O-CO_2±NaCl±CH_4, and 3) CO_2±H_2O inclusions.

1) H_2O-NaCl inclusions. H_2O-NaCl inclusions consist of liquid and a centrally located vapour bubble at room temperature. Solid phases were not recognized and thus the inclusions, at room temperature, are indistinguishable from pure H_2O fluid inclusions.

The presence of NaCl was determined by reheating the inclusions to determine the melting temperature of ice. Melting below 0°C indicates the presence of salt.

2) H_2O-CO_2±NaCl±CH_4 inclusions. H_2O-CO_2 inclusions occur as either two phase inclusions, consisting of a liquid phase and a vapour bubble or as three phase inclusions consisting of H_2O liquid, CO_2 liquid, and a vapour bubble consisting of CO_2.

At room temperature the two phase inclusions are indistinguishable from H_2O-NaCl inclusions. They are identified by the occurrence of clathrate ($CO_2 \cdot 5.75H_2O$) at > 0 °C (Roedder, 1984). The freezing of CO_2 was observed by the darkening of the inclusion and further crumpling of the vapour bubble at temperatures ≈ - 90 °C. Upon reheating, the CO_2 phase melted at temperatures below -56.6 °C. Also, CO_2(L) and CO_2(V) homogenized, by the liquid expanding to consume the vapour, at temperatures between 28.7 °C and 31 °C. The phase changes described for the two phase H_2O-CO_2 inclusions are also recognized in the three phase inclusions with the exception of CO_2 homogenization. The presence of CH_4 was determined in the

H_2O-CO_2±NaCl inclusions by the depression of the CO_2 melting temperature below that for pure CO_2 (-56.6 °C). In description that follows, these inclusions will be referred to more simply as H_2O-CO_2-NaCl inclusions.

3) CO_2±H_2O inclusions. CO_2 rich inclusions occur among a group of comparatively dark equant to highly irregularly shaped inclusions. CO_2 bearing inclusions are distinguished by the recognition of a phase change upon freezing below -90 °C and the presence of CO_2 solid at temperatures < -56.6 °C. In some cases, a small amount of H_2O is identified in these inclusions, usually at the junction of inclusion walls at temperatures > 31 °C.

4.33 Description of fluid inclusion sections

4.331 Arrowhead Pond Showing

Six sections from the two veins from the Arrowhead Pond Showing were examined. The sections consist of massive to banded quartz and magnesite. Quartz in the sections ranges from relatively clear, unstrained bands to comparatively fractured quartz with optically discontinuous quartz occurring along and forming grain boundaries.

All three compositional types of fluid inclusions are recognized in the Arrowhead Pond sections. In order of increasing abundance they are 1) H_2O-NaCl inclusions, 2) H_2O-

$CO_2 \pm NaCl \pm CH_4$ inclusions, and 3) $CO_2 \pm H_2O$ inclusions.

H_2O-NaCl inclusions occur as primary inclusions throughout the sections. They are variable in size and shape. The largest recognized is 32 μm long and they are typically < 20 μm. They range from oval shapes to highly irregular "wormlike" shapes (Plates 4.1 and 4.2). H_2O-NaCl inclusions commonly occur as secondary planes of inclusions of equal phase ratios. (Plate 4.3). The planar arrays emanate from grain boundaries and transgress grain boundaries. In some cases they terminate in a quartz grain. The secondary H_2O-NaCl inclusions are generally smaller than their primary counterparts.

H_2O-CO_2-NaCl (i.e. H_2O-$CO_2 \pm NaCl \pm CH_4$) inclusions are identified as primary inclusions dominantly in the earlier quartz and less commonly in the later, less strained quartz. They contain three phases at room temperature; $H_2O(L)$, $CO_2(L)$, and $CO_2(V)$. They are somewhat larger than the H_2O-NaCl inclusions, the largest was 42 μm. The CO_2/H_2O ratio is variable among these inclusions which is attributed to leakage after trapping as they are commonly characterized by trails of small inclusions emanating from highly angular apices. However, where H_2O-CO_2-NaCl inclusions occur as isolated primary inclusions (Plate 4.4) or inclusion clusters they have a consistent H_2O/CO_2 ratio of approximately 5/1. H_2O-CO_2-NaCl inclusions are not recognized in any other textural site. However, secondary trails of inclusions in some cases contain inclusions that have highly variable compositions ranging from CO_2 rich to H_2O-rich

Plate 4.1. Photomicrograph of H_2O-NaCl primary inclusions in Arrowhead Pond vein quartz. Width of the photo is 225 μm. Taken at room temperature.

Plate 4.2. Photomicrograph of H_2O-NaCl primary inclusions in Arrowhead Pond vein quartz. Field of view is the same as in plate 4.1 and indicates that the inclusions form a three dimensional array. Width of the photo is 225 μm. Room temperature.

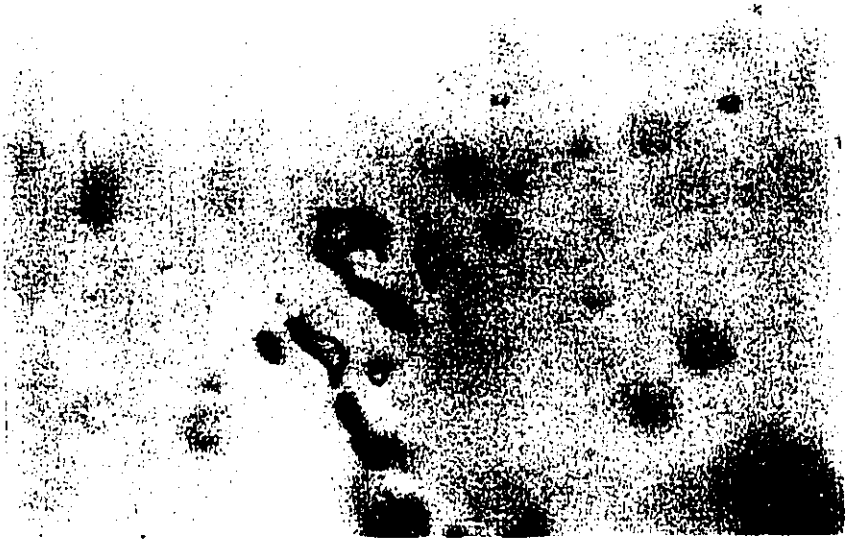

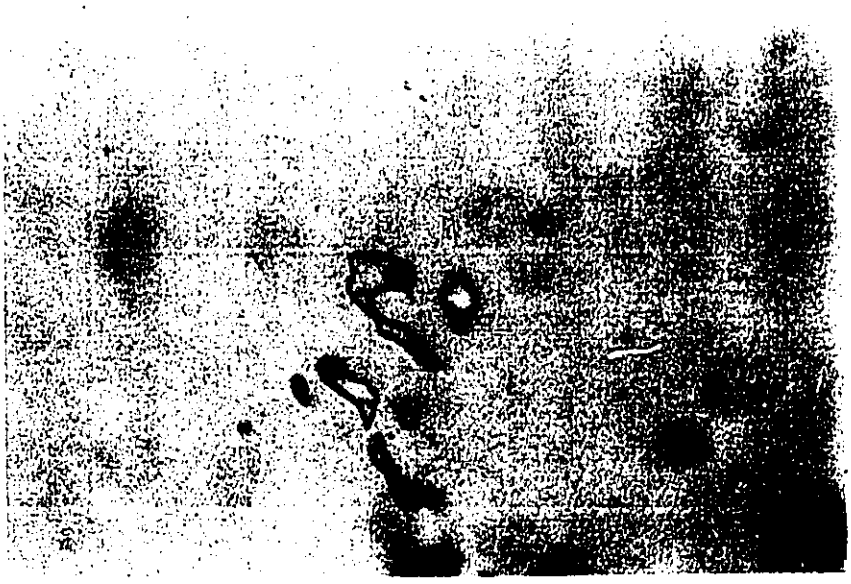

Plate 4.3. Photomicrograph of planar array of secondary H_2O-NaCl inclusions in Arrowhead Pond vein quartz. Note the similar phase ratios among the inclusions and with the primary inclusions in plates 4.1 and 4.2. Width of the photo is 225 μm. Taken at room temperature.

Plate 4.4. Photomicrograph of primary three phase H_2O-CO_2-NaCl inclusion in Arrowhead Pond vein quartz. Smaller, adjacent inclusions (out of focus) have similar phase ratios. Width of the photo is 225 μm. Taken at room temperature.

Plate 4.5. Photomicrograph of large primary H_2O-CO_2-NaCl inclusion in Long Pond vein quartz. Width of the photo is 225 μm. Taken at room temperature.

Plate 4.6. Photomicrograph of primary H_2O-CO_2-NaCl inclusion in Long Pond vein quartz. Width of the photo is 225 μm. Taken at room temperature.

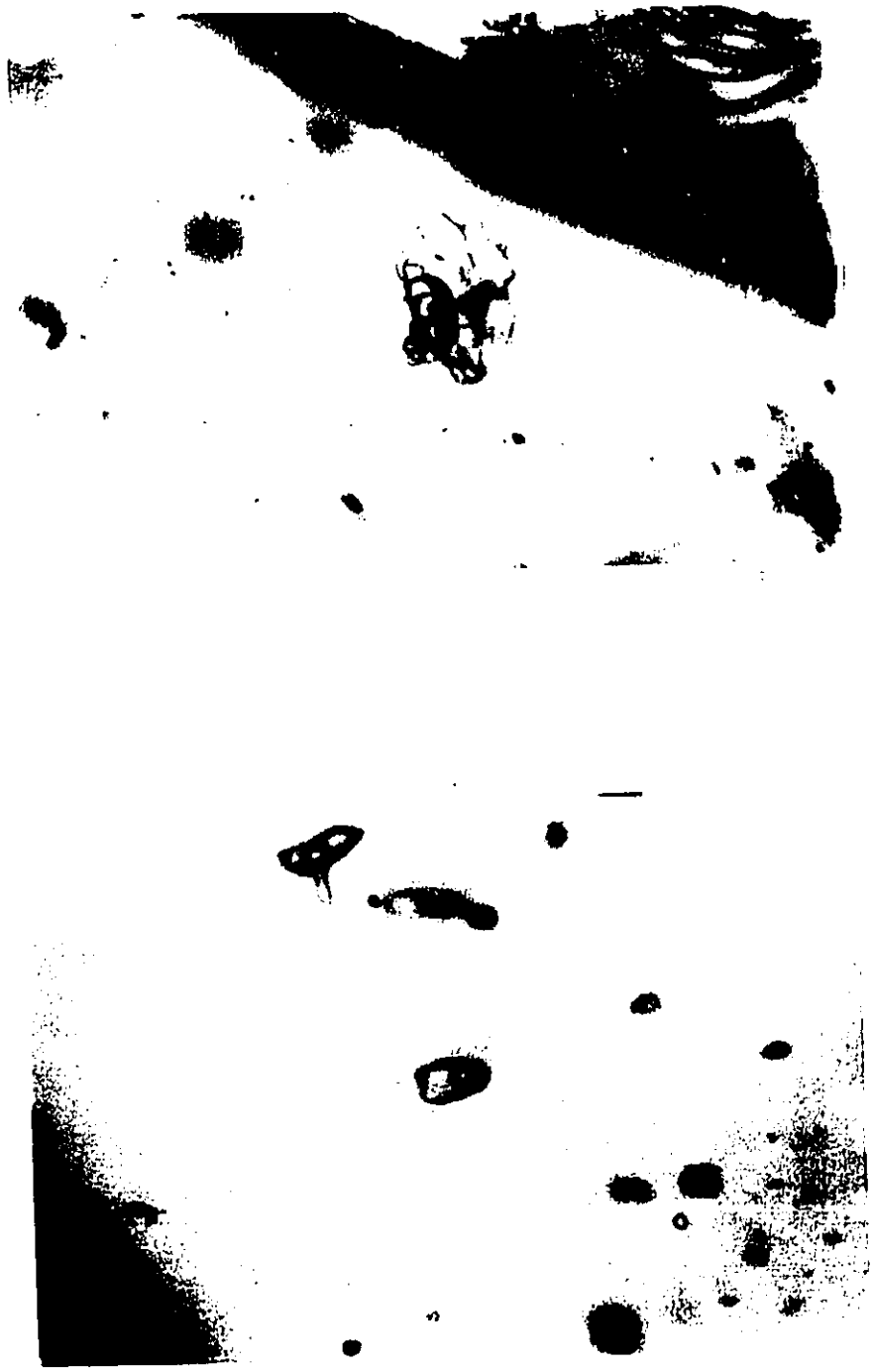

in adjacent inclusions may have originated through separation after trapping of H_2O-CO_2-NaCl fluids.

$CO_2 \pm H_2O$ inclusions occur dominantly as small (< 5 μm) oval shaped inclusions, a number of which form secondary trails and planes. In some cases the secondary trails of CO_2 inclusions cross quartz grain boundaries and in other cases are terminated at grain boundaries. The inclusions are recognized by freezing CO_2 at <-90 °C. The small size of the inclusions precludes detailed study, however, the presence of a small amount of H_2O is identified in a number inclusions.

4.332 Long Pond Vein

Samples of the Long Pond vein consist of clear and unstrained coarsely crystalline quartz crystals < 1.25 cm long that commonly terminate in vugs. Three sections from the Long Pond vein were examined.

Three phase inclusions consisting of $H_2O(L)$, $CO_2(L)$, and $CO_2(V)$ occur as primary inclusions in Long Pond vein quartz. The CO_2 contained in the inclusions estimated at room temperature ranges from .1 to .4 vol. % with the average of the estimates being .20. They range in size from 45 μm to < 1 μm and are typically 5 to 15 μm. The larger inclusions (> 30 μm) have an irregular angular shape due to crystal faces (Plate 4.5). The smaller primary inclusions, those of typical size, have more round to ellipsoid flat shapes (Plate 4.6). Rarely,

CO_2 rich inclusions occur as faceted, isolated (primary ?) inclusions. The Long Pond sections are characterized by fractures in quartz and grain boundaries that are occupied by trails of secondary inclusions. The trails possess inclusions with highly variable phase ratios that include H_2O inclusions, CO_2 rich inclusions, and single phase (empty ?) inclusions. The secondary inclusions are typically small (< 5 μm).

4.333 Betts Big Pond veins

Five doubly polished sections as well as three standard thin sections were made from veins that occur in serpentine-carbonate in the north-northeast trending fault zone between Betts Big Pond and Kitty Pond (Figure 2.3). It was not possible to identify the origin and composition of the fluid inclusions.

Veins in the fault zone consist dominantly of quartz. Rarely, magnesite is recognized in the veins. The quartz is strongly fractured, shows undulatory extinction and recrystallization. In addition, multiple veining events are distinguished by microveinlets of quartz cross cutting earlier, deformed quartz.

The "primary"-looking inclusions are rare, have a very irregular shape, and are characterized by the occurrence of smaller adjacent inclusion; thus the criteria for primary inclusions (Roedder, 1984) could not be satisfied. As a result, it is not possible to retrieve quantitative data from the fluid

inclusions. A number of attempts were made to determine melting temperatures to determine 1) the composition of the vapour phase and 2) if the inclusions contained a salt. However, the small size of the inclusions preclude confidant results. The only information of certainty is that the vein fluid was a H_2O-CO_2 mixture.

4.34 Microthermometry

Inclusions suitable for microthermometric determinations were identified in three of the Arrowhead Pond sections including both banded and massive vein material and in two of the three Long Pond sections.

The H_2O-CO_2-NaCl inclusions from the Arrowhead Pond and Long Pond veins are similar. The average homogenization temperatures are 261±7 °C and 248±9 °C for the Arrowhead Pond and Long Pond veins, respectively (Figure 4.7). The average CO_2 homogenization temperatures for the Long Pond vein of 30.5±.3 °C is similar to the 29.9±.7 °C average for the Arrowhead Pond vein which is somewhat more variable (Figure 4.8). Clathrate melting temperatures are 8.9±.7 °C and 8.4±.5 °C for the Arrowhead Pond and Long Pond veins respectively (Figure 4.9) and the CO_2 melting temperatures are -57.1±.2 °C and 57.3±.6 °C for the Arrowhead Pond and Long Pond veins respectively (Figure 4.10).

4.7a

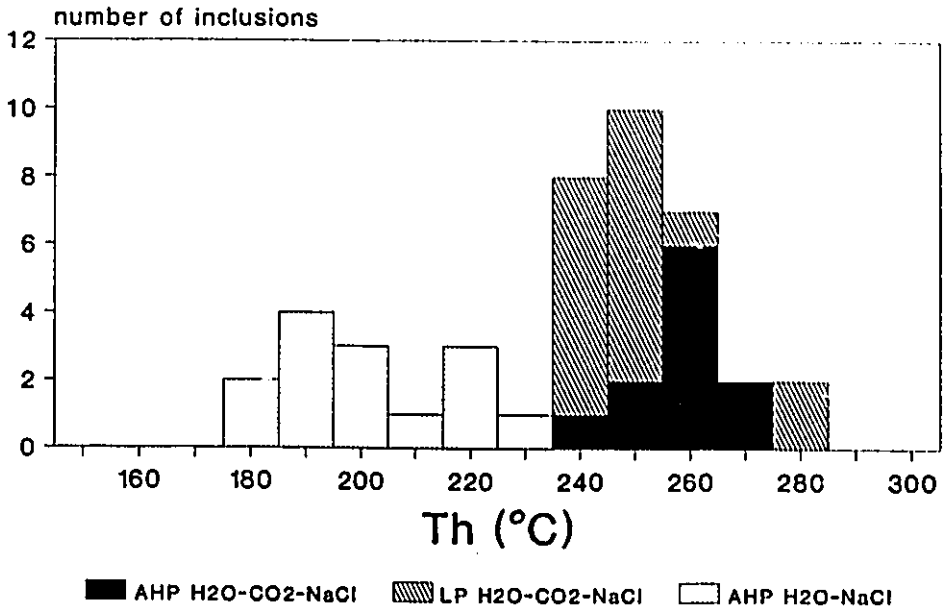

4.7b

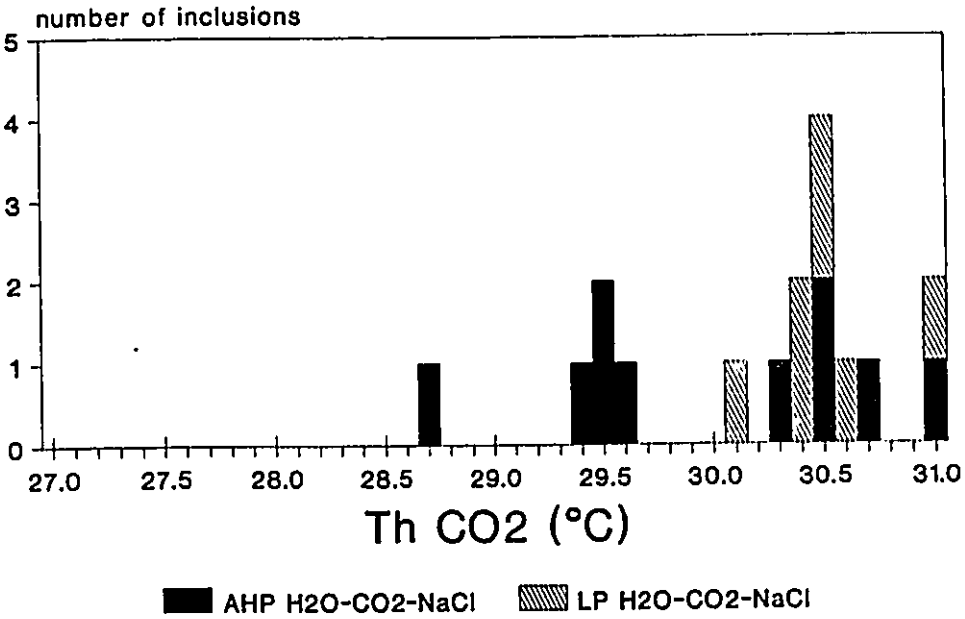

Figure 4.7. Fluid inclusion homogenization temperatures (Th). a) Total homogenization. b) CO_2 homogenization

4.8a

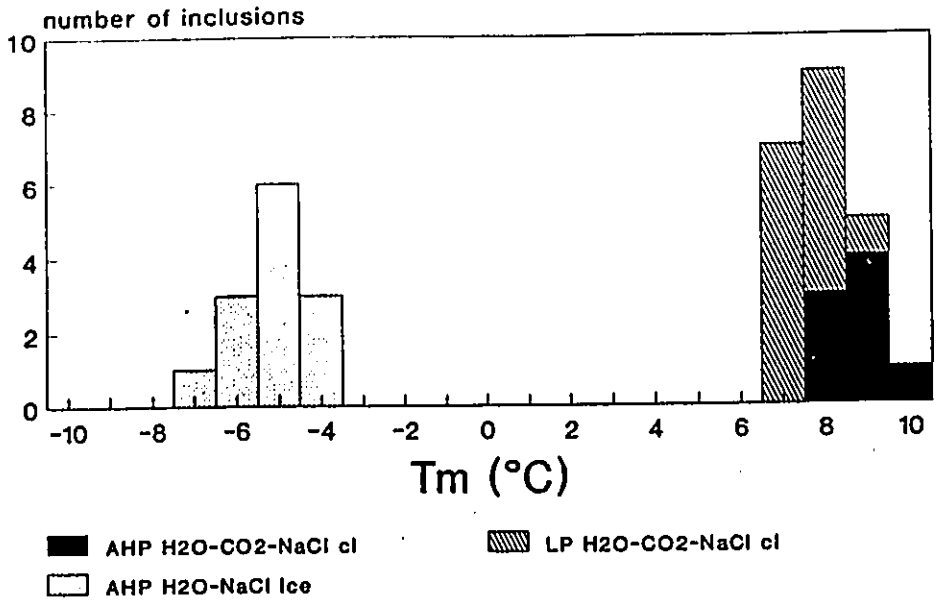

4.8b

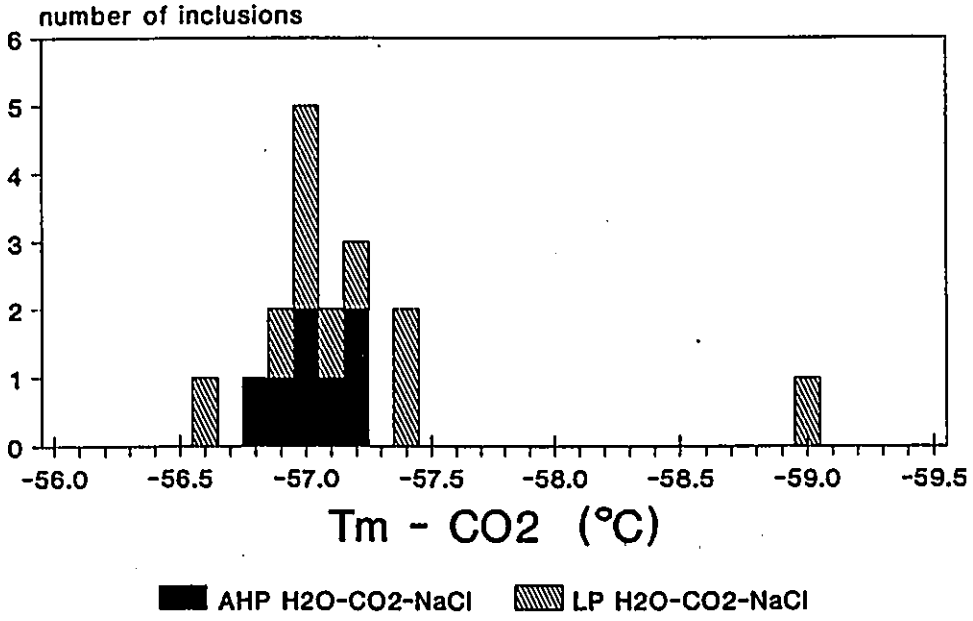

Figure 4.8. Fluid inclusion melting temperatures (Tm). a) Ice and clathrate melting temperatures. b) CO_2 melting temperatures.

The homogenization temperatures for the H_2O-NaCl inclusions in the Arrowhead Pond (Figure 4.7) vein are consistently lower than the H_2O-CO_2-NaCl inclusions averaging 203±13 °C. No difference was recognized between the homogenization temperatures of primary and secondary H_2O-NaCl inclusions. The average melting temperature of ice in the H_2O-NaCl inclusions was 4.2±.3 °C (Figure 4.9).

4.35 Interpretation

4.351 composition and density

The composition and density of the inclusion fluids are calculated from the microthermometric data and the estimates of phases present at room temperature. Calculations that rely only on microthermometric determinations may be both precise and accurate depending on the quality of the experimental and thermodynamic P-T-V-X data (Roedder, 1984). However, the inaccuracy of calculations that rely on phase ratio estimates is largely due to uncertainty of inclusion size in the third dimension (Bodnar, 1983).

Salinity (Figure 4.9) and CO_2 density (Figure 4.10), calculations do not involve phase ratio estimates and the results are similar for the Arrowhead Pond and Long Pond H_2O-CO_2-NaCl inclusions. For Arrowhead Pond, the average salinity is 2.1 ±1.2 wt % (NaCl equivalent) and for Long Pond it is 3.1

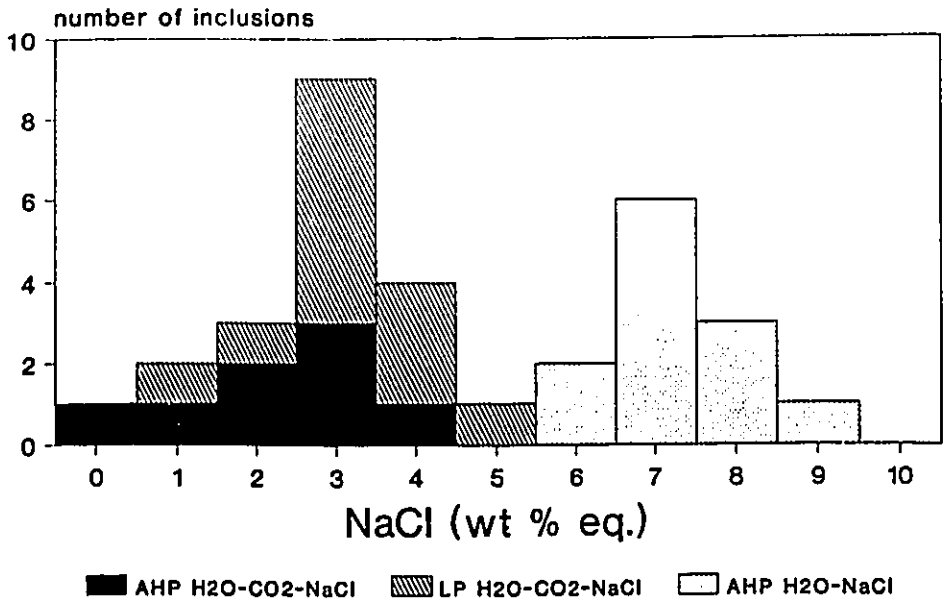

Figure 4.9. Fluid inclusion salinities calculated using FLINCOR (Brown, 1989)

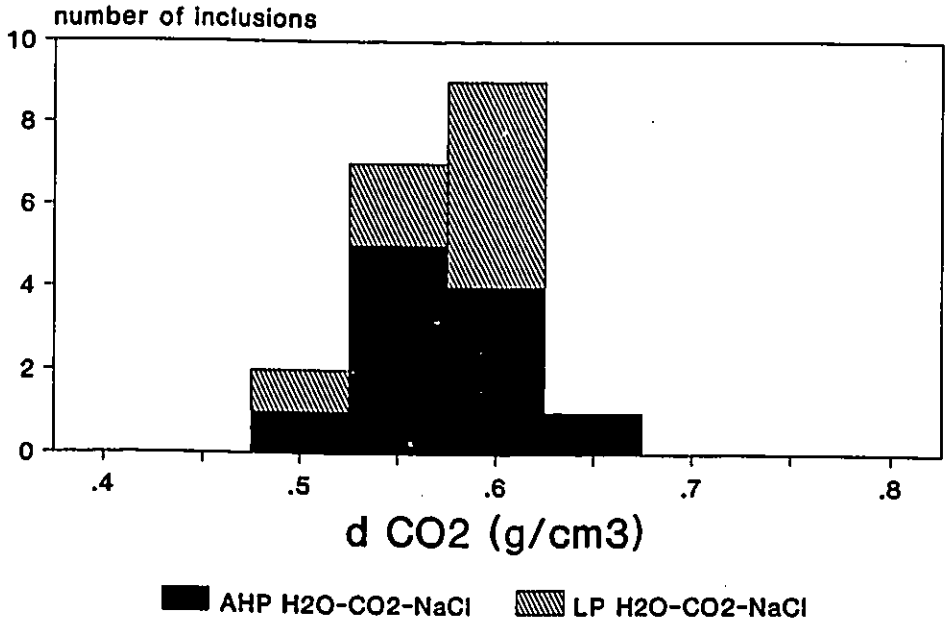

Figure 4.10. Density of CO_2 of inclusion fluids. Calculated using FLINCOR (Brown, 1989)

±1.0 (Figure 4.9). The H_2O-NaCl inclusions from Arrowhead Pond are significantly more saline, containing an average of 7.2 ±.8 wt % NaCl (equivalent) (Figure 4.10). The average density of CO_2 in the H_2O-CO_2-NaCl inclusions from Arrowhead Pond is .59 ±.04 g/cc is similar to that of .57 ±.02 g/cc in the Long Pond vein (Figure 4.12).

The depression of the CO_2 melting temperatures indicates the presence of other gases; the most common of which in hydrothermal minerals is usually CH_4 (Roedder, 1984). The presence of CH_4 was confirmed in some H_2O-CO_2-NaCl inclusions by the condensation of a liquid at temperatures <-90 °C (Roedder, 1984). According to Burruss (1981) the CO_2 melting temperatures for the H_2O-CO_2-NaCl inclusions in the Arrowhead Pond and Lond Pond veins would indicate <10 mole % CH_4 in CO_2.

4.352 temperature and pressure estimates

Estimates of the pressure for fluid inclusion formation was calculated using FLINCOR (Brown, 1989) utilizing the equations of state for H_2O-NaCl (Brown and Lamb, 1989) and for H_2O-CO_2-NaCl (Bowers and Helgeson, 1983). The calculations yield pressures that range from 420 bars to 1646 bars and average 934 bars for homogenization temperatures of 239 °C - 268 °C from the Long Pond H_2O-CO_2-NaCl inclusions (Figure 4.13). The Arrowhead Pond H_2O-CO_2-NaCl inclusions yield similar pressure estimates ranging from 834 bars to 1330 bars with an average of

1082 bars for homogenization temperatures ranging from 261 °C to 272 °C (Figure 4.13). The H_2O-NaCl inclusions from Arrowhead Pond have calculated pressures from 11 bars to 20 bars with an average of 15 bars for homogenization temperatures that range from 195 °C to 220 °C. (Figure 4.13).

The formation of the Long Pond vein, characterized by euhedral quartz crystals in vugs requires that the host structure remained open during mineral deposition (Hodgson, 1989). The trapping of a relatively homogeneous H_2O-CO_2-NaCl-CH_4 fluid is consistent with such a mode of vein formation and the homogenization temperatures of the primary inclusions represent the minimum trapping temperature during vein formation (Roedder, 1984).

The three types of fluid inclusions in the Arrowhead Pond veins could be representative of three distinct fluids during the history of vein formation. An alternative explanation is that the H_2O-NaCl and $CO_2 \pm H_2O$ fluids represent fluids that "unmixed" (Robert and Kelly, 1987) from the H_2O-CO_2-NaCl$\pm CH_4$ fluid due either to pressure or temperature decreases (Figure 4.12) and that the "parent" H_2O-CO_2-NaCl was occasionally trapped. Fluid unmixing has been documented in a number of Au vein deposits (e.g. Ho et al., 1985; Wood et al., 1986; Robert and Kelly, 1987). It is the preferred alternative for the Arrowhead Pond vein based on: 1) both H_2O-CO_2-NaCl and H_2O-NaCl inclusions occur as primary inclusions in older and younger (relatively) quartz; 2) secondary arrays of inclusions

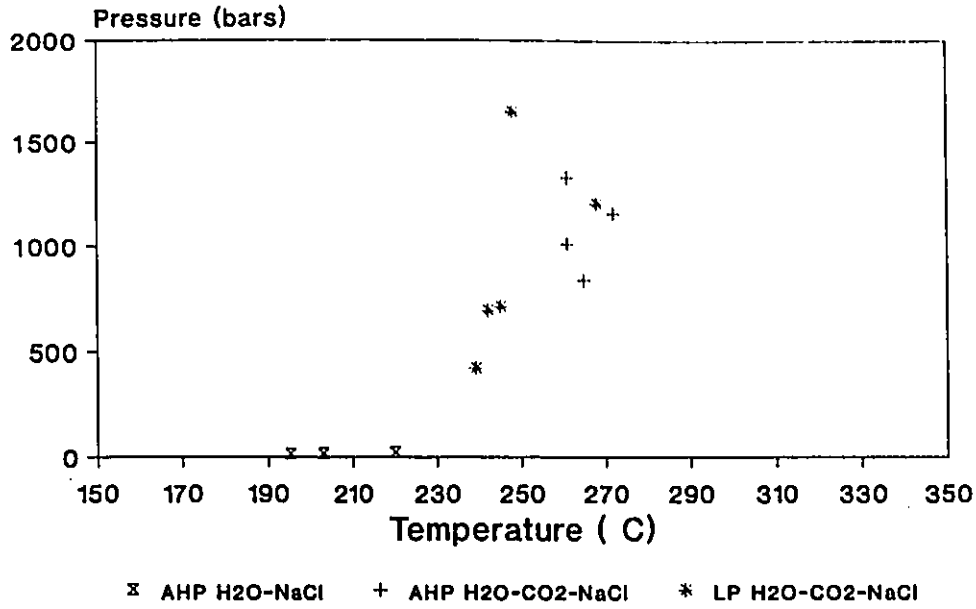

Figure 4.11. Temperature-pressure plot of fluid inclusion data. Point represent inclusion for which all of the microthermometric determinations necessary for the calculation of pressure were attained. Temperature is temperature of homogenization. Pressure is derived from FLINCOR (Brown, 1989).

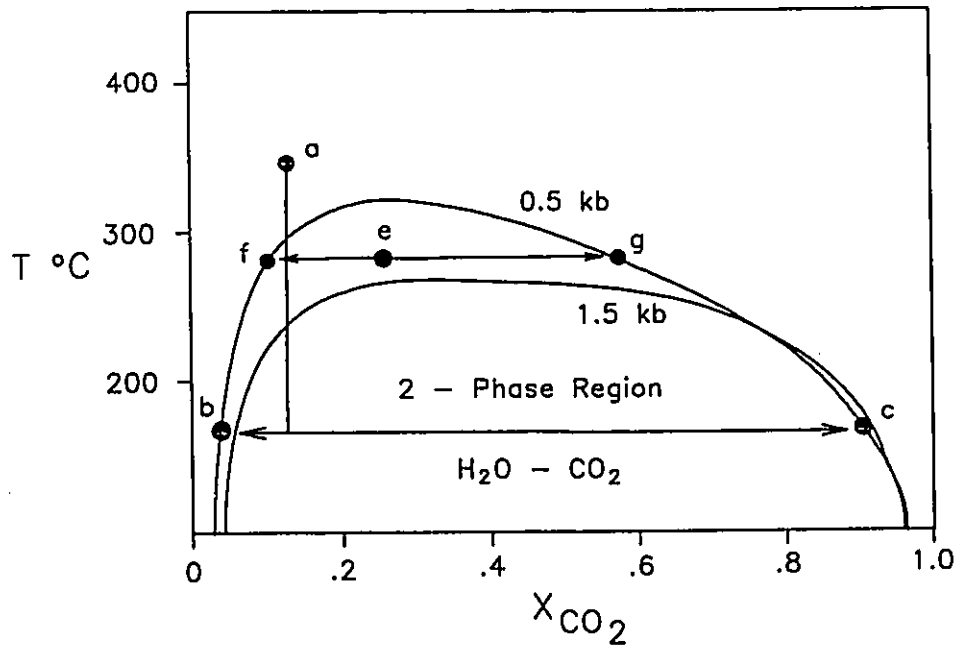

Figure 4.12. T-xCO_2 diagram illustrating fluid unmixing in the system H_2O-CO_2. A fluid at point "a" at 0.5 kbar if cooled to 175 °C would unmix to the two fluids with compositions at "b" and "c". A fluid at "e" at 1.5 kbar would unmix to fluids "f" and "g" upon a pressure drop to 0.5 kbars. Solvi from Crawford (1981)

consisting entirely of H_2O-NaCl or $CO_2 \pm H_2O$ inclusions occur in all quartz regardless of deformational state (i.e. earlier and later quartz); 3) the secondary arrays both emanate from and cut quartz grain boundaries. These petrographic observations indicate that the three fluid types represented by the three types of fluid inclusions circulated in the vein structure throughout vein formation rather than some being earlier and some being later. Also, the unmixing of a $CO_2 \pm H_2O$ fluid explains some compositional and microthermometric features of the fluid inclusions. The difference in homogenization temperatures for the H_2O-CO_2-NaCl inclusions (261 ±7 °C) and H_2O-NaCl inclusions (203 ±13 °C) would be expected due to enthalpy changes associated with unmixing (e.g. Henley et al., 1984). The separation of a CO_2 rich phase from the parent H_2O-CO_2-NaCl fluid would explain the contrasting salinities (2.1 ±1.2 wt % NaCl eq. for the H_2O-CO_2-NaCl$\pm CH_4$ inclusions and 7.2 ±.8 wt % NaCl eq. for the H_2O-NaCl inclusions) as salt will fractionate into the H_2O-rich phase rather than the CO_2-rich phase (Bowers and Helgeson, 1983).

The Arrowhead Pond veins, which have a banded to massive texture, have several generations of quartz in which quartz is variably fractured and annealed is consistent with a crack-seal mechanism of vein formation (Ramsay, 1980). In such a case it may be expected that fluid pressure fluctuate from a lower value during opening to a higher value when the vein is closed (Sibson et al., 1988). The relative homogenization temperatures

and pressure estimates are consistent with the trapping of H_2O-NaCl fluids at lower pressure during vein opening and H_2O-CO_2-NaCl at higher pressure during vein closing (Figure 4.11). It cannot be conclusively demonstrated that the H_2O-NaCl inclusions coexisted with the $CO_2 \pm H_2O$ on the solvus (Figure 4.12) in which case the homogenization temperature of the H_2O-NaCl inclusions would be the trapping temperature (Crawford, 1981). However, the average homogenization temperature of 203 ±13 °C is in good agreement with the bornite-chalcocite assemblage in the Arrowhead Pond veins (Al, 1990) which restricts the temperature of formation to 200 ±10 °C (Barton and Skinner, 1979). It is recognized that the chalcocite-bornite assemblage is commonly a secondary assemblage, however, there is no geochemical or petrographic evidence of supergene processes in the Arrowhead Pond vein.

Although the relative results of the pressure calculations which indicate that the H_2O-CO_2-NaCl inclusions from both the Arrowhead Pond and Long Pond veins formed at similar minimum pressure and the H_2O-NaCl inclusions in the Arrowhead Pond veins at a consistently lower pressure are consistent with the textural features of the vein quartz and the distribution and composition of the fluid inclusions, the absolute calculated pressure values are to be interpreted cautiously. This is because 1) The pressure calculations rely on phase ratio estimates of which uncertainty may exist due to the shape of the fluid inclusions (Bodnar, 1983); 2) Uncertainty in the

equations of state for the systems H_2O-CO_2-NaCl and H_2O-NaCl; 3) The unknown effect of small amounts of CH_4; and 4) Although described and modelled as H_2O-NaCl inclusions, it is probable that they contain small amounts of CO_2.

The similarity in composition between the primary H_2O-CO_2-NaCl-CH_4 inclusions in the Arrowhead Pond and Long Pond veins suggests that both veins formed from a similar H_2O-CO_2-NaCl-CH_4 fluid. The occurrence of H_2O-NaCl and $CO_2 \pm H_2O$ inclusions in the Arrowhead Pond veins and lack of these inclusions in the Long Pond vein can be ascribed to mineral deposition while dilatancy was maintained in the Long Pond vein and a crack-seal mechanism of vein formation in the Arrowhead Pond veins. The similar homogenization temperatures of the H_2O-CO_2-NaCl inclusions indicates a similar minimum temperature of trapping. Minimum pressure estimates based on the Long Pond data range from 420 bars to 1646 bars with an average of 934 bars. Minimum pressure estimates for the H_2O-CO_2-NaCl inclusions from the Arrowhead Pond vein range from 834 bars to 1330 bars with an average of 1082 bars. Thus, assuming that the range of pressure and temperature values can be ascribed to the uncertainties described above, a minimum pressure of $\approx$ 1 kbar and minimum temperature of $\approx$ 250 °C are reasonable round figure approximations for the temperature and pressure of the vein forming fluid.

4.4 Carbon and oxygen isotopes

4.41 Introduction

Investigations of C and O isotopic compositions in magnesite were undertaken in the Betts Big Pond area to determine: 1) if the Au bearing talc-carbonate has a unique isotopic signature that may be indicative of an isotopically unique Au bearing fluid; 2) to determine the isotopic composition of carbonate in the serpentine-carbonate unit; and 3) to compare carbonates in the Betts Big Pond area with vein carbonate from the northern part of the Betts Cove Complex.

4.42 Results

The isotope compositions of the samples from the Betts Big Pond area are very similar and are similar to those from the veins in the northern part of the Betts Cove Complex (Table 4.3). This similarity suggests that the carbonates were formed from hydrothermal fluids of similar C and O isotope compositions. To infer otherwise would require significant differences in the physical and chemical conditions of carbonate formation and that the shifts due to the differences fortuitously resulted in the same $\delta^{13}C$ and $\delta^{18}O$ values for the carbonate minerals.

Table 4.3. Carbon and oxygen isotopic compositions of magnesite

Sample	$\delta^{18}O_{SMOW}$	$\delta^{13}C_{PDB}$	Sample Characteristics
NT-016	10.49	-4.4	talc-carbonate; 360 ppb Au; 18.87 wt % CO_2; 2.6 wt % H_2O
NT-018	10.28	-4.1	talc-carbonate; < 1 ppb Au; 18.28 wt % CO_2; 2.2 wt % H_2O
NT-080	11.42	-4.3	green serpentine-carbonate; < 1 ppb Au; 6.49 wt CO_2 9.8 wt % H_2O
WPR-1*	10.13	-5.2	Au vein magnesite
LP-1*	12.28	-4.6	Au vein magnesite

* Unpublished GSC data. Abbreviations: NT-Betts Big Pond, WPR-West Pond Ridge, LP-Long Pond vein

The minimum temperature of carbonatization in the Betts Big Pond area is constrained to > 240 °C by the occurrence of antigorite coexisting with magnesite. A temperature of < 240 °C would have resulted in the retrograde replacement of antigorite by chrysotile (Chernosky et al, 1988). The fluid inclusion data indicate that the vein forming fluids at Long Pond and Arrowhead Pond existed at similar temperatures of > 250 °C. Given that the West Pond Ridge vein is within the continuous talc-carbonate belt that hosts the Arrowhead Pond showing (Figure 2.1) and the geochemical and mineralogical similarities in the Arrowhead Pond and West Pond Ridge veins (Al, 1990), the temperature of formation for the Arrowhead Pond veins is considered valid for the West Pond Ridge vein.

In the case of the Au-veins in the northern part of the Betts Cove Complex, Al (1990) constrained $fO_2 \approx 10^{-35}$ at 250 °C

based on the metallic mineral assemblages. In the Betts Big Pond area, the fO_2 attending talc-carbonate formation is similarly constrained to 10^{-34} at 250 °C by the occurrence of hematite and magnetite in both Au-bearing and non Au-bearing talc-carbonate. Little constraint exists for the fO_2 in the formation of the serpentine-carbonate unit. However, magnetite is replaced by carbonate in these rocks which is an oxygen generating reaction due to the reduction of Fe^{3+} in magnetite to Fe^{2+} in magnesite which may have resulted in fluid oxidation (Eckstrand, 1975; Frost, 1985). Furthermore, to produce a shift of 1 $^{o}/_{oo}$ in the C isotope composition in the green serpentine-carbonate relative to the talc-carbonate unit would require a decrease in fO_2 from the magnetite-hematite buffer of approximately 4 log units if the bulk carbon isotopic compositions of the hydrothermal fluid are the same (Ohmoto, 1972). Thus, it is concluded that the CO_2 bearing fluids that formed carbonate in Au bearing talc-carbonate, non-Au bearing talc-carbonate, and in serpentine-carbonate in the Betts Big Pond as well as vein carbonate in the West Pond Ridge Showing (and therefore in the Arrowhead Pond Showing) and the Long Pond vein had similar C and O isotopic compositions.

CHAPTER 5

SUMMARY AND DISCUSSION

5.1 Introduction

A major objective of this study is to determine the effect of serpentinization and carbonatization on the distribution of Au in the ultramafic member of the Betts Cove Complex. Eckstrand (1975) derived a model from the study of the Dumont ultramafic body in which reaction between an externally derived fluid and the major rock forming minerals controlled the distribution of the minor nickeliferous opaque mineral assemblages. This general approach is followed here to determine the significance of serpentinization and carbonatization on the distribution of Au, irrespective of the source of Au, in the ultramafic member of the Betts Cove Complex.

In this study, mineral-fluid reactions that approximate the metasomatic processes of serpentinization and carbonatization are derived from mineral assemblages and textures and from the geochemical data. Constraints on some fluid characteristics are derived through comparison of the mineral reactions with experimentally derived and thermodynamically calculated mineral stabilities. The effect of reaction between a fluid and the major rock forming minerals on the solubility of Au is evaluated by comparison of the fluid

characteristics with experimentally determined Au solubilities.

5.2 Petrology of the metasomatized ultramafic rocks

5.21 Temperature and pressure estimates

Thermodynamic modelling of the presence of antigorite and the lack of chrysotile in serpentinite constrains the temperature of serpentinization in the Betts Big Pond area to > 260 °C at 1 kbar and > 240 °C at 4 kbar (Chernosky et al. 1988). As pointed out in the discussion of C and O isotopic compositions of magnesite, since carbonate forms an assemblage with antigorite which is not retrograded to chrysotile, the minimum temperature of carbonatization is similarly constrained. These minimum values are similar to the fluid inclusion data and pressure calculations which establish minimum temperature and pressure of vein formation to 250 °C and 1000 ±355 bars. Therefore, with the lack of upper P-T constraints in mind, 250 °C and 1 kbar will be used in further discussion.

5.22 Serpentinization

Serpentinization may be approximated by the general reaction

$$30\ \underset{(Fo)}{(Mg_{.9}Fe_{.1})_2SiO_4} + 41\ H_2O \qquad \text{(Reaction 1)}$$

$$= 15\ \underset{(Srp)}{Mg_3Si_2O_5(OH)_4} + 9\underset{(Brc)}{Mg(OH)_2} + 2\underset{(Mag)}{Fe_3O_4} + 2H_2$$

(Eckstrand, 1975) where forsterite (Fo) forms serpentine (Srp), brucite (Brc), and magnetite (Mag). It is widely recognized that serpentinization results in fluid reduction (e.g. Chamberlain et al., 1965; Thayer, 1966; Eckstrand, 1975; Frost, 1979; 1985, Coveny et al., 1987; Abrajano and Pasteris, 1989; Abrajano et al., 1990). Eckstrand (1975) indicates that fluid reduction is largely governed by the partial reaction

$$\underset{\text{(in olivine)}}{3\ FeO} + H_2O = \underset{\text{Mag}}{Fe_3O_4} + H_2 \qquad \text{(Reaction 2)}$$

Frost (1985) indicates that the assemblage olivine-antigorite-magnetite-brucite constrains the ambient fO_2 to four to seven log units below the fayalite-magnetite-quartz (FMQ) buffer which is therefore 10^{-44} - 10^{-47} (FMQ buffer = 10^{-40} at 250 °C (Myers and Eugster, 1983)). Although this assemblage is recognized locally, application of this buffer is limited as serpentinite in the Betts Big Pond area is dominantly antigorite-magnetite.

Chamberlain et al. (1965), Eckstrand (1975) and Frost (1985) indicate that the occurrence of native iron in partially

serpentinized ultramafic rocks resulted from the dissolution of magmatic Fe-sulphides. The dissolution of magmatic sulphides in the Betts Big Pond area serpentinite is common. However, native iron is not recognized. This appears to indicate that serpentinization proceeded in the magnetite stable field (Figure 5.1). Thus, fO_2 during serpentinization may locally have been in the range 10^{-46} - 10^{-44} (upper stability limit for native iron and upper stability limit for the assemblage antigorite-magnetite-brucite) but more generally, is constrained only by the magnetite stability field (10^{-46} - 10^{-34}). It has been suggested by Abrajano et al. (1990) that reaction to form the hydrated minerals in locally closed systems may result in a fluid with a greater H_2/H_2O ratio than expected in an open system.

Barnes et al. (1978) determined pH values that range from 9.2 to 11.75 (at temperatures from 20 °C to 34 °C) of natural fluids that have reacted to form serpentinite. Moody (1976) measured the pH of experimentally derived serpentinizing fluids that range from 10.9 to 11.6. The experiments were conducted at temperatures and pressures from 304 °C to 331 °C and pressures from 540 bars to 1470 bars. Jánecky and Seyfried (1986) have shown through experimental investigation that formation of magnetite during serpentinization requires that the fluid be alkaline. Thus, the pH during serpentinization in the Betts Big Pond area is interpreted to be alkaline.

A zone of magnetite rich rock is located adjacent to a

chromite body in the green serpentine-carbonate unit north of Betts Big Pond in the Betts Big Pond area. In the Beaver Cove Pond area (Figure 2.3), a similar zone of magnetite occurs in basalt of the Cape St. John Group at the fault contact with the ultramafic member of the Betts Cove Complex (Lavigne, 1988). On an island in Red Cliff Pond (Figure 2.3), a zone of magnetite rich basalt in which magnetite comprises approximately 50 - 70 modal % of the rock, occurs where the ultramafic and basaltic members of the Betts Cove Complex are in fault contact. The distribution of these magnetite rich zones within and adjacent to the ultramafic rocks suggest that they are hydrothermal magnetite formed in chemically distinct rocks during serpentinization.

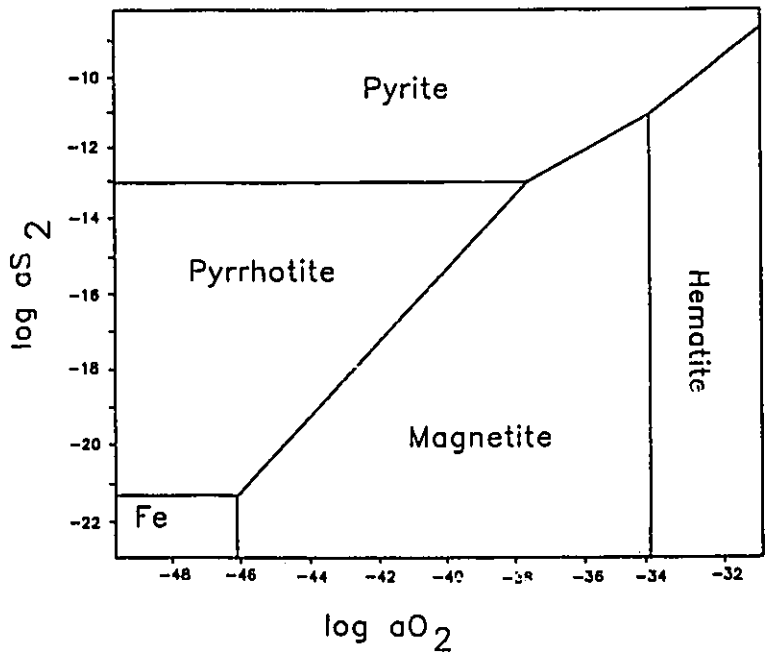

Figure 5.1. Log a(S_2) - log a(O_2) diagram for the system Fe-O-S at 250 °C.

Mineralogically, the magnetite rich zone in the Betts Big Pond area is characterized by high magnetite/antigorite ratios (Figure 3.5), chromite grains and disseminated and fine grained sulphides occur within massive magnetite. Chlorite is intergrown with antigorite. The departure in chemical composition of the magnetite rich rocks from typical serpentinite in the Betts Big Pond area largely reflects the higher magnetite/antigorite ratio. Exceptions include enrichments of S, As, Cu, and Au relative to serpentinite. In the magnetite rich samples from the Betts Big Pond area, CO_2 concentrations are near detection limit (samples NT-326 and NT-327 in appendix II) and no carbonate was observed in the rocks. The magnetite rich samples from Beaver Cove Pond are similarly low in CO_2 (Lavigne, 1988). The occurrence of magnetite and chlorite rims of chromite is widely regarded as being due to alteration during serpentinization (e.g. Ulmer, 1974; Bliss and MacLean, 1975). Thus, the magnetite rich rocks in the Betts Big Pond area most likely formed during serpentinization.

5.23 Carbonatization

The net effect of the conversion of serpentinite to talc-carbonate may be approximated by the reaction

$$\underset{(Srp)}{18\ Mg_3Si_2O_5(OH)_4} + \underset{(Mag)}{Fe_3O_4} + 30\ CO_2 \qquad \text{(Reaction 3)}$$

$$= \underset{(Tlc)}{9\ Mg_3Si_4O_{10}(OH)_2} + \underset{(Mgs)}{30\ (MgFe)CO_3} + 27\ H_2O + (1/2)O_2$$

(Eckstrand, 1975). However, this does not account for a number of field, petrographic, and geochemical observations from the Betts Big Pond area.

Rock textures and contact relationships indicate that serpentine-carbonate formed by the carbonatization of serpentinite and that talc-carbonate formed from serpentine-carbonate.

Talc is not ubiquitous in the serpentine-carbonate unit at Betts Big Pond. This is observed in thin section and in the normative molar mineral calculations where a number of samples are talc free or have very low molar talc abundances (Figure 3.5). This suggests the reaction

$$\underset{(Srp)}{Mg_3Si_2O_5(OH)_4} + 3\ CO_2 = \underset{(Mgs)}{3\ MgCO_3} + 31\ H_2O + 34\ SiO_{2\,(aq)} \qquad \text{(Reaction 4)}$$

in which serpentine was carbonatized to form magnesite without the production of talc at Betts Big Pond. Consistent with this reaction is: 1) the serpentine content decreases as the magnesite content increases with progressive carbonatization (Figure 3.5); 2) A number of samples do not contain talc, which is seen in thin section and in the normative mineral calculations where some rocks, with up to 7.5 wt % CO_2, do not contain talc (Figure 3.5); 3) There is a consistent loss in SiO_2 from the rock with increasing CO_2 content to a maximum loss at approximately 16 wt % CO_2 (Figure 3.7a), and 4) There is a consistent loss in H_2O from the rock with increasing CO_2

content.

Fine grained mixtures of talc and serpentine are recognized in the serpentine-carbonate unit as revealed by mineral compositions intermediate between talc and serpentine (Figure 3.4). This feature may reflect the reaction

$$\underset{(Srp)}{Mg_3Si_2O_5(OH)_4} + 2\ SiO_{2\,(aq)} \qquad \text{(Reaction 5)}$$

$$= \underset{(Tlc)}{Mg_3Si_4O_{10}(OH)_2} + H_2O$$

In the normative mineral plots (Figure 3.5), there is a sharp increase in the abundance of talc at approximately 16 wt % CO_2. The increase in talc abundance is greater than the trend in increasing talc from 0 to < 16 wt % CO_2. Also at approximately 16 wt % CO_2, there is a decrease in serpentine content which is greater than the trend of decreasing serpentine with CO_2 contents < 16 wt % (Figure 3.5). These "abrupt" changes in the mineralogical composition correspond with: 1) a sharp increase in the SiO_2 content of the rocks about 16 wt % CO_2 and 2) a sharp decrease in H_2O content which is greater than the loss of H_2O in the rocks with < 16 wt % CO_2 (Figure 3.7d)

Summation of reactions 4 and 5 results in the reaction

$$2\ \underset{(Srp)}{Mg_3Si_2O_5(OH)_4} + 3\ CO_2 \qquad \text{(Reaction 6)}$$

$$= \underset{(Tlc)}{Mg_3Si_4O_{10}(OH)_2} + 3\ \underset{(Mgs)}{MgCO_3} + 3\ H_2O$$

which describes the conservation of SiO_2 in the conversion of serpentine to talc and magnesite. The observation that SiO_2 is

increasingly lost from the rock with increasing CO_2 contents (< 16 wt % CO_2) indicates a net loss of SiO_2. However, in the rocks with < 16 wt % CO_2 the variable serpentine/talc ratio (Figure 3.5d) may indicate that carbonatization of serpentinite in the rocks with < 16 wt % CO_2 proceeded by a combination of reactions 3, 4, and 5.

Magnetite grains are truncated by magnesite veins in the green serpentine-carbonate unit. Where magnetite is recognized in magnesite, it is corroded and embayed. Within the talc-carbonate unit, magnetite commonly occurs as highly irregular to skeletal inclusions in magnesite. This suggests the following reaction takes place during the formation of magnesite

$$2\ \underset{(Mag)}{Fe_3O_4} + 6\ CO_2 = 6\ \underset{(in\ Mgs)}{FeCO_3} + O_2 \qquad \text{(Reaction 7)}$$

Combination of this reaction with Reaction 6 yields the general reaction of Eckstrand (1975) (Reaction 3 above) which describes the conversion of serpentinite to talc-carbonate.

Inclusions of talc in magnesite is common in talc-carbonate suggesting the replacement of talc by magnesite via the reaction:

$$\underset{(Tlc)}{Mg_3Si_4O_{10}(OH)_2} + 3\ CO_2 = 3\ \underset{(Mgs)}{MgCO_3} + 4\ SiO_{2\,(aq)} + H_2O \qquad \text{(Reaction 8)}$$

Further evidence supporting the reaction comes from the

geochemical calculations which indicate a loss of SiO_2 (Figure 3.7a) and a decrease in the molar abundance of talc with increasing whole rock CO_2 contents (Figure 3.5).

The phase relations represented in figure 5.2 indicate 1) that Reaction 4, which is recognized in the serpentine-carbonate unit is constrained to a lower $a(SiO_2)$ than reactions 5 and 6; 2) The occurrence of the assemblage antigorite-talc-magnesite (reaction 6), constrains the system to an invariant point until antigorite is eliminated; and 3) Reaction 8, will not proceed in the presence of antigorite and is constrained to lie at a higher $a(SiO_2)$. 4) Since quartz is not present in talc-carbonate in the Betts Big Pond area, the $aSiO_2$ was less than that required for quartz formation. It is suggested that the SiO_2 required for the formation of talc be derived through reaction 4.

The fO_2 during carbonatization is indicated by the distribution of magnetite and hematite. Magnetite occurs in all of the carbonatized rocks whereas hematite occurs in only some talc-carbonate indicating that fO_2 was as high as hematite stability in some parts of the talc-carbonate unit.

Eckstrand (1975) and Frost (1985) suggest that the dominant equilibria controlling $f(O_2)$ in carbonate bearing serpentinite is that of reaction 7. Figure 5.3 indicates that the assemblage magnetite-antigorite-talc-magnesite is constrained to the invarient point at the intersection of reactions 6, the conversion of antigorite (Mg endmember) to

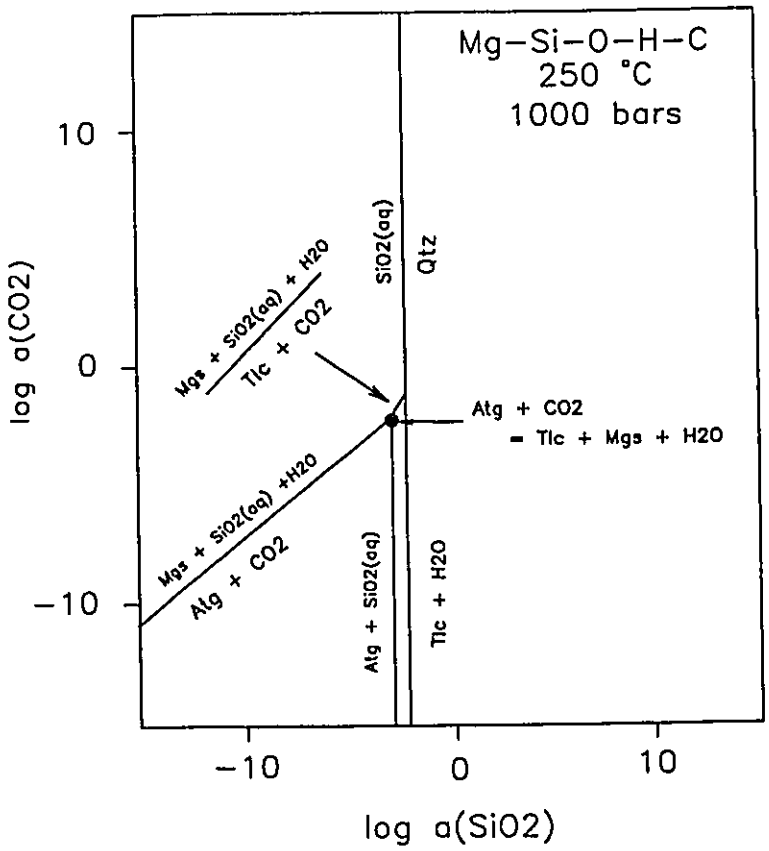

Figure 5.2. Log a(SiO_2) - Log a(CO_2) diagram calculated with TWEEQU (Berman, 1991). Reactions and mineral formulae as indicated in the text.

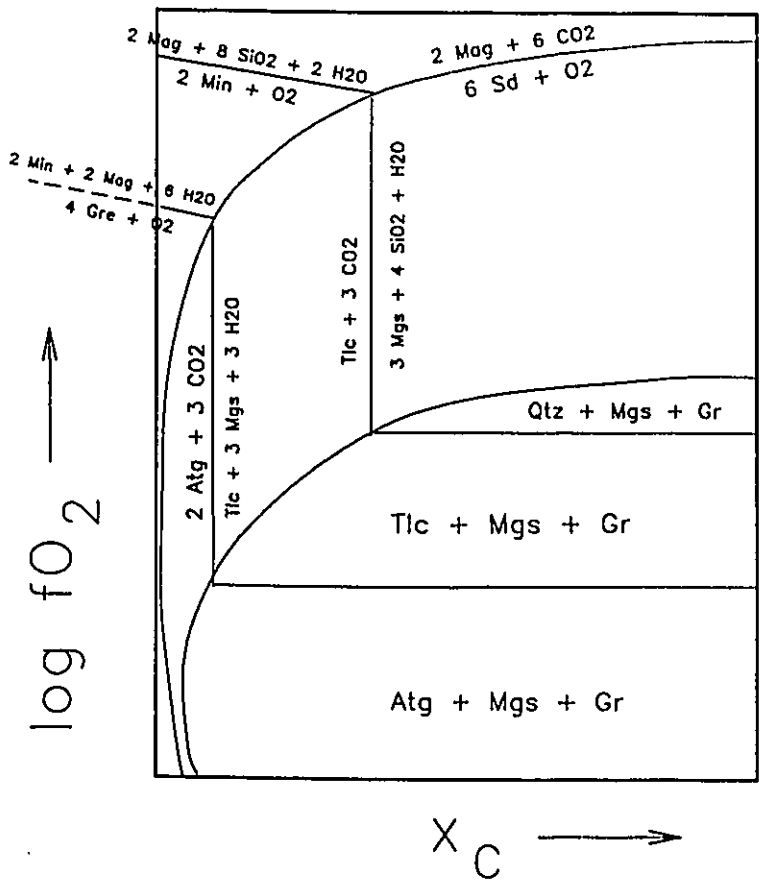

Figure 5.3. Schematic log $f(O_2)$ - xC diagram from Frost (1985) showing general topology of phase relationships. xC = xCO_2 + xCO + xCH_4 and xC + xH_2O = 1. Abbreviations and mineral formulae: Atg - antigorite, $Mg_3Si_2O_5(OH)_4$; Gre - greenalite, $Fe_3Si_2O_5(OH)_4$; Tlc - talc, $Mg_3Si_4O_{10}(OH)_2$; Min - minnesotiate, $Fe_3Si_4O_{10}(OH)_2$; Mgs - magnesite, $MgCO_3$; Sd - siderite, $FeCO_3$; Mag - magnetite, Fe_3O_4; Gr - graphite, C; Qtz - quartz, SiO_2.

talc (Mg endmember) and magnesite; reaction 7, the conversion of magnetite to siderite; and the formation of minnesotaite (Fe endmember of talc) and magnetite from the reaction of greenalite (Fe endmember of antigorite) and O_2. The carbonatization of magnetite in the serpentine-carbonate unit in the Betts Big Pond area is evident in thin section. However, the net conservation of magnetite in serpentine-carbonate is indicated by there being no detectable decrease in the molar magnetite abundance with increasing whole rock CO_2 content in the presence of serpentine (< 16 wt % CO_2 in figure 3.5). In the absence of serpentine (i.e. talc-carbonate, CO_2 > 16 wt %) there is a consistent decrease in magnetite abundance with increasing whole rock CO_2 content. Furthermore, the average ratio Fe/(Fe+Mg) (mole ratios) decreases from .058 in serpentine to .033 in talc and the carbonate in the serpentine-carbonate rocks is magnesite (Fe/(Fe+Mg) < .05) whereas in talc-carbonate the carbonate is breunnerite (Fe/(Fe+Mg) > .05). There is a consistent increase Fe/(Fe+Mg) in breunnerite with increasing whole rock CO_2 contents of talc-carbonate samples (Figure 3.3 and Table 3.3). The distribution of magnetite and hematite in the Betts Big Pond area, in which magnetite is ubiquitous but hematite only occurs in some talc-carbonate, is consistent with fO_2 being constrained to magnetite stability in the presence of antigorite (and greenalite) due to the consumption of O_2, liberated by the carbonatization of magnetite (reaction 7), in the formation of magnetite and

minnesotaite from greenalite. Upon the elimination of serpentine, continued carbonatization of magnetite (reaction 7) resulted in a higher Fe content in carbonate, fluid oxidation (reaction 7) and hematite stability.

Magnesite may be stabilized from serpentinite through reaction with a relatively low xCO_2 fluid. In a study of fluid inclusions hosted by carbonate in talc-carbonate, Schandl and Naldrett (1992) determined that the fluid was H_2O rich containing < 1 mole % CO_2. Also, the occurrence of the assemblage talc-serpentine-magnesite requires that the fluid have a relatively low xCO_2 (Johannes, 1969).

The pH during carbonatization is interpreted to be have been alkaline as carbonate is being formed and the first dissociation constant of carbonic acid, $H_2CO_3 = H^+ + HCO_3^-$ is at pH 7.7 at 250 °C (Henley et al., 1984). The $a(S_2)$ during carbonatization is not constrained due to the lack of sulphide minerals. However, given that the $f(O_2)$ is buffered by hematite and magnetite in some talc-carbonate, then dissolved sulphur would be dominantly SO_4^{2-} at $a(S_2) < 10^{-12}$. Barite, due to its low solubility, is not nescessarily a reliable indicator of $f(O_2)$, however, given the relatively low concentrations of Ba in the rocks, its occurrence in the hematite bearing talc-carbonate samples is consistent with a sulphate > sulphide fluid.

5.3 Au mineralization

5.31 Introduction

With the possible exception of trace amounts of magmatic magnetite and chromite, Au- bearing talc-carbonate is composed exclusively of hydrothermal minerals. Therefore, the occurrence of native gold in talc-carbonate is ascribed to its deposition from a hydrothermal fluid. Similarly, with the exception of chromite, magnetite rich serpentinite is composed of hydrothermal minerals including secondary sulphides. Au analyses of the adjacent chromite lens returned Au values less than detection limit. Thus, the slight Au enrichment in these rocks is interpreted to be due to its depostion during the formation of magnetite rich serpentinite. Au mineralization at Arrowhead Pond occurs in veins and in the hydrothermal alteration halo and was clearly deposited from a hydrothermal fluid. Thus, description of the solubility of Au in hydrothermal fluids is a nescessary pre-requisite to consideration of the effect of serpentinization and carbonatization on the distribution of Au.

5.32 Solubility of Au

Au forms stable complexes in a hydrothermal fluid (e.g. Seward, 1973; Kerrich and Fyffe, 1981; Schwarcz, 1986). Most

often implicated complexes in the process of Au concentration are aurous chloride and bisulfide complexes (e.g. Krauskopf, 1951; Helgeson and Garrels, 1968; Henley, 1973, Weissberg, 1970; Seward, 1973, 1984; Romberger, 1985). The solubility of Au as chloride and bisulphide complexes depends on $a(O_2)$, pH, and temperature (Figure 5.4). At 250 °C, the greatest solubility of Au as $Au(HS)_2^-$ occurs within the pyrite stablity field at relatively reduced conditions and alkaline pH. This is contrasted with the solubility of Au as $AuCl_2^-$ (under the same conditions indicated in figure 5.4) which is five orders of magnitude lower where the solubility of $Au(HS)_2^-$ is greatest. Under more oxidized and acidic conditions and at higher temperatures, the solubility of $AuCl_2^-$ may predominate over $Au(HS)_2^-$ (Figure 5.4). Although S and Cl concentrations in the fluid attending metasomatism in the Betts Big Pond area are not known, the minimum temperature inferred above, as well as the relatively reduced and alkaline conditions are consistent with Au being soluble dominantly as a bisulphide complex in the Betts Big Pond area.

5.33 Effect of serpentinization

Au is a siderophile element with a secondary chalcophile tendancy. Thus, Au will be strongly concentrated in the sulphide phase. Peach et al. (1990) determined partition coefficients (Au in sulphide melt/Au in silicate melt) based on

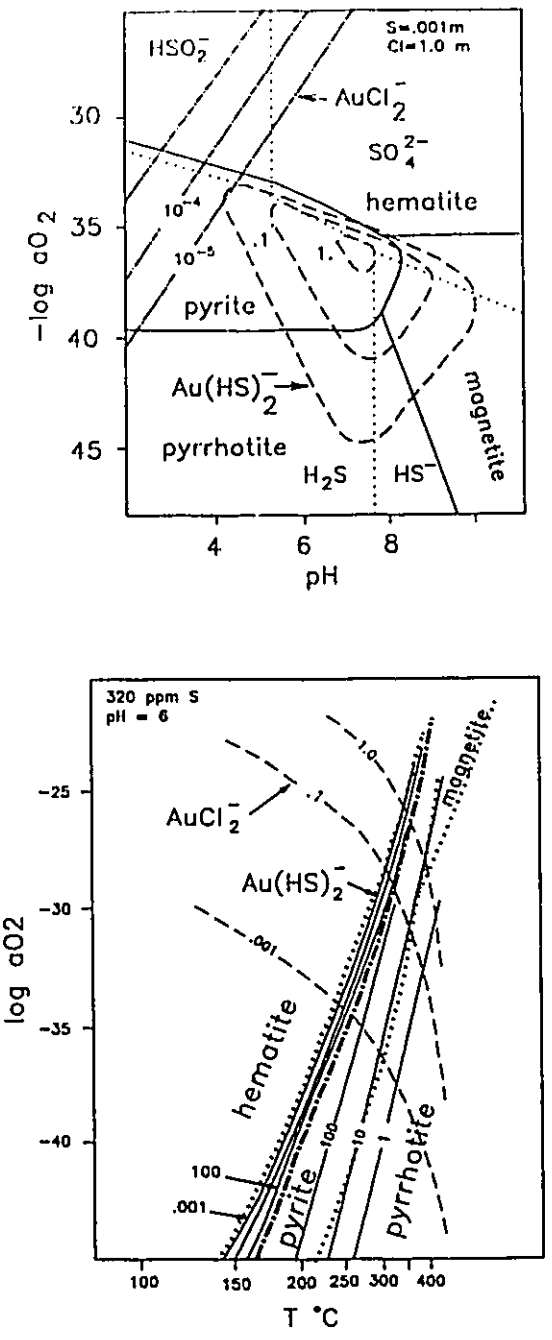

Figure 5.4. Diagrams with the calculated solubilities of $Au(HS)_2^-$ and $AuCl_2^-$ a) pH - log $a(O_2)$ diagram (Fe-O-S) at 250 °C. Solid lines separate mineral species. Dotted lines separate fields of dominant ionic species (from Seward, 1982). b) log $a(O_2)$ - T (Fe-O-S). Dotted lines separate fields of minerals species. (From Romberger, 1990). Other conditions indicated on the diagrams.

analyses of MORB that are $1.5\text{-}1.9\times10^{4}$. Similarly, Stone et al. (1990) report an experimentally derived partition coefficient of $1.0\pm.9\times10^{3}$ for Au. Vincent and Crocket (1960) showed that Au prefered copper sulphides to iron sulphides, oxides, or silicates in the Skaergard intrusion. Lorand and Pinet (1984) determined that Au is concentrated in Fe-Ni sulphides and arsenides in ultramafic rocks of several ophiolites. Similarly, Leblanc and Johan (1986) indicate that magmatic arsenides from a lherzolite massif in Morocco contain from 6 to 11 ppm gold.

Hamlyn et al. (1985) and Hamlyn and Keays (1986) have proposed a model in which the sulphides in melts derived from a depleted mantle source will be relatively enriched in chalcophile and siderophile elements such as PGE and Au. The main elements of the model are as follows: The sulphide component of the mantle has a low melting point (Naldrett, 1973) and is largely involved in mantle melting (Garuti et al., 1984). During partial melting of fertile mantle and extraction of magma, the system becomes sulphur saturated and immiscible sulphide droplets form and remain in the residue. Because of its affinity for sulphide, Au will partition from the silicate magma into the sulphide droplets (Campbell and Barnes, 1984). Subsequent partial melting of the residue (depleted mantle) will produce magmas with high concentrations of chalcophile elements such as Au (Hamlyn et al., 1985; Hamlyn and Keays, 1986).

Boninitic magamas are products of the partial melting of

depleted mantle and have been implicated in the process of Au and PGE concentration (e.g. Hamlyn and Keays, 1986). The Betts Cove Complex is interpreted to have been derived from a boninitic parental magma. Thus, it follows that magmatic sulphide disseminated in the ultramafic member of the Betts Cove Complex would be Au-bearing. The Au concentration determined for the layered cumulate rocks is dominantly < 1 ppb with one sample containing 4 ppb. It is probable that a larger sample set may more accurately define the Au contents of the layered cumulate rocks. In this respect, it is significant that Oshin and Crocket (1982) determined an average of 1.3 ppb Au with a range of .21 to 6.4 ppb Au from cumulate dunite in the Thetford Ophiolite Complex. Church (1977) indicates that the Thetford and Betts Cove Complexes are lithologically and geochemically correlative and probably formed in a similar tectonic environment.

The mobility of Au during serpentinization of ultramafic rocks has been demonstrated by Razin et al. (1965) and Crocket and Chyi (1972). In a previous section of this chapter (section 5.22) the fO_2 was estimated to be in the range 10^{-46} - 10^{-34} and the pH was suggested to be alkaline. Comparison of these characteristics of the fluid attending serpentinization with the solubility of Au as $Au(HS)_2^-$ in $f(O_2)$-pH space (Figure 5.4) indicate that serpentinization may have resulted in dissolution of Au as $Au(HS)_2^-$. Furthermore, if Au was preferentially concentrated in sulphide during crystallization of the Betts

Big Pond ultramafic rocks, the dissolution of the sulphides during serpentinization provides the necessary complexing agent, S, as well as Au.

Anomalous Au values were attained from massive magnetite samples which contain finely disseminated sulphides. The Au bearing rocks also contain anomalous concentrations of Cu, S, and As. In a previous section (section 5.22) it was suggested that the magnetite occurrence resulted by reaction of the serpentinizing fluid with the chromitite body causing magnetite deposition. The occurrence of finely disseminated Cu- and Fe-sulphides and Au (presumably within the sulphide given the Au-Cu-S-As association) is consistent with the destabilization of Au- and Cu-bisulphide complexes concomitant with the deposition of magnetite due to reaction with the chromitite body.

Although the Au values in the magnetite rich samples are small, this occurrence is significant in that 1) it is very similar to other magnetite rich occurrences in the ultramafic member of the Betts Cove Complex (e.g. Beaver Cove Pond) which contain significant Au and 2) it indicates the presence of Au in the serpentinizing fluid.

5.34 Effect of carbonatization

A number of physical or chemical changes affecting the hydrothermal fluid can lead to the deposition (or enhanced solubility) of Au from $Au(HS)_2^-$. Of the fluid parameters

illustrated in figure 5.4, the solubility of Au as $Au(HS)_2^-$ decreases most rapidly with an increase in $f(O_2)$ corresponding closely to the boundary between the sulphide and sulphate dominant fields.

All of the samples of ultramafic rocks containing > 100 ppb Au come from talc-carbonate in the northern part of the Betts Big Pond area. The Au bearing samples contain hematite, which is not ubiquitous in talc-carbonate, and barite, which was identified in two of the Au bearing samples. Otherwise, the Au bearing talc-carbonate is mineralogically and chemically identical to unmineralized talc-carbonate.

In a previous section of this chapter (section 5.23) it was established that the $f(O_2)$ during carbonatization is constrained by the presence of Fe-bearing antigorite. It was suggested that the higher $f(O_2)$ indicated by the occurrence of hematite in talc-carbonate was due to the carbonatization of magnetite in the absence of Fe-bearing antigorite. Thus, the occurrence of native gold in talc-carbonate due to fluid oxidation upon the elimination of Fe-bearing antigorite is consistent with the solubility of $Au(HS)_2^-$ (Figure 5.4). The occurrence of native gold in talc-carbonate may be ascribed to the reaction

$$Au(HS)_2^- + 18\ O_2 = 2\ Au^\circ + 4\ SO_4^{2-} + 2H_2O \qquad \text{(Reaction 9)}$$

A number of studies have invoked oxidation in the process

of Au deposition. In general, these models indicate the reaction of a relatively reduced Au bearing fluid with a precursor oxidized mineral assemblage (e.g. MacDonald, 1984; Phillips and Groves, 1984; Romberger, 1985; Roberts, 1987). One effect of this interaction is the replacement of Fe bearing oxide and silicate minerals by sulphide minerals thus reducing the activity of reduced sulphur and therefore the solubility of Au-bisulphide complexes (e.g. Phillips and Groves, 1984; Roberts, 1987). If this mechanism were inferred for the Betts Big Pond area then the replacement of magnetite and hematite by sulphide would be expected. However, this is not the case at Betts Big Pond where sulphide is replaced by magnetite, hematite replaces magnetite (Plate 2.17), and sulphide is comparitively rare. It is recognized that a pH change or desulphidation reaction will result in the destabilization of $Au(HS)_2^-$. The occurrence of barite in two of the Au bearing samples is consistent with fluid oxidation resulting in $SO_4^{2-} > H_2S$ and gold deposition in talc-carbonate in the Betts Big Pond area.

5.35 Arrowhead Pond Showing

Mineralization at Arrowhead Pond consists of two parallel veins enclosed in an alteration halo. The mineralogical and chemical similarities between talc-carbonate at Arrowhead Pond and Betts Big Pond and between talc-carbonate and the

alteration halo allow application of the phase relations established above and extension of them to include the occurrence of quartz. The veins are chemically very similar to the alteration halo and show no enrichment of elements exotic to the alteration halo. The exception is the occurrence of Cu-Fe sulphides with which native gold is associated.

The phase relations depicted in figure 5.2 indicate that a small increase in the $a(SiO_2)$ after elimination of antigorite can lead to quartz formation and the assemblage talc-magnesite-quartz. Although the carbonatization reactions provide a source for SiO_2, the geochemical calculations (Figures 4.5 and 4.6) indicate that SiO_2 was added to the alteration halo relative to the host talc-carbonate. Furthermore, the amount of quartz occuring in the alteration is irrespective of CO_2 content in the talc-carbonate rocks that are otherwise chemically the same as quartz free talc-carbonate.

Allowing for the dominance of quartz in the Arrowhead Pond vein, it is otherwise mineralogically and compositionally similar to the alteration halo. The occurrence of the vein represents brittle deformation in a body of talc-carbonate that is otherwise undergoing ductile deformation. Brittle failure may take place as a result of a combination of the effects of crustal level, shearing stress, and fluid pressure. In this respect, two possibilities for the formation of the Arrowhead Pond veins are apparent. First, it may be possible that the alteration halo represent a zone of high fluid pressure in

talc-carbonate which led to brittle failure (i.e. the vein structure) possibly resulting in pressure and temperature decreases leading to quartz saturation and possibly fluid unmixing (fluid inclusions, section 4.3). Second, the occurrence of quartz in the alteration halo could represent quartz deposition from fluid flow from the vein structure due to a temperature gradient. The occurrence of quartz interstitial to talc and magnesite in the alteration halo, rather than quartz veins or veinlets pervading the vein wall rock, and the observation that the veins are relatively short may be evidence in favor of the first alternative.

The Arrowhead Pond veins have not been studied in sufficient detail during this study to conclusively comment on mechanism(s) of Au deposition. However, fluid immiscibility has been implicated in the deposition of Au in Archean Au deposits (e.g. Robert and Kelly, 1987) which is consistent with the fluid inclusion data at the Arrowhead Pond Showing. Furthermore, the occurrence of native gold associated with Cu-Fe sulphides at Arrowhead Pond is consistent with this interpretation (Drummond and Ohmoto, 1985).

5.4 Summary

The following paragraphs summarize the observations made during this study emphasizing the mineralogical and geochemical aspects of the ultramafic rocks in the Betts Big Pond area and

comparison with the Arrowhead Pond area. Field aspects of this study, emphasizing the history of the ultramafic bounding faults and the significance of the timing of serpentinization and carbonatization are summarized in the following section.

5.41 Betts Big Pond area

1) Ultramafic rocks in the Betts Big Pond area consist of: 1) layered cumulate rocks including dunite and harburgite and minor lherzolite and wehrlite; 2) serpentinite; 3) green weathering serpentine-carbonate; 4) red weathering serpentine-carbonate; talc-carbonate. The metasomatic sequence in the Betts Big Pond area in terms of the dominant mineral assemblages is:

- olivine ± orthopyroxene ± clinopyroxene replaced by
  serpentine and magnetite
- serpentine and magnetite replaced by
  serpentine, magnetite, magnesite ± talc
- serpentine, magnetite, magnesite ± talc
  to serpentine, magnetite, magnesite, talc
- serpentine, magnetite, magnesite, talc
  to talc, breunnerite, magnetite ± hematite

2) Pentlandite, pyrrhotite, and chalcopyrite occur in the layered cumulate ultramafic rocks. These minerals are recognized locally in serpentinite but are strongly corroded.

3) Au mineralization, up to 1300 ppb, in the Betts Big

Pond area occurs as a zone of hematite bearing talc-carbonate in the northern part of the map area. In addition, slightly anomalous Au values (23 and 26 ppb) occur in serpentinite.

4) Au in serpentinite occurs in magnetite rich samples in which disseminated secondary sulphides occur.

5) Mineralogically, Au bearing talc-carbonate is similar to non-Au-bearing talc-carbonate. The exceptions are the occurrence of hematite, which is not ubiquitous in talc-carbonate and barite, although the distribution of barite remains unknown.

6) Chemically, Au bearing talc-carbonate is similar to non-Au-bearing talc-carbonate. There is no trace element concentration that correlates with Au. Mineral compositions in Au-bearing talc-carbonate and non-Au-bearing talc-carbonate are the same.

7) C and O isotopic compositions of carbonate from Au-bearing talc-carbonate, non-Au-bearing talc-carbonate, and serpentine-carbonate are very similar.

8) The Au anomaly in serpentinite is associated with Cu, S, and As enrichment.

9) With the exception of the addition of H_2O, serpentinization appears to be an isochemical process. During serpentinization, the fluid was alkaline. The $f(O_2)$ during serpentinization may been in the range 10^{-44} to 10^{-47} indicated by the assemblage antigorite-magnetite-brucite. However, the dominant assemblage in serpentinite being antigorite-magnetite,

the lack of native iron, and the dissolution of magmatic sulphides indicate that serpentinization proceeded under conditions of $f(O_2)$ 10^{-46} - 10^{-34}.

10) Carbonatization in the Betts Big Pond area is characterized by the addition of CO_2 and the loss of Si, H_2O, and possibly Al, Fe, and Cr. During carbonatization, the pH of the fluid may have been alkaline. The $a(SiO_2)$ was lower in the presence of antigorite than that in talc-carbonate. The $f(O_2)$ in the carbonatized rocks is constrained by the occurrence of Fe-bearing antigorite. In the case of the Betts Big Pond area, the $f(O_2)$ associated with serpentine-carbonate was constrained to below the magnetite-hematite buffer whereas in some talc-carbonate the $f(O_2)$ was at the magnetite-hematite buffer.

11) Although the details of the composition of the fluid attending serpentinization are not known, it is thought, based on estimated fO_2 and pH, that the conditions of serpentinization may have been favourable for the solution of Au as $Au(HS)_2^-$. If, as predicted by the model of Hamlyn et al. (1985) and Hamlyn and Keays (1986), the magmatic sulphides in the Betts Cove Complex ultramafic rocks were Au bearing, then through their dissolution may have provided Au as well as S.

12) The occurrence of Au in magnetite rich serpentinite may be due to the reaction of the serpentinizing fluid with massive chromite causing the precipitation of Au and Fe-Cu sulphides. Although the Au contents are slight, they indicate the presence of Au in the fluid.

13) The occurrence of Au in talc-carbonate at Betts Big Pond is consistent with the destabilization of $Au(HS)_2^-$ due to fluid oxidation as a result of the carbonatization of magnetite upon the elimination of Fe-antigorite.

5.42 Vein mineralization in the northern Betts Cove Complex - summary and comparison with the Betts Big Pond area

Au vein mineralization occurs north of the Betts Big Pond area at Arrowhead Pond, Long Pond, and West Pond Ridge among others. Following is a summary of the characteristics of mineralization in the northern Betts Cove Complex determined during this study and a comparison with the Betts Big Pond area.

1) Talc-carbonate at Arrowhead Pond is mineralogically and chemically similar to talc-carbonate in the Betts Big Pond area.

2) The alteration halo at Arrowhead Pond is enriched in SiO_2 as quartz relative to talc-carbonate. Otherwise, the alteration halo and talc-carbonate are similar.

3) The vein is not enriched in elements exotic to the talc-carbonate.

4) The composition of carbonate from the Betts Big Pond area is similar to that in the alteration halo and in the veins at Arrowhead Pond.

5) C and O isotopic compositions of carbonate from Au veins in the northern Betts Cove Complex are generally similar to those in the Betts Big Pond area.

6) The composition of vein forming fluids at Arrowhead Pond and Long Pond, determined from the analyses of fluid inclusions, are similar. In the case of the Long Pond vein, a single compositional type of primary fluid inclusion is consistent with the vuggy and crystalline nature of the vein (section 4.35). In the Arrowhead Pond veins, the trapping of three different fluid inclusion types is consistent with fluid unmixing during vein formation which is consistent with the banded nature of some of the veins and the deformational state of the quartz (section 4.35). The fluid inclusions similar to the Arrowhead Pond and Long Pond veins (i.e. H_2O-CO_2-NaCl-CH_4) were trapped at similar minimum temperatures and pressures that average approximately 250 °C and 1 kbar. The aqueous inclusions in the Arrowhead Pond vein were trapped at a lower temperature and pressure (section 4.35)

5.43 Timing of serpentinization and carbonatization

5.431 Introduction

A number of studies have considered alteration assemblages similar to those in the ultramafic rocks in the Betts Big Pond area. Eckstrand (1975) related the observed alteration facies

in the Dumont ultramafic body to metasomatic "fronts"; the first front being the conversion of peridotite to serpentinite and the second front being the conversion of serpentinite to talc-carbonate. Studies by Groves and Keays (1979), Keays et al. (1979), Frost (1985) and others have described similar peridotite - serpentinite - talc-carbonate associations in terms of metasomatic fronts. All of these studies either implicitely state or infer a single metasomatic event resulting in serpentinized and carbonatized ultramafic rocks.

In contrast to these studies, Hess (1933) indicates that carbonatization of serpentinite is a much later process and not associated with serpentinization. Moody (1976) suggests that the common association of serpentinized and carbonatized ultramafic rocks is due to carbonatization after serpentinization.

Serpentinite hosted Au veins are enclosed in a halo of carbonatized serpentinite at Allegheny California (e.g. Bohlke, 1989). Bohlke (1989) assumed that the peridotite was completely serpentinized prior to CO_2 hydrothermal activity associated with Au mineralization. However, Coveny (1981) shows that no data exists to determine the absolute timing of serpentinization and mineralization at Allegheny. Marshall and Taylor (1981) indicate that some serpentinization occurred during mineralization in the Allgeheny district. A lack of consensus also exists on the timing of serpentinization and mineralization in the northern Canadian Cordillera and Alaska.

Nesbitt et al. (1986) imply that serpentinization and mineralization were the same event whereas Pickthorn et al. (1987) maintain that no such link exists. With respect to ultramafic hosted Au mineralization in Proterozoic ophiolites in Africa, Buisson and LeBlanc (1987) indicate that carbonatization and Au concentration occurred during the later stages of serpentinization.

5.432 Betts Big Pond area

Au mineralization in the Betts Cove Complex is related to carbonatization as indicated by: 1) The occurrence of Au bearing talc-carbonate in the Betts Big Pond area; 2) The occurrence of carbonate in Au veins in the northern part of the ultramafic member; and 3) CO_2 in the fluid inclusions. However, the temporal relationship between serpentinization and carbonatization remains unknown.

Three phases of deformation are recognized in the Betts Cove Complex consistent with Taconic, Salinic, and Acadian Orogenies which are constrained to the periods > 440 Ma, 440-390 Ma, and 390-340 Ma respectively. Lydon et al. (1990), on the basis of $^{40}Ar/^{39}Ar$ age spectra from the Long Pond vein and Tom Showing illustrated vein formation during the period 427 Ma - 395 Ma (D_2; Salinic) (Figure 1.3) and partial resetting at < 350 Ma (D_3; Acadian) (Figure 1.3). This is consistent with the overprinting of D_2 by D_3 in the Long Pond to Beaver Cove Pond

area.

The D_2 fault that bounds the ultramafic rocks to the northwest is traceable from Long Pond to Kitty Pond, south of which it extends to Burtons Pond. It is interpreted as a D_2 fault as it records the westward movement of the ophiolitic rocks up and over the Cape St. John Group and Cape Brule Porphyry which is different from the southward polarity of D_3 which overprints in the Long Pond to Beaver Cove Pond area. D_3 is not recognized in the Betts Big Pond area and its effect in the area between Betts Big Pond and Long Pond is not known. On the basis of these structural relationships, carbonatization and the occurrence of Au at Betts Big Pond is consistent with its emplacement during the Salinic Orogeny, similar to the time of Au emplacement at Long Pond. The mineralogical, geochemical, and isotopic similarities between Long Pond, Arrowhead Pond, and Betts Big Pond support a similar timing but by no means prove it.

D_1 in the Betts Big Pond area, indicated by the thrust fault that forms the contact with basalt, appears to have been accompanied largely by serpentinization. However, the D_2 structure is characterized by dominantly serpentinite near Kitty Pond and talc-carbonate in the northern part of the Betts Big Pond map area. This distribution could have several explanations, three of which are: 1) serpentinization and carbonatization proceeded as fronts during the same metasomatic event; 2) they occurred as separate events during the Salinic

Orogeny; and 3) the D_2 structure is a reactivated D_1 structure, for example a ramp in a thrust zone, that was sepentinized during D_1 and carbonatized during D_2.

If serpentinization and carbonatization occurred as a single event, it may be reasonable to examine the hypothesis that Au in talc-carbonate was derived through the serpentinization of peridotite. In this respect it may be significant that:

1) Magmatic sulphides, which are thought to be Au bearing, were dissolved during serpentinization.

2) Fluid characteristics during serpentinization at Betts Big Pond appear to be favourable for the solution of $Au(HS)_2^-$.

3) The occurrence of Au in magnetite-rich Fe-Cu sulphide bearing serpentinite may indicate an Au-bearing serpentinizing fluid. Although this does not necessarily mean that the Au was derived from the dissolution of the magmatic sulphides.

4) The fluid during both serpentinization and carbonatization were > 250 °C and alkaline. Combined with the range of fO_2 defined by a minimum during serpentinization and a maximum during Au deposition in talc-carbonate, the fluid therefore has characteristics favourable to carry $Au(HS)_2^-$.

Further work to evaluate the role of serpentinization and carbonatization in the Betts Big Pond area in the concentration of Au could be:

1) Although the overall evolution of the fault is reasonably well constrained, details within the broad events

(i.e. Taconic, Salinic, and Acadian) are lacking, especially in the immediate areas of Au-vein mineralization. Thus, detailed structural mapping is required.

2) A detailed C, O, and H isotopic study of metasomatic minerals emphasizing their distribution with respect to deformational events.

3) An evaluation of the stability of magnesite during serpentinization in the Betts Big Pond area.

4) Analyses of magmatic sulphides to determine if, as predicted, they are Au bearing.

CONCLUSIONS

The ultramafic rocks in the Betts Big Pond area consist of dunite, harzburgite, orthopyroxenite, websterite, and wehrlite. These rocks are altered to serpentine and magnetite, serpentine, magnetite, and magnesite, serpentine, magnetite, magnesite, and talc, and talc, breunnerite, magnetite ± hematite. All peridotite sampled has Au abundances below detection limit (1 ppb) with one exception of 4 ppb. All serpentinite analyses have Au abundances below detection limit of 1 ppb with the exception of two samples that contain 22 and 26 ppb respectively. These slightly anomalous samples are magnetite-rich Cu-Fe sulphide bearing serpentinite. The Au content of the carbonate bearing rocks is variable and ranges from below detection limit to 1300 ppb in talc-carbonate. All of the samples with Au > 100 ppb are from a zone of talc-carbonate-hematite in the northern part of the map area.

Serpentinization resulted in the dissolution of magmatic sulphides. It is concluded that conditions attending serpentinization may have been favourable for the mobilization of Au and S from the magmatic sulphides. The occurrence of Au-bearing serpentinite may support this but does not preclude the possibility of an Au source outside the ultramafic rocks.

The occurrence of native gold in talc-carbonate is attributed to fluid oxidation due the carbonatization of magnetite in talc-carbonate. The Au-vein occurrences and

associated alteration in the northern part of the ultramafic member are similar with respect to mineralogy and chemistry and magnesite has similar C and O isotopic compositions. Au-vein mineralization in the northern Betts Cove Complex and disseminated Au mineralization in the Betts Big Pond area appear to have been emplaced at a similar time and under similar conditions.

REFERENCES

Abrajano, T.A., Sturchio, N.C., Kennedy, B.M., Lyon, G.L., Muehlenbachs, K., and Bohlke, J.K. 1990. Geochemistry of reduced gas related to serpentinization of the Zambales ophiolite, Phillipines. Applied Geochemistry, **5**: 625-630.

Abrajano, T.A. and Pasteris, J.D. 1989. Zambales ophiolite, Phillipines II. Sulphide petrology of the critical zone of the Acoje Massif. Contribution to Mineralogy and Petrology, **103**: 64-77.

Al, T. 1990. The character and setting of gold mineralization associated with the Betts Cove Complex. Unpublished MSc thesis, Memorial University of Newfoundland, St. Johns, Newfoundland.

Anonymous. 1972. Penrose field conference on ophiolites. Geotimes, **17**: 24-25.

Barnes, I., LaMarche, V.C., and Himmelberg, G. 1967. Geochemical evidence of present day serpentinization. Science, **156**: 830-832.

Barnes, I. and O'Neil, J.R. 1978. Present day serpentinization in New Caledonia, Oman, and Yugoslavia. Geochimica et Cosmochimimca Acta, **42**: 144-145.

Barnes, I. and O'Neil, J.R. 1969. The relationship between the fluids in some fresh alpine type ultramafic rocks and possible modern day serpentinization, Western United States. Geological Society of America Bulletin, **80**: 1947-1960.

Barton, P.B.Jr and Skinner, B.J. 1979. Sulphide mineral stabilities. *In* Geochemistry of Hydrothermal Ore Deposits. *Edited by* H.L. Barnes. John Wiley and Sons, New York. 278-403.

Bell, R. and Beischer, G. A. 1991. Gold exploration in the Betts Cove ophiolite. *In* Ore Horizons. *Edited by* H.S. Swinden and A. Hogan. Dept. of Mines and Energy, Government of Newfoundland and Labrador.

Bell, K. and Blenkinsop, J. 1977. Geochronological evidence of Hercynian activity in Newfoundland. Nature, **265**: 616-618.

Berman. R.G. 1991. Thermobarometry using multiequilibrium calculations: a new technique with petrologic applications. Canadian Mineralogist. **29**: 833-855.

Best. M.G. 1982. Igneous and metamorphic petrology. W.H. Freeman and Company, San Francisco, 630 p.

Blackwood, R.F. 1982. Geology of the Gander Lake (2D/15) and Gander River (2E/2) area. Department of Mines and Energy, Government of Newfoundland and Labrador, Report 82-4, 56 p.

Bliss, N.W. and MacLean, W.H. 1975. The paragenesis of zoned chromite from central Manitoba. Geochemica et Cosmochimica Acta, **39**: 973-990.

Bodnar, R.J. 1983. A method of calculating fluid inclusion volumes based on vapour bubble diameters and P-V-T-X properties of inclusion fluids. Economic Geology, **78**: 535-542.

Bohlke, J.K. 1989. Comparison of metasomatic reactions between a common CO_2-rich vein fluid and diverse wall rocks: Intensive variables, mass transfers, and Au-mineralization at Allegheny, California. Economic Geology, **84**: 291-327.

Bowers, T.S. and Helgeson, H.C. 1983. Calculation of the thermodynamic and geochemical consequences of nonideal mixing in the system H_2O-CO_2-NaCl on phase relations in geologic systems: Equations of state H_2O-CO_2-NaCl fluids at high pressures and temperatures. Geochimica et Cosmochimica Acta, **47**: 1247-1275.

Boyle, R.W. 1979. The geochemistry of gold and its deposits. Geological Survey of Canada Bulletin 280, 584 p.

Boyle, R.W. 1961. The geology, geochemistry and origin of gold deposits of the Yellowknife District. Geological Survey of Canada Memoir 310, 193 p.

Brimhill, G.H.Jr., Cunninghan, A.B., and Stoffgren, R. 1984. Zoning in precious metal distribution within base metal sulphides: A new lithologic approach using generalized inverse methods. Economic Geology, **79**: 556-589.

Brown, P.E. 1989. FLINCOR: A microcomputer program for the reduction and investigation of fluid inclusion data. American Mineralogist, **74**: 1390-1393.

Brown, P.E. and Lamb, W.M. 1989. P-V-T properties of fluids in the system H_2O-CO_2-NaCl; New graphical presentations and implications for fluid inclusion studies. Geochimica et Cosmochimica Acta, **53**: 1209-1221.

Buisson, G. and LeBlanc, M. 1986. Gold bearing listweanites (carbonatized ultramafic rocks) from ophiolite complexes. *In* Metallogney of basic and ultrabasic rocks. *Edited by* M.J. Gallagher, R.A. Ixer, C.R. Neary, and H.M. Prichard. The Institution of Mining and Metallurgy, 121-132.

Buisson, G. and LeBlanc, M. 1987. Gold in mantle peridotite from Upper Proterozoic ophiolites in Arabia, Mali, and Morocco. **82**: 2091-2097.

Bursnall, J.T. 1975. Stratigraphy, structure, and metamorphism west of Baie Verte, Burlington Peninsula, Newfoundland. Unpub. Phd thesis, Cambridge University, England, 337 p.

Bursnall, J.T. and de Wit, M.J. 1975. Timing and development of the orthotectonic zone in the Appalachian orogen of northwest Newfoundland. Canadian Journal of Earth Sciences, **12**: 1712-1722.

Cameron, W.E., Nisbet, E.G., and Dietrich, V.J. 1979. Boninites, komatiites, and ophiolitic basalts. Nature, **280**: 550-553.

Chamberlain, J.A., McLeod, C.R., Traill, R.J., and LaChance, G.R. 1965. Native metals in the muskox intrusion. canadian Journal of Earth Sciences, **2**: 188-215.

Campbell, I.H. and Barnes, S.J. 1984. A model for the geochemistry of the platinum group elements in magmatic sulphide deposits. Canadian Mineralogist, **22**: 151-160.

Chandler, F.W., Sullivan, R.W., and Currie, K.L. 1987. The age of the Springdale Group, Western Newfoundland, and correlative rocks-evidence for a Llandovery overlap assemblage in the Canadian Appalachians. Transactions of the Royal Society of Edinburgh, **78**: 41-49.

Chernosky, J.V.Jr., Berman, R.G., and Bryndzia, L.T. 1988. Stability, phase relations, and thermodynamic properties of chlorite and serpentine group minerals. *In* Hydrous phyllosilicates exclusive of micas. *Edited by* S.W. Bailey. Reviews In Mineralogy, Mineralogical Society of America, **1** 295-346.

Church, W.R. 1977. The ophiolites of southern Quebec: Oceanic crust of the Betts Cove type. Canadian Journal of Earth Sciences, **14**: 1668-1673.

Church, W.R. and Riccio, L. 1974. The sheeted dike layer of the Betts Cove Ophiolite Complex does not represent spreading: Discussion. Canadian Journal of Earth Sciences, **11**: 1499-1502.

Church, W.R. and Stevens, R.K. 1971. Early Paleozoic ophiolite complexes of the Newfoundland Appalachians as mantle-crust sequences. Journal of Geophysical Research, **76-5**: 1460-1466.

Coish, R.A. and Church, W.R. 1979. Igneous geochemistry of mafic rocks in the Betts Cove ophiolite, Newfoundland. Contributions to Mineralogy and Petrology, **70**: 29-39

Coish, R.A., Hickey, R. and Frey, F.A. 1982. Rare earth element geochemistry of the Betts Cove ophiolite, Newfoundland: complexities in ophiolite formation. Geochimical et Cosmochimica Acta, **46**: 2117-2134.

Colman-Sadd, S.P. 1982. Two stage continental collision and plate driving forces. Tectonophysics, **90**: 263-282.

Colman-Sadd, Hayes, J.P., and Knight, I. 1990. Geology of the Island of Newfoundland. Geological Survey Branch, Government of Newfoundland and Labrador, Map 90-01.

Coveny, R.M.Jr. 1981. Gold quartz veins and auriferous granite at the Oriental Mine, Allegheny District, California. Economic Geology, **76**: 2176-2199.

Coveny, R.M.Jr., Goebel, E.D., Zeller, E.J., Dreschhoff, G.A.M., and Angino, E.E. 1987. Serpentinization and the origin of hydrogen gas in Kansas. American Association of Petroleum Geologists, Bulletin, **71**: 39-48.

Coyle, M.L. 1990. Geology, Geochemistry, and Geochronology of the Springdale group, an Early Silurian caldera in central Newfoundland. Unpublished PhD thesis. Memorial University of Newfoundland, St. Johns, Newfoundland.

Coyle, M. and Strong, D.F. 1987. Geology of the Springdale Group: A newly recognized epicontinental-type caldera in Newfoundland. Canadian Journal of earth Sciences, **24**: 1135-1148.

Crawford, M.L. 1981. Fluid inclusions in metamorphic rocks - Low and medium grade. *In* Short Course in fluid inclusions: Applications to petrology. *Edited by* L.S. Hollister and M.L. Crawford. Mineralogical Association of Canada Short Course Handbook, **6**: 157-181.

Crocket, J.H. and Chyi, L.L. 1972. Abundances of Pd, Ir, Os, and Au in an alpine ultramafic pluton: 24th International Geological Congress, Montreal, Sec.10 p. 202-209.

Dallmeyer, R.D. 1977. $^{40}Ar/^{39}Ar$ age spectra of minerals from the Fleur de Lys Terrane in northwestern Newfoundland: Their bearing on chronology of metamorphism within the Appalachian orthotectonic zone. Journal of Geology, **85**: 89-103.

Dallmeyer, R.D. and Hibbard, J. 1984. Geochronology of the Baie Verte Peninsula, Newfoundland: Implications for the tectonic development of the Humber and Dunnage Zones of the Appalachian Orogen. Journal of Geology, **92**: 489-512.

DeGrace, J.R., Kean, B.F., Hsu, E., and Green, T. 1976. Geology of the Nippers Harbour map area (2E/13). Newfoundland, Dept. of Mines and Energy, Report 76-3.

de Wit, M.J. 1972. The geology around Bear Cove, eastern White Bay, Newfoundland. Phd thesis, Cambridge University, England, 232 p.

Dunning, G.R., Swinden, H.S., Kean, B.F., Evans, D.T.W. and Jenner, G.A. 1991. A Cambrian island arc in Iapetus: geochronology and geochemistry of the Lake Ambrose volcanic belt, Newfoundland Appalachians. Geological Magazine, **128**: 1-17.

Dunning, G.R., O'Brien, S.J., Colman-Sadd, S.P., Blackwood, R.F., Dickson, W.L., O'Neill, P.P., and Krogh, T.E. 1990. Silurian orogeny in the Newfoundland Appalachians. Journal of Geology, **98**: 895-913.

Dunning, G.R. and Krogh, 1985. Geochronolgy of ophiolites of the Newfoundland Appalachians. Canadian Journal of Earth Science, **22**: 1659-1670.

Drummond, S.E and Ohmoto, H. 1985. Chemical evolution and mineral deposition in boiling hydrothermal systems. Economic Geology, **80**: 126-147.

Eckstrand, O.R. 1975. The Dumont Serpentinite: A model for control of nickeliferous opaque mineral assemblages by alteration reactions in ultramafic rocks. Economic Geology, **70**: 183-201.

Erdmer, P. 1986. Geology of the Long Range Inlier in the Sandy Lake map area, western Newfoundland. Geological Survey of Canada, Paper 86-1b: 19-29.

Fabiani, W.M.B. 1984. Archean gold-copper mineralization in the Athens Mine, Mvuma, Zimbabwe. *In* Gold '82: The geology, geochemistry, and genesis of gold deposits. *Edited by* R.P. Foster. Geological Society of Zimbabwe Special Publication No. 1: 449-468.

Ferguson, H.G. and Gannett, R.W. 1932. Gold quartz veins of the Allegheny district, California. U.S. Geological Survey Proffessional Paper No. 172, 139 p.

Ferrill, B. A. and Thomas, W.A. 1988. Acadian dextral transpression and synorogenic sedimentary successions in the Appalachians. Geology, **16**: 604-608.

Foster, R.P. and Wilson, J.F. 1984. Geological setting of Archean gold deposits in Zimbabwe. *In* Gold '82: The geology, geochemistry, and genesis of gold deposits. *Edited by* R.P. Foster. Geological Society of Zimbabwe Special Publication No. 1: 521-552.

Frost, B.R. 1979. Mineral equilibria involving mixed volatiles in a C-O-H fluid phase: The stabilities of siderite and graphite. American Journal of Science, **279**: 1033-1059.

Frost, B.R. 1985. On the stability of sulphides, oxides, and native metals in serpentinite. Journal of Petrology, **26**: 31-63.

Fyon, J.A., Crocket, J.H., and Schwarz, H.P. 1983. Magnesite abundance as a guide to gold mineralization associated with ultramafic flows, Timmins area. Journal of Geochemical Exploration, **18**: 245-266.

Fyffe, L.R. and Swinden, H.S. 1991. Paleotectonic setting of Cambro-Ordovician volcanic rocks in the Canadian Appalachians. Geoscience Canada, **18**: 145-157.

Gale, G.H. 1973. Paleozoic basaltic komatiite and ocean floor type basalts from northeast Newfoundland. Earth and Planetary Science Letters, **18**: 22-28.

Garuti, G., Gorgoni, C., and Sighinolfi, G.P. 1984. Sulphide mineralogy and siderpohile element abunadnces in the Ivrea-Verbano mantle peridotites (western Italian Alps), Earth and Planetary Science Letters, **70**: 69-87.

Goodwin, L.B. and Williams, P.F. 1990. Strike-slip motion along the Baie Verte Line, Newfoundland. Atlantic Geoscience Society Colloquium, 1990, Program with Abstracts: 13

Gower, D., Graves, G., Walker, S., and MacInnis, D. 1990. Lode gold mineralization at Deer Cove, Point Rousse Complex, Baie Verte Peninsula. *In* Metallogenic framework of base and precious metal deposits, central and western Newfoundland. *Edited by* H.S. Swinden, D.T.W. Evans, and B.F. Kean. Geological Survey of Canada Open File 2156: 165-172.

Grant, J.A. 1986. The isocon diagram - A simple solution to Gresens' equation for metasomatic alteration. Economic Geology, **81**: 1976-1982.

Greenwood, H.J. 1967. Mineral equilibria in the system MgO-SiO_2-H_2O-CO_2. *In* Researches in geochemistry. *Edited by* P.H. Abelson. John Wiley and Sons, New York: 542-567.

Gresens, R.L. 1967. Composition-volume relationships of metamorphism. Chemical Geology, **2**: 47-65.

Groves, D.I., Phillips, G.N., Ho, S.E., Henderson, C.A., Clark, M.E., and Wood, G.M. 1984 Controls on distribution of Arcean hydrothermal gold deposits in Australia. *In* Gold '82: The geology, geochemistry, and genesis of gold deposits. *Edited by* R.P. Foster. Geological Society of Zimbabwe Special Publication No. 1: 689-712.

Groves, D.I. and Phillips, G.N. 1987. The genesis and tectonic control on Archean gold deposits of the Western Australian shield - A metamorphic replacement model. Ore Geology Reviews, **2**: 287-322.

Groves, D.I. and Keays, R.R. 1979. Mobilization of ore-forming elements during alteration of dunites, Mt. Keith-Betheno, Western Australia. Canadian Mineralogist, **17**: 373-389.

Hamlyn, P.R. and Keays, R.R. 1986. Sulphur saturation and second stage melts. Economic Geology, **81**: 1431-1445.

Hamlyn, P.R., Keays, R.R., Cameron, W.E., Crawford, A.J., Waldron, H.M. 1985. Precious metals in megnesian low-Ti lavas: Implications for metallogenesis and sulphur saturation in primary magmas. Geochemica et Cosmochimica Act, **49**: 1797-1811.

Helgeson, H.C. and Garrels, R.M. 1968. Hydrothermal transport and deposition of gold. Economic Geology, **63**: 622-635.

Henley, R.W. 1973. Solubility of gold in hydrothermal chloride solutions. Chemical Geology, **11**: 73-87.

Henley, R.W., Truesdall, A.H., and Barton, P.B.Jr., 1894. Fluid-mineral equilibria in hydrothermal systems. Reviews in Economic Geology, volume 1, Society of Economic geologists.

Hess, H.H. 1933. The problem of serpentinization and the origin of certain chrysotile asbestos and talc soapstone deposits. Economic Geology, **28**: 634-657.

Hibbard, J. 1983. Geology of the Baie Verte Peninsula, Newfoundland. Newfoundland Department of Mines and Energy, Memoir 2, 279 p.

Hibbard, J. 1987. Ophiolitic melange along the Baie Verte Line, Coachmans Harbour, Newfoundland. Geological Society of America Centennial Field Guide-Northeastern Section, 457-462.

Hickey, R.L. and Frey, F.A. 1982. Geochemical characteristics of boninite series volcanics: implications for their source. Geochimica et Cosmochimica Acta, **46**: 2099-2115.

Ho, S.E., Groves, D.I., and Phillips, G.N. 1985. Fluid inclusions as indicators of the nature and source of ore fluids and ore depositional conditions for Archean gold deposits of the Yilgarn block, Western Australia. Transactions of the Geological Society of South Africa, **88**: 149-158.

Hodgson, C.J. 1989. The structure of shear related, vein-type gold deposits: A review. Ore Geology Reviews, **4**: 231-273.

Hodgson, C.J. and MacGeehan, P.J. 1982. Geological characteristics of gold deposits in the Superior Province of the Canadian Shield. Canadian Institute of Mining and Metallurgy, Special Volume 24: 211-231.

Huard, A.A. 1990. The Noranda/Impala Stog'er Tight gold deposit.*In* Metallogenic framework of base and precious metal deposits, central and western Newfoundland. *Edited by* H.S. Swinden, D.T.W. Evans, and B.F. Kean. Geological Survey of Canada Open File 2156: 173-177.

Jacobs, G.K. and Kerrick, D.M. 1981. Methane: An equation of state with application to the ternary system H_2O-CO_2-CH_4. Geochimica et Cosmochimica Acta, **45**: 607-614.

Jamieson, R.A. 1990. Metamorphism of an Early Paleozoic continental margin, western Baie Verte Peninsula, Newfoundland. Journal of Metamorphic Geology, **8**: 269-288.

Jamieson, R.A. and Vernon, R.H. 1987. Timing of porphyroblast growth in the Fleur de Lys Supergroup, Newfoundland. Journal of Metamorphic Geology, **5**: 273-288.

Janecky, D.R. and Seyfried, W.E.Jr. 1986. Hydrothermal serpentinization of peridotite within the oceanic crust: Experimental investigations of mineralogy and major element chemistry. Geochimica et Cosmochimica Acta, **50**: 1357-1378.

Jenner, ,G.A., Swinden, H.S., Dunning, G., Szybinski, A., and Kean, B. 1990. Tectonic setting and petrogenesis of central Newfoundland ophiolites: Geochemical and Sm/Nd isotopic constraints. Symposium on ophiolite genesis and evolution of oceanic lithosphere. Ministry of Petroleum and Minerals, Oman. Volume of abstracts.

Jenner, G.A., Dunning, G.R., Malpas, J., Brown, M., and Brace, T. 1991. Bay of Islands and Little Port Vomplexes revisited: age, geochemical, and isotopic evidence confirm suprasubduction zone origin. Canadian Journal of Earth Sciences, **28**: 1635-1652.

Johannes, W. 1969. An experimental investigation of the system $MgO-SiO_2-H_2O-CO_2$. American Journal of Science, **267**: 1083-1105.

Keays, R.R. 1987. Principles of mobilization (dissolution) of metals in mafic and ultramafic rocks - The role of immiscible magmatic sulphides in the generation of hydrothermal gold and volcanogenic massive sulphide deposits. Ore Geology Reviews, **2**: 47-63.

Keays, R.R. 1984. Archean gold deposits and their source rocks: The upper mantle connection. *In* Gold '82: The geology, geochemistry, and genesis of gold deposits. *Edited by* R.P. Foster. Geological Society of Zimbabwe Special Publication No. 1: 17-52.

Kean, B.F., Dean, P.L., and Strong, D.F. 1981. Regional geology of the Central Volcanic Belt of Newfoundland. Geological Association of Canada Special Paper 22: 65-78.

Kennedy, M.J. 1971. Structure and stratigraphy of the Fleur de Lys Supergroup in the Fleur de Lys area, Burlington Peninsula, Newfoundland. Geological Association of Canada, Proceedings, **24**: 59-71.

Kerrich, R. and Fyffe, W.S. 1981. The gold-carbonate association: Souirce of CO_2 and CO_2 fixation reactions in Archean lode deposite. Chemical Geology, **33**: 265-294.

Kidd, W.S. 1974. The evolution of the Baie Verte Lineament, Burlington Peninsula, Newfoundland. Phd thesis, Cambridge University, England, 294 p.

Kidd, W.S.. Dewey, J.F., and Bird, J.M. 1978. The Mings Bight Ophiolite Complex, Newfoundland: Appalachian oceanic crust and mantle. Canadian Journal of Earth Sciences, **15**: 781-804.

Knopf, A. 1929. The Motherlode system of California. U.S. Geological Survey professional paper 157, 103 p.

Krauskopf, K.B. 1951. The solubility of gold. Economic Geology, **46**: 858-870.

Kretz, R. 1983. Symbols for rock forming minerals. American Mineralogist, **60**: 277-279.

Lavigne, J. 1988. Stratigraphic position and gold enrichment of the Beaver Cove Pond Gold Occurrence. BSc thesis, Memorial University of Newfoundland, 75 p.

Lydon, J.W. and Galley, A. 1986. Chemical and mineralogical zonation in the Mathiati alteration pipe, Cyprus, and its genetic significance. *In* Metallogney of basic and ultrabasic rocks. *Edited by* M.J. Gallagher, R.A. Ixer, C.R. Neary, and H.M. Prichard. The Institution of Mining and Metallurgy, 49-68.

Lydon, J.W., Lavigne, J., and Roddick, J.C.M. 1990. The relationship of gold mineralization to the thermal and tectonic history of the Baie Verte Peninsula, Newfoundland. Geological Survey of Canada, Mineral Colloquium, Program with Abstracts: 26.

Mattinson, J.M. 1977. U-Pb ages of some crystalline rocks from the Burlington Peninsula, Newfoundland, and implications for the age of the Fleur de Lys metamorphism. Canadian Journal of Earth Sciences, **14**: 2316-2324.

MacDougall, C. and MacInnis, D. 1990 The Dorset Showing: A structurally controlled lode gold occurrence adjacent to the Baie Verte Line. *In* Metallogenic framework of base and precious metal deposits, central and western Newfoundland. *Edited by* H.S. Swinden, D.T.W. Evans, and B.F. Kean. Geological Survey of Canada Open File 2156: 162-164.

Marshall, B. and Taylor, B.E. 1981. origin of hydrothermal fluids responsible for gold deposition, Allegeheny district, Sierra County, California. U.S. Geological Survey Open file report **81-355**: 280-293.

Moody, J.B. 1976. Serpentinization: A review. Lithos, **9**: 125-138

Neale, E.R.W. 1957. Ambiguous intrusive relationship of the Betts Cove-Tilt Cove Serpentinite Belt, Newfoundland. Geological Association of Canada Proceedings, **9**: 95-107.

Neale, E.R.W. and Nash, W.A. 1963. Sandy Lake (east half) Geological Survey of Canada Paper 62-28: 40 p.

Neale, E.R.W., Kean, B.F., and Upadhyay, H.D. 1975. Posy-ophiolite unconformity, Tilt Cove-Betts Cove area, Newfoundland. Canadian Journal of earth Sciences, **12**: 880-886.

Neale, E.R.W. and Kennedy, M.J. 1967. Relationship of the Fleur de Lys Group to younger groups of the Burlington Peninsula, Newfoundland. In Geology of the Atlantic region,Sd. E.R.W. Neale and H. Williams, Geological Association of Canada Special Paper **4**: 139-169.

Nesbitt, B.E., Murowchick, J.B., Muehlenbachs, K. 1986. Dual origins of lode gold deposits in the Canadian Cordillera, **14**: 506-509.

Norman, R.E. and Strong, D.F. 1975. The geology and geochemistry of ophiolitic rocks exposed at Ming Bight, Newfoundland. Canadian Journal of earth Sciences, **12**: 777-797

Ohmoto, H. 1972. Systematics of sulfur and carbon isotopes in hydrothermal ore deposits. Economic Geology, **67**: 551-578.

Oshin, I.O. and Crocket, J.H. 1982. Noble metals in Thetford Mine ophiolites, Quebec, Canada. Part I: Distribution of gold iridium, platinum, and palladium in the ultramafic and gabbroic rocks. Economic Geology, **77**: 1556-1570.

Peach, C.L., Mathez, E.A., and Keays, R.R. 1990. Sulphide melt-silicate melt distribution coefficients for noble metals and other chalcophile elements as deduced from MORB: Implications for parial melting. Geochemica et Cosmochimica Act, **54**: 3379-3389.

Pearce, J.A. 1975. Basalt geochemistry used to investigate past tectonic environments on Cyprus. Tectonophysics, **25**: 41-67.

Phillips, G.N. and Groves, D.L. 1984. Fluid access and fluid-wall rock interaction in the genesis of the Archean gold-quartz vein deposit at Hunt Mine, Kambalda, Western Australia. *In* Gold '82: The geology, geochemistry, and genesis of gold deposits. *Edited by* R.P. Foster. Geological Society of Zimbabwe Special Publication No. 1: 389-416.

Pickthorn, W.J., Goldfarb, R.J., and Leach, D.L. 1987. Comment on "Dual origin of gold deposits in the Canadian Cordillera". Geology, **15**: 471-473.

Piasecki, M.A.J. 1988. Strain-induced mineral growth in ductile shear zones and a preliminary study of ductile shearing in western Newfoundland. Canadian Journal of Earth Sciences, **25**: 2118-2129.

Pringle, G.J. 1993. MINREP: A fortran computer program to produce tables of mineral analyses with formula and endmembers. Geological Survey of Canada Open File 2596.

Pyke, D.R. 1976. On the relationship between gold mineralization and ultramafic volcanic rocks in the Timmins area, northeastern Ontario. Canadian Institute of Mining and Metallurgy Bulletin, **69**: 79-87.

Ramsay, J.G. 1980. The crack-seal mechanism of rock deformation. Nature, **284**: 135-139.

Razin, L.V., Khvostov, V.P., and Novikov, V.A. 1965. Platinum metals in the essential and accessory minerals of ultramafic rocks. Geochemistry International, **2**: 118-131.

Robert, F. and Kelly, W.C. 1987. Ore forming fluids in Archean gold bearing quartz veins at the Sigma Mine, Abitibi Greenstone Belt, Quebec, Canada. Economic Geology, **82**: 1464-1482.

Roberts, R.G. 1987. Archean lode gold deposits. Geoscience Canada, **14**: 1-14.

Rodgers, G. and Neale, E.R.W. 1969. Possible "Taconic" klippen in western Newfoundland. American Journal of Science, **261**: 713-730.

Roedder, E. 1984. Fluid Inclusions. Reviews in mineralogy, Mineralogical Society of America, **12**: 646 p.

Romberger, S.B. 1895. Geochemistry of gold in hydrothermal deposits. *In* Introduction to geology and resources of gold and the geochemistry of gold. pp A9-A25.

Ross, J.R. and Keays, R.R. 1979. Precious metals in volcanic type nickel sulphide deposits in Western Australia, 1. Relationship with the composition of the ores and their host rocks. Canadian Mineralogist, **17**: 417-435.

Saunders, A.D., Marsh, N.G., and Wood, D.A. 1980. Ophiolites as ocean crust or marginal basin crust. *In* Ophiolites: Proceedings of the International Ophiolite Symposium. *Edited by* A. Panayiotou. Cyprus Ministry of Agriculture d Natural Resources, Nicosia, pp. 193-204.

Schwarcz, H.P. 1986. Cyanide in gold deposits. Ontario Geological Survey Miscellaneous Paper 130, 161-164.

Searle, M.P. and Stevens, R.K. 1984. Obduction processes in ancient, modern and future ophiolites. *In* Ophiolites and oceanic lithosphere. *Edited by* I.G. Gass, S.J. Lippard, and A.W. Shelton. Geological Society Special Publication No. 13: 303-320.

Serri, G. 1981. The petrochemistry of ophiolte gabbroic complexes: A key for the classification of ophiolites into low-Ti and high-Ti types. Earth and Planetary Science Letters, **52**: 203-212.

Seward, T.M. 1984. The transport and deposition of gold in hydrothermal systems. *In* Gold '82: The geology, geochemistry, and genesis of gold deposits. *Edited by* R.P. Foster. Geological Society of Zimbabwe Special Publication No. 1: 165-181.

Seward, T.M. 1973. Thiocomplexes of gold and the transport of gold in hydrothermal solutions. Geochimica et Cosmochimica Acta, **37**: 379-399.

Shervais, J.W. 1982. Ti-V plots and the petrogenesis of modern and ophiolitic lavas. Earth and Planetary Science Letters, **59**: 101-118.

Sibson, R.H., Robert, F., and Poulsen, K.H. 1988. High angle reverse faults, fluid pressure cycling and mesothermal gold deposits. Geology, **16**: 551-555.

Stevens, R.K. 1970. Cambro-Ordovician flysch sedimentation and tectonics in west Newfoundland and their possible bearing on a proto-Atlantic ocean. In Flysch Sedimentation, Ed. J. Lajoie, Geological Association of Canada, Special Paper 7: 165-177.

Stevens, R.K., Church, W.R., and St. Julien, P. 1969. Age of ultramafic rocks in the northwestern Appalachians. Geological Society of America, Program with abstracts: 215-216.

Stone, W.E., Crocket, J.H., and Fleet, M.E. 1990. Partitioning of palladium, iridium, platinum, and gold between sulphide liquid and basalt melt at 1200 °C. Geochemica et Cosmochimica Act, **54**: 2341-2344.

Streckeisen, A. 1979. Classification and nomenclature of volcanic rocks, lamprophyres, carbonatites, and melilitic rocks: Recomendations and suggestions of the IUGS subcommision on the systematic of igneous rocks. Geology. **7**; 331-335.

Sun, S. and nesbitt, R.W. 1978. Geochemical regularities and genetic significance of ophiolitic basalts. Geology, **6**: 689-693.

Thayer, T.P. 1966. Serpentinization considered as a constant volume metasomatic process. American Mineralogist, **51**: 685-710.

Thompson, J.B. 1982. Composition space: An algebraic and geometric approach. *In* Characterization of metamorphism through mineral equilibria. *Edited by* J.M. Ferry. Mineralogical Society of America, Reviews in Mineralogy, **10**: 1-31.

Touret, J. 1987. Fluid distribution in the continental lithosphere. *In* Proterozoic Lithosphere Evolution. *Edited by* A. Kroner. American Geophysical Union, Geodynamic Series, **17**.

Trommsdorff, V. and Evans, B.W. 1977. Antigorite-ophiocarbonates: phase relations in a portion of the system $CaO-MgO-SiO_2-H_2O-CO_2$. Contributions to Mineralogy and Petrology, **60**: 39-56.

Tuach, J., Dean, P.L., Swinden, H.S., O'Driscoll, C.F., Kean, B.F., and Evans, D.T.W. 1988. Gold mineralization in Newfoundland: A 1988 review. Department of Mines, Government of Newfoundland and Labrador, **88-1**: 279-306.

Ulmer, G.C. 1974. Alteration of chromite during serpentinization in the Pennsylvania-Maryland district. American Mineralogist, **59**: 1236-1241.

Upadhyay, H.D. 1973. The Betts Cove ophiolite and related rocks of the Snooks Arm Group, Newfoundland, Unpublished PhD thesis, Memorial University of Newfoundland, St. John Newfoundland.

Upadhyay, H.D. 1982. Ordovician komatiites and associated boninite-type magnesian lavas from Betts Cove, Newfoundland. *In* Komatiites. *Edited by* N.T. Arndt and E.G. Nisbet. George Allen and Unwin, Boston: 187-198.

van der Pluijm, B.A. and van Stall, C.R. 1988. Characteristics and evolution of the Central Mobile Belt, Canadian Appalachians. Journal of Geology, **96**: 535-548.

Viljoen, M.J. 1984. Archean gold mineralization and komatiites in southern Africa. *In* Gold '82: geology, geochemistry, and genesis of gold deposits. *Edited by* R.P. Foster. Geological Society of Zimbabwe Special Publication No. 1: 583-594.

Vincent, E.A. and Crocket, J.H. 1960. Studies on the geochemistry of gold, I, The distribution of gold in rocks and minerals of the Skaergaard Intrusion, East Greenland. Geochimical et Cosmochimica Acta. **18**: 130-142,

Weissberg, B.G. 1970. Solubility of gold in hydrothermal alkaline sulphide solutions. Economic Geology, **65**: 551-556.

Whalen, J.B., Currie, K.L., and van Breeman, O. 1987. Episodic Ordovician-Silurian plutonism in the Topsails igneous terrane, western Newfoundland. Transactions of the Royal Society of Edinburgh,, **78**: 17-28.

Williams, H. 1964. The Appalachians in northeast Newfoundland - a two-sided symmetrical system. American Journal of Science, **262**: 1127-1158.

Williams, H. 1977. Ophiolitic melange and its significance in the Fleur de Lys Supergroup, northern Appalachians. Canadian Journal of Earth Sciences, **14**: 987-1003.

Williams, H. 1979. The Appalachian Orogen in Canada. Canadian Journal of Earth Sciences, **16**: 792-807.

Williams, H., Colman-Sadd, S.P., and Swinden, H.S. 1988. Tectonic-stratigraphic subdivisions of central Newfoundland. Geological Survey of Canada, Paper 88-1B: 91-98.

Williams H. and Smyth, W.R. 1973. Metamorphic aureoles beneath ophiolite suites and alpine peridotites: tectonic implications with west Newfoundland examples. American Journal of Science, **273**: 592-621.

Williams, H, and Stevens, R.K. 1974. The ancient continental margin of eastern North America. In The Geology of the Continental Margins, Edited bya. Burk and C.L. Drake. Springer-Verlag, New York, pp. 781-796.

Williams, H. and St. Julien, P. 1982. The Baie Verte_Brompton Line: Early Paleozoic continent ocean interface in the Canadian Appalachians. *In* major structural zones and faults of the northern Appalachians. *Edited by* P. St. Julien and J. Beland. Geological Association of Canada Special Paper 24: 177-208.

Williams, H., Hibbard, J., and Bursnall, J. 1977. Geologic setting of asbestos-bearing ultramafic rocks along the Baie Verte Lineament, Newfoundland. Geological Survey of Canada, Paper 77-1A: 351-360.

Wood, D.A., Joron, J.L., and Treuil, M. 1979. A re-appraisal of the use of trace elements to classify and discriminate between magma series erupted in different tectonic settings. Earth and Planetary Science Letters, 50: 326-336.

Wood, P.C., Burrows, D.R., Thomas, A.V., and Spooner, E.T.C. 1986. The Hollinger-McIntyre Au-quartz vein system , Timmins Ontario, Canada: geologic characteristics, fluid properties, and light stable isotope geochemistry. *In* Gold'86. *Edited by* A.J. MacDonald. Konsult International Inc., Willowdale, Ontario. p. 56-80.

Appendix I - Analytical Methods

Whole rock chemical analyses

Table of whole rock analytical methods, detection limits, and precision

	Method	Unit	Limit	Precision (± %)		Method	Unit	Limit	Precision (± %)
SiO_2	XRF	%	0.01	1.0	Cd	DCP	ppm	1.00	31.4
Al_2O_3	XRF	%	0.01	1.0	Mo	DCP	ppm	1.00	13.6
TiO_2	XRF	%	0.01	2.2	Pb	DCP	ppm	2.00	24.7^b
MgO	XRF	%	0.01	1.6	Se	GFAA	ppm	0.10	na
CaO	XRF	%	0.01	1.4	Y	XRF	ppm	2.00	6.4
K_2O	XRF	%	0.01	2.2	Zr	XRF	ppm	3.00	7.3^a-1.8^b
Na_2O	XRF	%	0.01	2.6	Nb	XRF	ppm	10.00	14.2^a-18.3^b
Fe_2O_3	XRF	%	0.01	2.8	Ba	XRF	ppm	10.00	9.5^a-3.7^b
MnO	XRF	%	0.01	1.4	Cr	DCP	ppm	2.00	na
P_2O_5	XRF	%	0.01	3.0	Sr	XRF	ppm	2.00	18.6^a-2.6^b
CO_2	WET	%	0.01	3.0	Rb	XRF	ppm	2.00	40.9^a-14.9^b
H_2O	WET	%	0.01	na	As	XRF	ppm	3.00	13.2^a-4.9^b-2.6^c
S	XRF	%	0.01	50.0	Tl	DCP	ppm	2.00	3.3
Co	DCP	ppm	1.00	4.0^b-1.3^c	Ag	DCP	ppm	0.50	15.3
Ni	DCP	ppm	1.00	4.0^a-2.1^b-0.8^c	Au	FADCP	ppb	1.00	20.0^a-10.0^b-5.0^c
Cu	DCP	ppm	0.50	26.4^a-6.4^b	Pt	FADCP	ppb	10.00	na
Zn	DCP	ppm	0.50	3.0^a-6.0^b	Pd	FADCP	ppb	2.00	na

Abbreviations: XRF - X-ray fluorescence (fused disk)
DCP - Direct current plasma
wet - Wet chemistry; H_2O - combustion/infrared; CO_2 - acid evolution/infrared
FADCP - Fire assay/direct current plasma
GFAA - Graphite furnace/atomic absorption

Precision: Reported by XRAL X-ray Assay Laboratories
a = precision for the concentration which ranges from 1 - 10 times the detection limit
b = precision for the concentration which ranges from 10 - 100 times detection limit
c = precision for the concentration which ranges from 100 - 1000 times the detection limit
na = not available

All chemical analyses were provided by the Geological Survey of Canada through the Canada-Newfoundland Mineral Development Agreement (1985-1989). They were completed at XRAL X-ray Assay Laboratories, Don Mills, Ontaio. Tabulated are the analytical methods, detection limits, and precision data.

Mineral compositions

All mineral compositions were determined by the author at the Geological Survey of Canada with a Cameca Electron Microprobe. The analyses were obtained from carbon coated polished thin sections. Operating conditions were 15 kV accelerating voltage, a 10 nA beam current, a 10-20 s counting time, and approximately 1 μm spot size. Analyses are accurate to 0.1 wt. %. The method of Pouchou and Pichoir (1984) was used to calculate wt %. Standards used are as follows:

Serpentine and talc	Carbonate	Chromite and magnetite
Na - NaCl	Ca - calcite	Mg - periclase
K - KBr	Mg - magnesite	Al - corumdum
Fe - magnetite	Fe - siderite	V - vanadium
Mg - periclase	Mn - rhodocrosite	Si - quartz
Si - quartz	Sr - celestite	Ti - rutile
Ca - wollastonite	Ba - barite	Fe - magnetite
Mn - rhodonite		Ni - nickel
Ti - rutile		Cr - chromite
Cr - chromite		Mn - rhodonite
Al - corundum		Zn - zinc
Ni - millerite		

Mineral formulaes were calculated with the computer program of Pringle (1993). Formulae for average compositions are reported with the oxide data in Appendix II.

Isotope compositions

Carbon and oxygen isotope compositions of magnesite were determined in the Stable Isotope Laboratory at the University of Ottawa. This includes both the data obtained during this study and the unpublished GSC data used in this study. Magnesite was digested with 100 % H_3PO_4 for 21 days at 50 °C. $^{13}C/^{12}C$ and $^{18}O/^{16}O$ ratios of evolved CO_2 were determined with a VG SIRA 12 mass spectrometer. Carbon and oxygen isotope ratios are reported using the normal δ-notation relative to PeeDee Belemnite (PDB) and Standard Mean Ocean Water (SMOW) respectively. Precision on $^{13}C/^{12}C$ and $^{18}O/^{16}O$ ratios are 0.1 and 0.2 $^{0}/_{00}$ respectively.

X-ray diffraction analyses

Mineral identification of whole rock powders was carried out at the Geological Survey of Canada using a PW-1830 X-ray diffractometer. Operating conditions were: Cu Kα radiation; 50 KV; 30 m amps; and sample rotation from 3° to 63°.

Fluid inclusion methodology

Fluid inclusion studies were carried out in the Fluid Inclusion Laboratory at the University of Ottawa. Petrographic studies and microthermometric determinations utilized approximately 100 μm thick, doubly polished sections using a modified USGS Fluid Inc. gas flow heating and freezing stage. The USGS stage is fully described by Roedder (1984). It was calibrated at CO_2 melting temperature (-56.6 °C), H_2O melting temperature (±0.0 °C), and the H_2O triple point (374.1 °C) using synthetic inclusions from Synflinc Inc. Calibration was checked regularly and no correction was required. Microthermometric determinations were made by temperature cycling. Precision for melting temperatures and CO_2 homogenization are ±0.1 °C and ±1.0 °C for total homogenization temperatures.

Appendix II - Whole Rock Chemical Data

Peridotite

Sample	NT-1	NT-3	NT-4	NT-5	NT-6	NT-0423	NT-0424
SiO2	41.60	37.80	38.20	44.30	40.80	40.30	39.60
Al2O3	0.76	0.58	0.64	1.79	0.38	0.49	0.50
TiO2	b.d	b.d	b.d	b.d	b.d	0.02	0.02
MgO	36.50	38.95	39.30	30.45	40.50	37.40	37.10
CaO	0.82	b.d	0.00	5.14	b.d	0.08	0.08
Na2O	0.07	0.01	0.01	0.05	0.01	0.04	0.03
K2O	0.01	b.d	0.01	0.01	b.d	b.d	b.d
Fe2O3	9.23	10.76	9.23	9.37	6.77	9.38	9.28
MnO	0.14	0.14	0.07	0.17	0.10	0.16	0.17
P2O5	0.01	b.d	b.d	b.d	b.d	0.01	0.01
CO2	0.01	0.01	0.01	0.01	0.01	0.08	0.10
H2OP	10.94	11.25	12.21	8.02	11.80	11.40	7.70
S	0.01	0.01	0.01	0.01	0.01	b.d	0.01
TOTAL	100.10	99.51	99.69	99.32	100.38	99.37	94.61
Co	91	111	117	85	84	98	96
Ni	1200	1300	1600	700	2000	1600	1400
Cu	b.d	b.d	b.d	11	b.d	b.d	b.d
Zn	27	40	12	31	39	32	34
Mo	b.d	b.d	b.d	b.d	b.d	b.d	b.d
Cd	b.d	b.d	b.d	b.d	b.d	b.d	b.d
Pb	b.d	b.d	b.d	b.d	b.d	b.d	b.d
Y	4	4	4	4	4	4	6
Zr	12	12	12	14	10	13	11
Nb	b.d	b.d	b.d	b.d	b.d	b.d	b.d
Ba	10	10	10	10	10	10	15
Cr	3500	3500	2800	3000	2200	2000	1600
Se	b.d	b.d	b.d	b.d	b.d	b.d	b.d
Sr	5	2	2	5	2	2	2
Rb	b.d	b.d	b.d	b.d	b.d	14	7
As	b.d	b.d	6	b.d	3	7	7
Tl	b.d	b.d	b.d	b.d	b.d	b.d	b.d
Ag	b.d	b.d	b.d	b.d	b.d	b.d	b.d
Au	b.d	4	b.d	b.d	b.d	b.d	b.d
Pt	b.d	b.d	b.d	b.d	b.d	20	b.d
Pd	b.d	b.d	b.d	b.d	b.d	9	5

b.d - below detection limit
total iron as Fe_2O_3
significant figures for Ni and Cr = 2; all others as in detection limits (Appendix I)

Peridotite

Sample	NT-0422
SiO2	38.90
Al2O3	0.98
TiO2	0.03
MgO	36.60
CaO	0.09
Na2O	0.03
K2O	b.d
Fe2O3	8.83
MnO	0.12
P2O5	0.01
CO2	0.13
H2OP	11.90
S	0.02
TOTAL	97.64
Co	99
Ni	1500
Cu	b.d
Zn	24
Mo	b.d
Cd	b.d
Pb	b.d
Y	5
Zr	12
Nb	11
Ba	24
Cr	1700
Se	b.d
Sr	3
Rb	5
As	b.d
Tl	b.d
Ag	b.d
Au	b.d
Pt	b.d
Pd	5

b.d - below detection limit
total iron as Fe_2O_3
significant figures for Ni and Cr = 2; all others as in detection limits (Appendix I)

Serpentinite

Sample	NT-0301	NT-0326	NT-0327	NT-0328	NT-0329	NT-0426	NT-0427
SiO2	41.20	21.20	12.20	40.40	41.40	38.90	38.20
Al2O3	0.36	0.50	0.37	0.26	0.25	0.68	0.66
TiO2	0.02	0.01	0.02	0.02	0.02	0.02	0.02
MgO	38.10	18.00	10.16	36.50	37.40	37.80	37.10
CaO	0.13	0.07	0.08	0.13	0.08	0.07	0.08
Na2O	0.02	0.07	0.06	0.06	0.04	0.02	b.d
K2O	b.d	b.d	b.d	b.d	0.02	b.d	b.d
Fe2O3	7.44	52.70	74.34	9.07	6.41	8.92	9.86
MnO	0.08	0.07	0.06	0.08	0.08	0.11	0.10
P2O5	0.01	0.01	0.01	0.01	0.01	0.01	0.01
CO2	0.13	0.06	0.02	0.14	0.06	0.10	0.16
H2OP	12.10	6.20	3.40	11.50	12.10	12.20	11.30
S	b.d	0.06	0.13	0.06	0.04	0.01	b.d
TOTAL	99.60	98.96	100.85	98.23	97.91	98.84	97.50
Co	93	180	130	180	91	93	78
Ni	2500	1700	1700	2700	2400	1500	1200
Cu	1	310	590	28	5	b.d	b.d
Zn	24	54	71	37	30	24	32
Mo	b.d	b.d	b.d	b.d	b.d	b.d	b.d
Cd	2	b.d	b.d	b.d	1	b.d	b.d
Pb	b.d	b.d	b.d	b.d	b.d	b.d	6
Y	4	b.d	b.d	7	8	5	3
Zr	11	18	12	18	17	14	16
Nb	b.d	20	25	b.d	b.d	18	b.d
Ba	18	34	52	41	37	53	18
Cr	1600	3000	4500	2200	1500	2100	2300
Se	b.d	0.10	0.10	0.10	b.d	b.d	b.d
Sr	4	12	11	2	2	2	2
Rb	9	2	3	16	6	8	17
As	19	276	528	122	101	6	6
Tl	b.d	b.d	b.d	b.d	b.d	b.d	b.d
Ag	b.d	b.d	b.d	b.d	b.d	b.d	b.d
Pt	b.d	10	b.d	10	10	10	20
Pd	b.d	11	9	9	6	3	4

b.d - below detection limit
total iron as Fe_2O_3
significant figures for Ni and Cr = 2; all others as in detection limits (Appendix I)

Serpentinite

Sample	NT-0428	NT-0429	NT-0430	NT-0431
SiO2	38.20	38.70	39.30	39.00
Al2O3	0.82	2.00	0.63	0.76
TiO2	0.02	0.04	0.02	0.02
MgO	37.40	37.60	37.90	36.50
CaO	0.18	0.08	0.07	0.08
Na2O	0.03	0.05	0.02	0.03
K2O	b.d	b.d	b.d	b.d
Fe2O3	9.11	8.45	8.51	9.54
MnO	0.09	0.11	0.10	0.19
P2O5	0.01	0.01	0.01	0.01
CO2	0.19	0.04	0.07	0.06
H2OP	12.10	11.70	12.20	11.60
S	0.01	0.01	b.d	0.01
TOTAL	98.17	98.79	98.84	97.81
Co	96	77	91	100
Ni	1700	1100	1300	1400
Cu	b.d	b.d	b.d	b.d
Zn	21	31	20	55
Mo	b.d	b.d	b.d	b.d
Cd	b.d	b.d	b.d	b.d
Pb	b.d	4	b.d	b.d
Y	9	4	6	6
Zr	13	15	11	17
Nb	b.d	14	b.d	b.d
Ba	b.d	22	15	b.d
Cr	2000	2200	1500	1500
Se	b.d	b.d	0.20	0.30
Sr	b.d	b.d	b.d	3
Rb	6	5	8	8
As	7	b.d	b.d	b.d
Tl	b.d	b.d	b.d	b.d
Ag	b.d	b.d	b.d	b.d
Pt	20	20	b.d	10
Pd	12	4	8	7

b.d - below detection limit
total iron as Fe_2O_3
significant figures for Ni and Cr = 2; all others as in detection limits (Appendix I)

Serpentine - Carbonate

Sample	NT-0036	NT-0037	NT-0042	NT-0050	NT-0051	NT-0052	NT-0053
SiO2	39.10	38.80	29.20	39.00	38.70	38.40	40.80
Al2O3	0.19	0.34	0.06	0.22	0.19	0.60	0.31
TiO2	0.02	0.02	0.02	0.02	0.02	0.02	0.02
MgO	37.70	38.20	39.20	38.00	39.30	37.50	38.40
CaO	0.08	0.08	0.11	0.11	0.12	0.08	0.08
Na2O	0.02	b.d	0.04	b.d	b.d	0.03	0.04
K2O	b.d	b.d	b.d	0.02	b.d	b.d	b.d
Fe2O3	8.26	7.34	9.72	6.76	5.50	6.72	6.72
MnO	0.10	0.10	0.31	0.11	0.12	0.08	0.08
P2O5	0.01	0.01	0.01	0.01	0.01	0.01	0.01
CO2	4.61	2.48	10.90	4.50	3.98	2.26	0.95
H2OP	9.70	11.40	8.40	10.60	10.80	11.70	10.70
S	0.03	0.01	0.03	0.02	0.02	0.01	b.d
TOTAL	99.82	98.79	98.00	99.37	98.77	97.43	98.12
Co	85	79	160	95	88	83	94
Ni	2200	2100	5100	2600	2200	2100	2100
Cu	b.d	b.d	9.50	b.d	b.d	b.d	b.d
Zn	28	34	38	19	24	24	27
Mo	b.d	b.d	b.d	b.d	b.d	b.d	b.d
Cd	b.d	1	b.d	b.d	b.d	b.d	1
Pb	b.d	b.d	b.d	b.d	4	b.d	b.d
Y	3	5	8	5	6	4	5
Zr	16	16	10	11	10	12	14
Nb	10	b.d	14	25	17	11	b.d
Ba	25	b.d	29	10	25	25	15
Cr	2100	2400	1200	1400	1500	2200	2000
Se	b.d	0.30	b.d	b.d	b.d	b.d	b.d
Sr	b.d	b.d	2	b.d	3	b.d	b.d
Rb	16	15	17	18	18	15	16
As	25	56	49	28	42	40	11
Tl	b.d	b.d	b.d	b.d	b.d	b.d	b.d
Ag	b.d	b.d	b.d	b.d	b.d	b.d	b.d
Pt	b.d	10	40	b.d	20	20	b.d
Pd	3	5	770	b.d	82	3	b.d

b.d - below detection limit
total iron as Fe_2O_3
significant figures for Ni and Cr = 2; all others as in detection limits (Appendix I)

Serpentine - Carbonate

Sample	NT-0054	NT-0055	NT-0056	NT-0075	NT-0076	NT-0077	NT-0078
SiO2	35.30	34.40	40.00	33.80	34.70	39.80	39.40
Al2O3	0.26	0.28	0.35	0.17	0.22	0.23	0.19
TiO2	0.02	0.02	0.02	0.02	0.02	0.02	0.02
MgO	39.50	39.50	38.30	37.90	37.90	38.40	39.70
CaO	0.25	0.16	0.80	0.41	0.38	0.07	0.21
Na2O	b.d	0.02	0.03	0.02	0.05	0.02	0.03
K2O	b.d	b.d	b.d	b.d	b.d	b.d	b.d
Fe2O3	5.95	6.12	6.08	6.11	6.59	7.38	6.05
MnO	0.18	0.14	0.09	0.15	0.16	0.11	0.10
P2O5	0.01	0.01	0.01	0.01	0.01	0.01	0.01
CO2	7.85	8.47	2.22	14.58	11.56	2.88	3.79
H2OP	10.30	9.80	11.20	5.70	7.10	10.70	10.60
S	b.d	b.d	0.01	b.d	b.d	b.d	b.d
TOTAL	99.63	98.93	99.11	98.88	98.70	99.63	100.11
Co	76	82	78	76	87	88	74
Ni	1900	2000	2100	1800	2100	2200	1700
Cu	b.d	b.d	b.d	b.d	b.d	b.d	b.d
Zn	28	23	30	18	22	18	19
Mo	b.d	b.d	b.d	b.d	b.d	b.d	b.d
Cd	1	1	1	2	2	2	1
Pb	b.d	4	4	b.d	b.d	b.d	92
Y	7	8	6	8	6	8	7
Zr	15	15	15	10	10	12	10
Nb	15	b.d	11	b.d	18	b.d	16
Ba	20	21	b.d	28	b.d	34	b.d
Cr	1900	1900	1700	1300	1800	1600	1500
Se	b.d	b.d	b.d	b.d	b.d	b.d	b.d
Sr	15	4	27	15	11	2	11
Rb	15	19	20	17	8	14	9
As	30	31	6	b.d	6	7	14
Tl	b.d	b.d	b.d	b.d	b.d	b.d	b.d
Ag	b.d	b.d	b.d	b.d	b.d	b.d	b.d
Pt	b.d	b.d	b.d	b.d	b.d	10	b.d
Pd	b.d	3	3	3	b.d	6	2

b.d - below detection limit
total iron as Fe_2O_3
significant figures for Ni and Cr = 2; all others as in detection limits (Appendix I)

Serpentine - Carbonate

Sample	NT-0079	NT-0080	NT-0081	NT-0300	NT-0314	NT-0318	NT-0319
SiO2	39.60	35.70	37.90	39.90	42.90	37.30	37.40
Al2O3	0.20	0.22	0.27	0.40	0.34	0.07	0.34
TiO2	0.02	0.02	0.02	0.02	0.02	0.02	0.02
MgO	39.20	39.10	38.30	37.50	31.80	38.00	38.60
CaO	0.09	0.10	0.07	0.77	0.17	0.24	0.11
Na2O	0.02	0.04	0.03	0.07	0.02	b.d	0.04
K2O	b.d	b.d	b.d	b.d	b.d	b.d	b.d
Fe2O3	6.25	7.59	8.03	7.28	7.63	7.56	7.01
MnO	0.11	0.11	0.10	0.09	0.07	0.12	0.12
P2O5	0.01	0.01	0.01	0.01	0.01	0.01	0.01
CO2	3.51	6.49	2.48	1.19	12.42	5.65	3.96
H2OP	10.80	9.80	11.40	11.80	3.90	10.10	11.30
S	b.d	b.d	b.d	0.01	b.d	0.02	0.03
TOTAL	99.82	99.19	98.62	99.04	99.29	99.10	98.94
Co	80	80	93	87	79	79	90
Ni	1800	2000	2300	2300	2300	1900	2100
Cu	b.d	b.d	b.d	b.d	b.d	b.d	b.d
Zn	22	23	25	24	31	32	27
Mo	b.d	b.d	b.d	b.d	b.d	b.d	b.d
Cd	2	b.d	b.d	1	b.d	b.d	b.d
Pb	b.d	b.d	b.d	b.d	b.d	b.d	b.d
Y	5	8	5	5	7	6	8
Zr	10	9	11	10	12	12	12
Nb	b.d	b.d	18	13	b.d	b.d	12
Ba	19	10	17	b.d	13	27	19
Cr	1500	1800	1900	1800	2300	1800	1900
Se	b.d	b.d	b.d	b.d	b.d	b.d	b.d
Sr	b.d	b.d	2	15	b.d	10	b.d
Rb	8	15	18	17	7	17	6
As	18	18	17	30	b.d	28	98
Tl	b.d	b.d	b.d	b.d	b.d	b.d	b.d
Ag	b.d	b.d	b.d	b.d	b.d	b.d	b.d
Pt	b.d	b.d	b.d	b.d	b.d	b.d	b.d
Pd	b.d	b.d	4	24	3	3	3

b.d - below detection limit
total iron as Fe_2O_3
significant figures for Ni and Cr = 2; all others as in detection limits (Appendix I)

Serpentine - Carbonate

Sample	NT-0324	NT-0325	NT-0330	NT-0332	NT-0333	NT-6154	NT-6155
SiO2	40.30	44.90	37.30	35.30	36.30	38.80	35.60
Al2O3	0.34	0.33	0.25	0.26	0.22	0.45	0.45
TiO2	0.02	0.02	0.02	0.02	0.02	0.02	0.02
MgO	36.90	34.60	36.20	36.90	36.70	38.00	39.10
CaO	1.27	1.24	1.78	4.28	3.22	0.18	0.03
Na2O	0.04	0.03	0.04	0.03	0.05	0.03	0.02
K2O	b.d	b.d	b.d	b.d	b.d	0.02	0.02
Fe2O3	7.21	6.38	9.30	5.79	6.27	7.71	7.24
MnO	0.07	0.07	0.11	0.17	0.13	0.09	0.15
P2O5	0.01	0.01	0.01	0.01	0.01	0.01	0.01
CO2	1.89	2.02	2.79	7.26	5.52	2.82	5.85
H2OP	11.70	8.80	11.20	10.30	10.50	10.50	10.10
S	0.02	0.05	0.03	0.04	0.03	b.d	b.d
TOTAL	99.78	98.45	99.04	100.37	98.98	98.62	98.58
Co	84	87	97	85	89	85	110
Ni	2100	2300	2400	2500	2300	1900	2200
Cu	18	4	16	5	11	74	b.d
Zn	24	27	20	18	14	39	14
Mo	b.d	b.d	b.d	b.d	b.d	b.d	b.d
Cd	2	1	b.d	1	b.d	b.d	b.d
Pb	b.d	b.d	b.d	b.d	b.d	22	b.d
Y	3	6	4	7	6	b.d	b.d
Zr	10	15	13	14	15	21	21
Nb	b.d	b.d	b.d	b.d	14	12	b.d
Ba	25	15	b.d	15	24	34	b.d
Cr	2300	2200	2200	2300	1500	2200	1700
Se	b.d	0.10	0.10	b.d	b.d	b.d	b.d
Sr	21	18	27	89	68	19	7
Rb	7	9	14	8	7	7	4
As	83	123	293	234	210	56	114
Tl	b.d	b.d	b.d	b.d	b.d	b.d	b.d
Ag	b.d	b.d	b.d	b.d	b.d	b.d	b.d
Pt	10	b.d	b.d	10	b.d	20	20
Pd	12	4	2	b.d	b.d	3	b.d

b.d - below detection limit
total iron as Fe_2O_3
significant figures for Ni and Cr = 2; all others as in detection limits (Appendix I)

Serpentine - Carbonate

Sample	NT-6156	NT-6171	NT-6172	NT-6174
SiO2	35.20	33.40	28.90	35.40
Al2O3	0.40	0.27	0.24	0.15
TiO2	0.02	0.02	0.02	0.02
MgO	38.20	39.00	40.00	40.20
CaO	0.46	0.04	0.05	0.27
Na2O	0.05	0.01	0.02	0.02
K2O	0.03	b.d	b.d	b.d
Fe2O3	7.44	8.24	8.12	6.80
MnO	0.13	0.18	0.27	0.13
P2O5	0.01	0.01	0.01	0.01
CO2	7.90	6.97	10.98	2.97
H2OP	8.80	4.30	8.70	6.90
S	b.d	b.d	b.d	b.d
TOTAL	98.63	92.44	97.29	92.85
Co	74	98	85	88
Ni	2000	2400	2400	1900
Cu	b.d	b.d	b.d	b.d
Zn	20	33	21	33
Mo	b.d	b.d	b.d	b.d
Cd	b.d	b.d	b.d	b.d
Pb	b.d	b.d	b.d	6
Y	b.d	b.d	b.d	b.d
Zr	17	23	19	20
Nb	b.d	b.d	15	b.d
Ba	b.d	27	18	b.d
Cr	1700	2300	2100	1700
Se	b.d	b.d	b.d	b.d
Sr	27	8	10	13
Rb	9	6	7	8
As	7	106	126	225
Tl	2	b.d	b.d	b.d
Ag	b.d	b.d	b.d	b.d
Au	13	0.50	0.50	0.50
Pt	10	10	b.d	b.d
Pd	b.d	3	4	b.d

b.d - below detection limit
total iron as Fe_2O_3
significant figures for Ni and Cr = 2; all others as in detection limits (Appendix I)

Talc - Carbonate

Sample	NT-0035	NT-0073	NT-0071	NT-6175	NT-0228	NT-0072	NT-6157
SiO2	39.30	35.00	35.30	25.50	39.90	35.70	37.10
Al2O3	0.35	0.24	0.22	0.08	0.31	0.13	0.26
TiO2	0.02	0.02	0.02	0.01	0.02	0.01	0.02
MgO	34.10	35.70	34.60	40.70	33.50	35.80	34.30
CaO	0.13	0.14	0.15	0.05	0.10	0.16	0.10
Na2O	0.04	0.03	0.02	0.05	0.02	b.d	0.01
K2O	b.d	b.d	0.01	b.d	b.d	b.d	b.d
Fe2O3	6.53	7.58	8.28	8.58	7.08	7.25	7.20
MnO	0.08	0.12	0.12	0.39	0.07	0.13	0.09
P2O5	0.01	0.01	0.01	0.01	0.01	0.01	0.01
CO2	15.37	15.52	15.73	15.74	15.91	15.97	15.98
H2OP	2.70	4.40	3.50	7.60	3.20	3.70	2.20
S	0.01	0.01	0.01	b.d	0.01	0.01	b.d
TOTAL	98.65	98.77	97.97	98.69	100.13	98.88	97.27
Co	74	84	86	160	74	78	73
Ni	1900	2100	2200	4600	2100	2100	2200
Cu	b.d	b.d	b.d	15	b.d	b.d	b.d
Zn	33	17	35	12	17	15	18
Mo	b.d	b.d	b.d	b.d	b.d	b.d	b.d
Cd	1	2	b.d	b.d	2	2	b.d
Pb	4	10	b.d	b.d	b.d	6	b.d
Y	6	9	4	b.d	8	3	b.d
Zr	15	10	12	19	10	10	19
Nb	b.d	b.d	16	b.d	b.d	b.d	b.d
Ba	22	33	18	16	b.d	b.d	b.d
Cr	2100	1800	1600	280	1600	1300	1700
Se	0.10	b.d	b.d	b.d	b.d	b.d	b.d
Sr	b.d	b.d	b.d	8	b.d	b.d	10
Rb	18	16	6	5	8	17	8
As	18	b.d	b.d	67	b.d	b.d	7
Tl	b.d	b.d	b.d	b.d	b.d	b.d	b.d
Ag	b.d	b.d	b.d	b.d	b.d	b.d	b.d
Pt	b.d	10	20	10	10	10	10
Pd	b.d	b.d	b.d	310	b.d	6	4

b.d - below detection limit
total iron as Fe_2O_3
significant figures for Ni and Cr = 2; all others as in detection limits (Appendix I)

Talc - Carbonate

Sample	NT-0074	NT-0015	NT-6173	NT-0218	NT-0316	NT-0223	NT-0222
SiO2	33.50	39.00	24.40	38.60	35.40	35.60	37.90
Al2O3	0.21	0.38	0.22	0.31	0.10	0.25	0.27
TiO2	0.02	0.02	0.02	0.02	0.02	0.02	0.02
MgO	36.10	33.50	41.50	32.90	34.20	34.80	35.00
CaO	0.18	1.24	0.10	0.69	0.18	0.10	0.09
Na2O	b.d	0.05	0.01	b.d	0.03	b.d	0.03
K2O	b.d	b.d	0.01	b.d	b.d	b.d	b.d
Fe2O3	7.60	5.60	6.96	7.52	8.24	7.11	6.02
MnO	0.13	0.07	0.43	0.09	0.11	0.06	0.12
P2O5	0.01	0.01	0.01	0.01	0.01	0.01	0.01
CO2	16.10	16.28	16.54	16.54	17.09	17.39	17.90
H2OP	4.40	2.80	3.40	3.00	3.20	3.00	3.20
S	0.01	b.d	b.d	0.01	0.02	0.01	b.d
TOTAL	98.27	98.96	93.59	99.70	98.61	98.36	100.57
Co	85	120	96	89	73	80	81
Ni	2300	2300	2400	2300	2000	2100	2100
Cu	b.d	b.d	1	b.d	b.d	b.d	b.d
Zn	24	16	47	26	25	14	29
Mo	b.d	b.d	b.d	b.d	b.d	b.d	b.d
Cd	1	b.d	b.d	2	b.d	1	2
Pb	b.d	b.d	b.d	b.d	b.d	b.d	b.d
Y	6	5	b.d	6	5	7	8
Zr	10	9	22	9	11	11	11
Nb	b.d	15	15	b.d	b.d	b.d	b.d
Ba	b.d	b.d	b.d	24	b.d	23	b.d
Cr	2000	1600	2100	1700	1400	1600	1800
Se	b.d	b.d	b.d	b.d	b.d	b.d	b.d
Sr	b.d	11	4	6	3	b.d	2
Rb	7	6	6	8	14	10	6
As	b.d	b.d	223	b.d	10	b.d	3
Tl	b.d	b.d	b.d	b.d	b.d	b.d	b.d
Ag	b.d	b.d	b.d	b.d	b.d	b.d	b.d
Pt	10	b.d	10	b.d	b.d	b.d	b.d
Pd	b.d	b.d	5	2	b.d	3	b.d

b.d - below detection limit
total iron as Fe_2O_3
significant figures for Ni and Cr = 2; all others as in detection limits (Appendix I)

Talc - Carbonate

Sample	NT-0018	NT-6177	NT-0016	NT-0315	NT-0070	NT-0027	NT-6158
SiO2	34.70	30.70	34.80	35.80	30.40	32.50	30.10
Al2O3	0.28	0.21	0.25	0.27	0.23	0.16	0.33
TiO2	0.02	0.01	0.02	0.02	0.02	0.02	0.02
MgO	34.80	36.10	35.10	34.60	37.10	35.30	36.10
CaO	0.12	0.04	0.19	0.20	0.32	0.12	0.33
Na2O	0.04	0.02	0.02	b.d	0.06	0.02	0.02
K2O	0.01	b.d	b.d	b.d	0.02	b.d	0.02
Fe2O3	7.11	6.72	6.77	6.83	5.55	6.71	7.47
MnO	0.10	0.11	0.12	0.11	0.17	0.10	0.13
P2O5	0.01	b.d	0.01	0.01	0.02	0.01	b.d
CO2	18.28	18.84	18.87	18.94	20.38	21.30	22.38
H2OP	2.20	1.60	2.60	3.30	3.40	3.00	4.70
S	b.d	b.d	0.01	b.d	b.d	b.d	b.d
TOTAL	97.68	94.32	98.76	100.09	97.67	99.25	101.58
Co	83	71	71	78	66	72	75
Ni	2100	1900	1900	2100	1500	2000	2300
Cu	b.d	b.d	b.d	3	b.d	b.d	b.d
Zn	21	11	20	22	16	20	17
Mo	b.d	b.d	b.d	b.d	b.d	b.d	b.d
Cd	1	b.d	1	b.d	b.d	b.d	b.d
Pb	b.d	b.d	30	b.d	b.d	b.d	b.d
Y	5	b.d	8	7	7	6	b.d
Zr	10	17	17	10	12	10	21
Nb	b.d	b.d	b.d	b.d	14	14	b.d
Ba	b.d	26	b.d	b.d	10	b.d	36
Cr	1500	1400	1900	1600	1400	1500	2000
Se	b.d	b.d	b.d	b.d	b.d	b.d	b.d
Sr	2	7	b.d	b.d	6	b.d	13
Rb	17	7	18	4	8	9	b.d
As	b.d	b.d	b.d	4	b.d	b.d	b.d
Tl	b.d	b.d	b.d	b.d	b.d	b.d	b.d
Ag	b.d	b.d	b.d	b.d	b.d	b.d	b.d
Pt	b.d	b.d	b.d	10	10	10	10
Pd	b.d	2	2	3	6	b.d	b.d

b.d - below detection limit
total iron as Fe_2O_3
significant figures for Ni and Cr = 2; all others as in detection limits (Appendix I)

Talc - Carbonate

Sample	NT-6176	NT-0224	NT-6153	NT-6151
SiO2	30.90	27.80	24.30	19.10
Al2O3	0.41	0.02	0.48	2.36
TiO2	0.02	0.02	0.02	0.05
MgO	36.20	37.00	35.00	33.60
CaO	0.11	0.32	0.15	0.22
Na2O	0.02	0.05	0.03	0.05
K2O	b.d	b.d	b.d	0.01
Fe2O3	6.79	6.23	7.63	7.63
MnO	0.09	0.16	0.06	0.05
P2O5	b.d	0.01	0.01	0.01
CO2	22.39	24.20	31.43	34.53
H2OP	1.70	2.10	1.10	1.30
S	b.d	b.d	b.d	b.d
TOTAL	98.60	97.92	100.19	98.90
Co	78	68	72	72
Ni	2200	2100	2100	1700
Cu	b.d	b.d	5	b.d
Zn	31	8.50	24	26
Mo	b.d	b.d	b.d	b.d
Cd	b.d	b.d	b.d	b.d
Pb	b.d	b.d	2	b.d
Y	b.d	9	b.d	b.d
Zr	18	17	22	28
Nb	b.d	12	b.d	15
Ba	b.d	19	52	41
Cr	2100	390	1700	1900
Se	b.d	b.d	b.d	b.d
Sr	5	3	6	7
Rb	6	14	6	4
As	b.d	b.d	b.d	b.d
Tl	b.d	b.d	b.d	b.d
Ag	b.d	b.d	b.d	b.d
Pt	10	b.d	40	b.d
Pd	4	b.d	3	3

b.d - below detection limit
total iron as Fe_2O_3
significant figures for Ni and Cr = 2; all others as in detection limits (Appendix I)

Arrowhead Pond

Sample	AHP-1	AHP-2	AHP-3	AHP-4	AHP-5	AHP-6	AHP-7
SiO2	36.20	29.40	19.10	26.30	11.60	38.60	26.80
Al2O3	1.15	0.67	1.20	1.01	1.82	0.46	0.62
TiO2	0.02	0.02	0.02	0.03	0.02	0.02	0.02
MgO	33.50	32.90	34.50	31.70	37.00	34.20	31.50
CaO	1.44	0.07	0.15	0.09	0.20	0.35	0.16
Na2O	0.01	0.05	0.03	0.04	0.05	0.02	0.03
K2O	b.d	b.d	b.d	b.d	b.d	b.d	b.d
Fe2O3	6.43	6.48	6.98	9.23	8.43	6.77	7.42
MnO	0.10	0.08	0.08	0.04	0.17	0.06	0.09
P2O5	0.01	0.01	0.01	0.01	0.01	0.01	0.01
CO2	15.47	29.63	36.73	30.72	35.44	16.82	33.54
H2OP	2.80	3.30	0.90	1.10	0.10	2.60	0.50
S	b.d	b.d	b.d	b.d	b.d	b.d	b.d
Total	97.13	102.61	99.70	100.27	94.84	99.91	100.69
Co	88	79	72	75	110	92	120
Ni	2000	1700	2200	2400	2300	2100	2200
Cu	19	b.d	3	b.d	1500	22	42
Zn	34	22	37	30	35	28	40
Mo	b.d	b.d	b.d	b.d	b.d	b.d	b.d
Cd	b.d	b.d	b.d	b.d	b.d	b.d	b.d
Pb	2	2	2	2	8	4	6
Y	b.d	b.d	b.d	b.d	b.d	b.d	b.d
Zr	20	22	21	27	22	22	18
Nb	b.d	b.d	13	11	13	11	b.d
Ba	107	23	b.d	b.d	b.d	b.d	16
Cr	1700	1300	2300	1700	2700	1600	1900
Se	b.d	b.d	b.d	b.d	b.d	b.d	b.d
Sr	18	9	4	3	7	8	6
Rb	6	7	8	6	5	9	8
As	18	b.d	b.d	b.d	b.d	6	b.d
Tl	b.d	b.d	b.d	b.d	b.d	b.d	b.d
Ag	b.d	b.d	b.d	b.d	21	b.d	b.d
Pt	10	10	10	b.d	b.d	b.d	10
Pd	5	4	6	5	4	b.d	8

b.d - below detection limit
total iron as Fe_2O_3
significant figures for Ni and Cr = 2; all others as in detection limits (Appendix I)

Arrowhead Pond

Sample	AHP-8	AHP-9	AHP-10(V)	AHP-11	AHP-12	AHP-13	AHP-14
SiO2	29.30	24.90	62.40	17.90	26.70	37.50	26.50
Al2O3	0.37	0.51	0.84	1.32	1.56	0.20	0.49
TiO2	0.02	0.02	0.01	0.04	0.04	0.02	0.02
MgO	31.40	33.00	15.70	35.00	30.90	30.40	33.20
CaO	0.11	0.18	0.65	0.15	0.11	0.89	0.12
Na2O	b.d	0.03	b.d	0.02	0.02	0.02	0.03
K2O	b.d	b.d	b.d	0.02	b.d	b.d	b.d
Fe2O3	6.93	7.04	2.84	7.22	6.74	9.76	6.45
MnO	0.03	0.09	0.14	0.10	0.06	0.10	0.08
P2O5	0.01	0.01	0.01	0.01	0.01	0.01	0.01
CO2	30.28	31.03	16.68	36.75	33.31	17.62	32.74
H2OP	0.60	0.80	0.50	0.80	1.00	2.30	0.60
S	b.d	b.d	b.d	b.d	b.d	b.d	b.d
Total	99.05	97.61	99.77	99.33	100.45	98.82	100.24
Co	90	70	30	74	63	86	75
Ni	2100	1900	630	2000	1500	1900	2000
Cu	b.d	b.d	450	b.d	b.d	b.d	b.d
Zn	48	30	12	30	47	22	22
Mo	b.d	b.d	b.d	b.d	b.d	b.d	b.d
Cd	b.d	b.d	b.d	b.d	b.d	b.d	b.d
Pb	4	4	b.d	b.d	4	4	2
Y	b.d	b.d	b.d	b.d	b.d	b.d	b.d
Zr	20	25	19	29	25	20	20
Nb	b.d	b.d	11	b.d	b.d	b.d	b.d
Ba	12	41	107	13	42	b.d	29
Cr	1400	1400	560	1800	1300	360	1400
Se	b.d	b.d	b.d	b.d	b.d	b.d	b.d
Sr	3	7	11	5	6	53	6
Rb	5	8	5	5	7	8	7
As	b.d	b.d	b.d	b.d	b.d	93	b.d
Tl	b.d	b.d	b.d	b.d	b.d	b.d	b.d
Ag	b.d	b.d	7	b.d	b.d	b.d	b.d
Pt	10	10	b.d	10	b.d	10	10
Pd	8	3	b.d	10	b.d	b.d	1

b.d - below detection limit
total iron as Fe_2O_3
significant figures for Ni and Cr = 2; all others as in detection limits (Appendix I)

Arrowhead Pond

Sample	AHP-15	AHP-16
SiO2	38.50	31.40
Al2O3	0.51	0.37
TiO2	0.01	0.03
MgO	34.30	35.50
CaO	0.21	0.23
Na2O	0.03	0.03
K2O	b.d	b.d
Fe2O3	6.74	8.43
MnO	0.03	0.09
P2O5	0.01	0.01
CO2	15.54	21.75
H2OP	2.70	2.50
S	b.d	b.d
Total	98.58	100.34
Co	87	85
Ni	2200	1800
Cu	b.d	280
Zn	27	36
Mo	b.d	b.d
Cd	b.d	b.d
Pb	2	4
Y	b.d	b.d
Zr	18	24
Nb	22	18
Ba	31	20
Cr	2100	1700
Se	b.d	b.d
Sr	9	10
Rb	4	4
As	b.d	11
Tl	b.d	b.d
Ag	b.d	1
Pt	5	10
Pd	1	3

b.d - below detection limit
total iron as Fe_2O_3
significant figures for Ni and Cr = 2; all others as in detection limits (Appendix I)

Appendix II - Mineral Chemical Data

Serpentine

	AC053-1	AC053-2	AC053-3	AC053-4	AC053-5	ACB053-1	SCM053-3	AC053-8	AC053-9	AVERAGE
SIO2	44.6	43.3	44.0	43.2	42.9	43.1	42.1	43.6	40.8	43.1
AL2O3	.2	.4	.1	.4	.4	.6	.2	.4	.6	.4
CR2O3	.n	.1	.n	.1	.n	.1	.n	.1	.2	.1
FEO	2.1	4.0	3.3	4.1	4.0	3.8	6.1	4.3	6.9	4.3
NIO	.1	.2	.1	.2	.3	.3	.1	.1	.3	.2
MNO	.1	.n	.n	.n	.n	.n	.n	.n	.n	.n
MGO	39.7	36.8	38.4	37.2	37.2	37.0	36.8	37.1	37.0	37.5
CAO	.n	.n	.1	.n	.n	.n	.n	.n	.n	.n
NA2O	.n	.1	.n	.2	.n	.n	.n	.n	.n	.n
K2O	.n	.1	.n	.n	.n	.n	.n	.n	.n	.n
TOTAL	87.0	85.4	86.2	85.8	85.2	85.2	85.6	85.9	86.0	85.8

Formula based on 7 O

SIO2	1.1	Si	2.054
AL2O3	.1	Al	0.000
CR2O3	.0		
FEO	1.4	Al	0.022
NIO	.0	Cr	0.044
MNO	.n	Fe	0.172
MGO	.9	Ni	0.009
CAO	.n	Mn	0.001
NA2O	.1	Mg	2.663
K2O	.n	Ca	0.003
		Na	0.005
TOTAL	.5	K	0.002

	P054-1	P054-2	P054-5	P054-6	P054-7	P054-8	P054-9	P054-10	P054-11	P054-13
SIO2	41.8	43.6	44.2	42.8	42.6	43.4	43.2	42.6	43.1	44.3
AL2O3	.3	.2	.4	.2	.4	.5	.5	.5	.2	.2
CR2O3	.1	.2	.n	.3	.1	.1	.n	.6	.4	.2
FEO	5.5	2.2	4.1	3.4	4.0	4.1	3.8	4.9	3.1	1.8
NIO	.3	.1	.3	.n	.4	.3	.2	.3	.2	.2
MNO	.n	.n	.n	.n	.n	.n	.n	.n	.1	.n
MGO	37.0	39.1	38.3	38.6	36.5	36.6	36.7	36.4	37.9	40.1
CAO	.n	.n	.n	.n	.n	.n	.n	.n	.n	.n
NA2O	.n	.n	.n	.n	.n	.n	.n	.n	.n	.n
K2O	.n	.n	.n	.n	.n	.n	.n	.n	.n	.n
TOTAL	85.4	85.7	87.7	85.6	84.4	85.2	84.7	85.8	85.3	87.0

	P054-14	P054-15	P054-17	P054-19	P054-23	P054-24	P054-25	P054-26	P054-28	P054-30
SIO2	41.3	42.2	42.0	43.8	42.2	43.5	43.1	43.1	42.6	43.7
AL2O3	.8	.5	.4	.2	.5	.3	.5	.2	.5	.2
CR2O3	.6	.1	.1	.3	.6	.2	.n	.4	.n	.4
FEO	6.0	4.5	4.6	2.9	4.3	3.5	3.9	3.6	4.1	3.0
NIO	.4	.3	.2	.1	.1	.1	.3	.n	.2	.2
MNO	.n	.n	.n	.n	.n	.n	.n	.n	.n	.n
MGO	36.3	36.8	36.9	39.1	37.8	38.8	37.6	38.6	36.7	38.6
CAO	.n	.n	.n	.n	.n	.n	.n	.n	.n	.n
NA2O	.n	.n	.n	.n	.n	.n	.n	.n	.n	.n
K2O	.n	.n	.n	.n	.n	.n	.n	.n	.n	.n
TOTAL	85.7	84.7	84.5	86.6	85.8	86.6	85.7	86.2	84.4	86.4

total Fe as FeO
n = calculated concentration below accuracy (.1 wt %)

Serpentine

	P054-31	P054-32	P054-33	P054-34	AVERAGE	SD	Formula based on 7 O
SIO2	42.1	41.6	41.9	42.8	42.8	.82	Si - 2.048
AL2O3	.4	.4	.4	.2	.2	.1	Al - 0.000
CR2O3	.3	.2	.1	.1	.2	.1	
FEO	4.4	4.9	5.1	4.0	4.0	.9	Al - 0.023
NIO	.3	.3	.3	.2	.2	.1	Cr - 0.010
MNO	.n	.n	.n	.n	.n	.n	Fe - 0.161
MGO	36.4	36.0	36.9	37.5	37.6	1.1	Ni - 0.010
CAO	.n	.n	.n	.n	.n	.n	Mn - 0.002
NA2O	.n	.n	.n	.n	.n	.n	Mg - 2.679
K2O	.n	.n	.n	.n	.n	.n	Ca - 0.002
							Na - 0.000
TOTAL	84.1	83.7	84.9	85.2	85.5	.9	K - 0.001

	P055-1	P055-2	P055-3	P055-4	P055-5	P055-6	P055-7	P055-9	P055-11	P055-12
SIO2	42.5	43.1	42.8	43.1	42.6	43.4	40.4	43.9	43.0	42.6
AL2O3	.1	.3	.3	.3	.5	.2	.8	.3	.5	.2
CR2O3	.1	.6	.4	.4	.2	.3	.4	.2	.2	.n
FEO	3.3	4.5	4.6	4.2	3.7	3.4	5.8	3.3	4.1	3.4
NIO	.2	.2	.2	.2	.2	.1	.2	.1	.2	.2
MNO	.1	.n	.n	.n	.n	.n	.n	.n	.n	.n
MGO	38.6	37.5	37.9	37.8	37.3	38.6	37.0	38.6	37.4	37.8
CAO	.n	.n	.n	.n	.n	.n	.n	.n	.n	.n
NA2O	.n	.n	.n	.n	.n	.n	.n	.n	.n	.n
K2O	.n	.n	.n	.n	.n	.n	.n	.n	.n	.n
TOTAL	85.0	86.5	86.4	86.2	84.7	86.3	85.0	86.7	85.6	84.5

	P055-14	P055-15	P055-16	P055-17	P055-18	P055-19	P055-19	P055-22	P055-23	P055-25
SIO2	42.0	43.0	40.6	42.3	42.6	41.9	41.8	43.7	42.4	43.7
AL2O3	.7	.5	1.0	.5	.4	.6	.7	.2	.5	.2
CR2O3	.8	.2	.5	.2	.5	.6	.9	.1	.4	.4
FEO	4.7	4.1	6.4	5.1	4.3	5.3	5.4	2.8	4.3	2.7
NIO	.3	.2	.2	.3	.1	.3	.2	.2	.4	.3
MNO	.n	.n	.n	.n	.n	.n	.n	.n	.1	.n
MGO	36.8	37.3	36.2	37.1	37.6	36.0	36.3	38.9	36.4	38.4
CAO	.n	.n	.n	.n	.n	.n	.n	.n	.n	.n
NA2O	.n	.n	.n	.n	.n	.n	.n	.n	.n	.n
K2O	.n	.n	.n	.n	.n	.n	.n	.n	.n	.n
TOTAL	85.6	85.6	85.3	85.8	85.8	85.0	85.6	86.2	84.9	86.0

	P055-27	AVERAGE	SD	Formula based on 7 O
SIO2	43.9	42.6	.9	Si - 2.040
AL2O3	.1	.4	.2	Al - 0.000
CR2O3	.2	.4	.2	
FEO	3.3	4.2	.9	Al - 0.026
NIO	.2	.2	.0	Cr - 0.015
MNO	.n	.n	.n	Fe - 0.169
MGO	38.3	37.5	.8	Ni - 0.010
CAO	.n	.n	.n	Mn - 0.002
NA2O	.n	.n	.n	Mg - 2.677
K2O	.n	.n	.n	Ca - 0.002
				Na - 0.000
TOTAL	86.4	85.7	.6	K - 0.001

total Fe as FeO
n = calculated concentration below accuracy (.1 wt %)

Talc

	MC228-3	CA228-1	SC228-2	MC228-7	MC228-8	MC228-9	CMA228-1	MC228-13	AVERAGE	SD
SIO2	63.1	62.2	61.8	62.6	63.4	62.0	62.1	60.5	62.2	.8
AL2O3	.n	.n	.1	.n	.1	.1	.n	.1	.1	.n
FEO	1.1	1.1	1.4	1.4	1.3	1.6	1.5	1.8	1.4	.2
MNO	.n	.n	.n	.n	.n	.n	.n	.n	.n	.n
MGO	30.0	30.3	30.4	30.4	30.4	30.3	30.5	30.3	30.3	.1
CR2O3	.0	.n	.1	.n	.n	.n	.n	.n	.n	.n
NIO	.3	.2	.2	.3	.3	.2	.3	.4	.3	.n
CAO	.n	.n	.n	.n	.n	.n	.n	.n	.n	.n
NA2O	.n	.n	.n	.n	.n	.n	.n	.n	.n	.n
K2O	.n	.n	.n	.n	.n	.n	.n	.n	.n	.n
TOTAL	94.8	94.1	94.2	94.9	95.9	94.5	94.9	93.4	94.6	.7

Formula based on 22 O

Si - 7.983
Al - 0.017

Al - 0.000
Fe - 0.157
Mn - 0.001
Mg - 5.806
Cr - 0.006
Ni - 0.034
Ca - 0.001
Na - 0.000
K - 0.003

	P027-2	P027-3	P027-4	P027-6	P027-7	P027-8	P027-9	P027-10	P027-11	P027-12
SIO2	61.8	61.2	61.8	61.7	61.6	62.0	62.5	62.4	61.6	62.3
AL2O3	.1	.1	.n	.n	.n	.n	.1	.n	.n	.n
FEO	1.6	1.6	1.8	2.2	2.6	1.7	2.2	1.7	2.7	1.9
MNO	.n	.n	.n	.n	.n	.n	.n	.n	.n	.n
MGO	29.7	29.5	29.4	29.1	28.3	29.5	29.7	29.7	28.5	29.9
CR2O3	.1	.n	.n	.n	.n	.n	.n	.n	.n	.1
NIO	.3	.2	.5	.5	.5	.5	.3	.3	.3	.4
CAO	.n	.n	.n	.n	.n	.n	.n	.n	.n	.n
NA2O	.n	.n	.n	.n	.n	.n	.n	.n	.n	.n
K2O	.n	.n	.n	.n	.n	.n	.n	.n	.n	.n
TOTAL	93.9	93.0	93.7	93.7	93.3	94.0	95.0	94.3	93.4	94.9

	P027-14	P027-15	P027-16	P027-17	P027-20	P027-21	P027-22	P027-23	P027-24	P027-25
SIO2	61.7	62.1	62.3	61.6	62.1	61.9	62.3	61.8	61.4	56.9
AL2O3	.1	.1	.n	.n	.n	.n	.n	.n	.2	.n
FEO	1.7	1.5	1.6	2.0	1.5	2.7	1.7	3.0	2.6	11.0
MNO	.n	.n	.n	.n	.n	.n	.n	.n	.n	.n
MGO	29.6	29.7	30.1	29.3	29.4	28.8	29.9	28.3	28.8	27.7
CR2O3	.n	.n	.n	.n	.n	.n	.n	.n	.n	.n
NIO	.2	.4	.1	.3	.4	.9	.4	.8	.6	.4
CAO	.n	.n	.n	.n	.n	.n	.n	.n	.n	.n
NA2O	.n	.n	.n	.n	.n	.n	.n	.n	.n	.n
K2O	.n	.n	.n	.n	.n	.n	.n	.n	.n	.n
TOTAL	93.61	93.9	94.4	93.7	93.7	94.2	94.6	94.3	94.1	96.2

total Fe as FeO
n = calculated concentration below accuracy (.1 wt %)

Talc

	P027-26	P027-27	P027-28	P027-30	P027-33	P027-34	P027-35	AVERAGE	SD
SIO2	62.4	62.2	61.9	62.3	61.3	62.5	62.2	61.8	1.0
AL2O3	.n	.1	.1	.1	.n	.1	.n	.n	.n
FEO	1.4	1.6	1.6	1.3	2.7	1.7	1.6	2.3	1.8
MNO	.n	.n	.n	.n	.n	.n	.1	.n	.n
MGO	30.1	29.7	29.6	29.8	29.0	29.7	29.8	29.4	.6
CR2O3	.n	.n	.n	.1	.n	.n	.n	.n	.n
NIO	.6	.2	.2	.4	.2	.2	.4	.4	.1
CAO	.n	.n	.n	.n	.n	.n	.n	.n	.n
NA2O	.n	.n	.n	.n	.n	.n	.n	.n	.n
K2O	.n	.n	.n	.n	.n	.n	.n	.n	.n
TOTAL	94.7	94.1	93.6	94.3	93.5	94.4	94.4	94.1	.6

Formula based on 22 O

Si - 7.999
Al - 0.001

Al - 0.013
Fe - 0.251
Mn - 0.003
Mg - 5.672
Cr - 0.005
Ni - 0.045
Ca - 0.003
Na - 0.000
K - 0.002

	TC224-1	TC224-2	TCM224-1	TC224-3	TCM224-2	MC224-1	TCM224-3	TC224-5	TC224-6	AVERAGE
SIO2	63.3	62.0	62.0	62.5	62.9	62.6	62.8	63.2	63.4	62.7
AL2O3	.1	.1	.1	.1	.1	.n	.1	.n	.1	.1
FEO	1.0	2.6	2.8	1.7	1.6	2.3	1.4	1.3	1.1	1.8
MNO	.n	.n	.n	.n	.n	.n	.n	.n	.n	.n
MGO	30.4	28.5	28.9	29.4	29.6	28.7	29.4	29.6	29.9	29.4
CR2O3	.n	.1	.n	.n	.n	.n	.n	.n	.n	.n
NIO	.4	.6	.8	.5	.5	.5	.5	.5	.4	.5
CAO	.n	.n	.n	.n	.n	.n	.n	.n	.n	.n
NA2O	.n	.n	.n	.n	.n	.n	.n	.n	.n	.n
K2O	.n	.n	.n	.n	.n	.n	.n	.n	.n	.n
TOTAL	95.4	94.2	94.9	94.6	94.9	94.5	94.5	95.0	95.2	94.8

	SD
SIO2	.5
AL2O3	.0
FEO	.6
MNO	.0
MGO	.6
CR2O3	.n
NIO	.1
CAO	.n
NA2O	.n
K2O	.n
TOTAL	.3

Formula based on 22 O

Si - 8.043
Al - 0.000

Al - 0.017
Fe - 0.193
Mn - 0.002
Mg - 5.622
Cr - 0.005
Ni - 0.059
Ca - 0.004
Na - 0.000
K - 0.002

total Fe as FeO
n = calculated concentration below accuracy (.1 wt %)

Carbonate

	CA053-1	CA053-2	CA053-4	CAB053-1	CAB053-2	CAB053-3	CMS053-1	CMS053-2	CMS053-3	CA053-7
CAO	.1	.1	.4	.1	.5	.n	.1	.1	.4	.1
MGO	46.1	42.5	45.1	45.6	45.7	46.9	46.2	45.0	46.1	46.1
MNO	1.1	.n	.1	.4	1.4	.7	1.1	.5	1.2	.7
FEO	1.5	3.5	3.3	3.5	1.1	2.1	1.5	3.2	1.9	2.5
BAO	.n	.n	.n	.1	.n	.n	.n	.1	.n	.n
SRO	.n	.n	.n	.n	.n	.n	.n	.n	.n	.n
TOTAL	49.0	46.4	49.1	49.9	48.8	49.9	49.0	49.1	49.7	49.5

	CA053-8	CA053-9	AVERAGE	SD
CAO	.2	.7	.2	.2
MGO	46.1	42.7	45.4	1.3
MNO	1.n	.2	.7	.4
FEO	1.3	7.2	2.7	1.6
BAO	.n	.n	.n	.n
SRO	.n	.n	.n	.n
TOTAL	48.8	50.9	49.2	1.0

Formula based on 6 O

Ca - 0.025
Mg - 5.725
Mn - 0.053
Fe - 0.195
Ba - 0.001
Sr - 0.000

	CO54-1	CO54-2	CO54-3	TEST2	CO54-4	CO54-5	CO54-6	CO54-7	PO54-12	CO54-8
CAO	.2	.1	.2	.n	.3	.1	.1	.1	.n	.1
MGO	45.0	45.1	44.8	40.2	44.5	45.1	45.1	45.4	43.2	45.3
MNO	.6	.7	.8	.n	.9	.7	.8	.8	.n	.9
FEO	1.9	2.8	2.4	3.8	1.8	2.1	2.8	2.0	1.5	1.9
BAO	.n	.n	.n	.n	.n	.n	.n	.n	.n	.n
SRO	.n	.n	.n	.n	.n	.n	.n	.n	.n	.n
TOTAL	47.9	48.8	48.4	44.1	47.8	48.2	48.9	48.6	45.1	48.4

	CO54-	CO54-10	CO54-11	CO54-13	CO54-14	CO54-15	CO54-16	CO54-17	CO54-18	AVERAGE
CAO	.n	.1	.1	.1	.n	.5	.4	.4	.n	.1
MGO	45.0	44.2	45.6	44.8	43.3	45.0	45.3	45.2	45.1	44.6
MNO	.7	.6	1.3	.7	.4	1.2	1.1	.9	.7	.7
FEO	2.5	3.3	.9	3.0	6.4	2.1	1.6	3.1	2.2	2.5
BAO	.n	.n	.n	.n	.n	.n	.n	.n	.n	.n
SRO	.n	.n	.n	.n	.n	.n	.n	.n	.n	.n
TOTAL	48.3	48.3	48.0	48.7	50.3	48.8	48.5	49.8	48.3	48.2

	SD
CAO	.1
MGO	1.2
MNO	.3
FEO	1.1
BAO	.n
SRO	.n
TOTAL	1.4

Formula based on 6 O

Ca - 0.018
Mg - 5.736
Mn - 0.056
Fe - 0.187
Ba - 0.001
Sr - 0.001

n = calculated concentration below accuracy (.1 wt %)

Carbonate

	C055-1	C055-2	C00	C055-4	C055-5	C055-8	C055-9	C055-10	C055-11	C055-12
CAO	.2	.n	.2	.1	.1	.1	.2	.1	.1	.2
MGO	45.0	45.5	45.5	45.6	45.8	45.6	45.6	45.0	45.6	45.5
MNO	.8	.7	1.0	.7	.8	.7	.5	.7	.7	.1
FEO	2.1	1.7	2.3	2.4	1.6	1.8	2.0	2.9	2.0	2.8
BAO	.n	.n	.1	.n	.n	.n	.n	.n	.n	.n
SRO	.n	.n	.n	.n	.n	.n	.n	.n	.n	.n
TOTAL	48.4	48.0	49.2	49.0	48.4	48.4	48.5	48.9	48.5	48.7

	C055-13	C055-14	C055-15	C055-16	C055-17	C055-18	C055-19	C055-20	C055-21	C055-22
CAO	.n	.2	.5	.1	.2	.1	.2	.1	.1	.1
MGO	45.2	43.2	42.7	45.5	45.6	42.9	44.3	45.2	45.7	45.9
MNO	.8	.6	.7	1.0	1.1	.6	.2	.5	.2	.9
FEO	1.9	6.4	5.8	2.0	1.6	6.3	3.5	2.4	2.3	1.7
BAO	.n	.n	.n	.n	.n	.1	.n	.n	.1	.n
SRO	.n	.n	.n	.n	.n	.n	.n	.n	.n	.n
TOTAL	48.1	50.6	49.9	48.8	48.7	50.1	48.4	48.5	48.6	48.7

	C055-23	C055-24	C055-25	C055-26	C055-27	AVERAGE	SD
CAO	.1	.1	.1	.3	.2	.2	.1
MGO	45.4	45.8	44.9	45.1	45.4	45.1	.8
MNO	.7	.n	.1	.1	.n	.6	.3
FEO	2.4	2.5	3.n	3.3	2.7	2.8	1.3
BAO	.1	.1	.1	.n	.n	.n	.n
SRO	.n	.n	.n	.n	.n	.n	.n
TOTAL	48.8	48.6	48.4	49.0	48.5	48.8	.6

Formula based on 6 O

Ca - 0.018
Mg - 5.764
Mn - 0.045
Fe - 0.171
Ba - 0.n01
Sr - 0.000

	CM228-1	CM228-2	CM228-3	CA228-1	CM228-5	CM228-6	CM228-7	CM228-8	CM228-9	CMA228-1
CAO	.4	.2	.3	.4	.2	.3	.5	.2	.4	.3
MGO	44.0	43.2	44.2	43.7	44.6	44.5	43.7	44.5	43.9	44.3
MNO	.3	.1	.n	.1	.n	.1	.n	.n	.n	.n
FEO	4.7	5.5	5.3	6.0	5.9	4.9	5.6	5.1	5.8	5.2
BAO	.n	.1	.n	.n	.n	.n	.1	.n	.n	.n
SRO	.n	.n	.n	.n	.n	.n	.n	.n	.1	.n
TOTAL	49.6	49.2	49.9	50.4	50.8	50.0	50.0	50.0	50.3	50.1

Carbonate

	CM228-10	CM228-11	CM228-12	CM228-13	CM228-14	CMA228-2	CMA228-3	CMA228-4	AVE.	SD
CAO	.2	.2	.2	.5	.3	.4	.3	.3	.3	.1
MGO	44.7	44.6	44.5	43.8	44.2	44.6	43.6	44.6	44.2	.4
MNO	.1	.n	.n	.n	.n	.n	.n	.2	.n	.n
FEO	5.2	4.9	4.9	5.1	5.6	5.3	5.6	4.5	5.3	.4
BAO	.n	.n	.n	.n	.n	.n	.n	.n	.n	.n
SRO	.n	.n	.n	.n	.n	.n	.n	.n	.n	.n
TOTAL	50.3	49.9	49.8	49.5	50.3	50.5	49.7	49.8	50.0	.4

Formula based on 6 O

Ca - 0.032
Mg - 5.583
Mn - 0.006
Fe - 0.377
Ba - 0.001
Sr - 0.001

n = calculated concentration below accuracy (.1 wt %)

Carbonate

	C027-2	C027-3	C027-4	C027-5	C027-6	C027-7	C027-8	C027-9	C027-10	C027-11
CAO	.n	.1	.n	.n	.n	.2	.1	.1	.n	.1
MGO	43.9	43.6	44.1	44.3	43.2	45.8	43.9	43.5	44.3	43.4
MNO	.n	.n	.n	.n	.n	.8	.1	.n	.n	.n
FEO	5.4	5.6	5.1	5.0	6.9	1.2	5.9	5.5	4.3	6.1
BAO	.n	.n	.n	.n	.n	.1	.1	.n	.n	.n
SRO	.n	.n	.n	.n	.n	.n	.n	.n	.n	.n
TOTAL	49.4	49.4	49.3	49.6	50.2	48.2	50.2	49.4	48.8	49.7

	C027-12	C027-13	C027-14	C027-15	C027-16	C027-17	C027-18	C027-19	C027-20	C027-21
CAO	.n	.n	.1	.2	.1	.n	.n	.1	.1	.1
MGO	45.5	44.3	42.8	43.1	44.3	44.3	45.2	44.6	45.7	45.1
MNO	.4	.n	.n	.n	.n	.1	.2	.1	.7	.1
FEO	3.1	5.2	7.0	7.0	4.7	4.4	3.8	4.8	2.2	4.5
BAO	.n	.n	.n	.n	.n	.n	.n	.n	.n	.n
SRO	.n	.n	.n	.n	.n	.n	.n	.n	.n	.n
TOTAL	49.1	49.7	50.0	50.5	49.3	49.0	49.4	49.8	48.8	50.0

	C027-21	P027-22	C027-23	C027-24	C027-25	C027-26	C027-27	C027-28	C027-29	C027-30
CAO	.n	.n	.1	.n	.n	.1	.1	.n	.1	.1
MGO	44.9	40.9	43.5	44.5	44.5	44.4	43.8	44.0	44.2	44.0
MNO	.1	.2	.n	.n	.1	.n	.n	.n	.n	.n
FEO	4.1	9.8	5.9	4.6	5.2	5.0	5.7	5.0	5.3	6.2
BAO	.n	.n	.n	.n	.n	.n	.1	.n	.n	.n
SRO	.n	.n	.n	.n	.n	.n	.n	.n	.n	.n
TOTAL	49.3	51.0	49.6	49.3	49.9	49.8	49.8	49.3	49.8	50.4

	C027-31	C027-32	AVERAGE	SD
CAO	.1	.n	.1	.n
MGO	44.1	40.5	44.0	1.1
MNO	.n	.3	.1	.2
FEO	5.9	10.2	5.3	1.7
BAO	.n	.n	.n	.n
SRO	.n	.n	.n	.n
TOTAL	50.3	51.2	49.7	.6

Formula based on 6 O

Ca - 0.009
Mg - 5.595
Mn - 0.010
Fe - 0.383
Ba - 0.001
Sr - 0.001

	CT224-1	CT224-2	CTM224-1	CT224-3	CTMS2241	CTM224-2	CT224-4	CM224-1	CTM224-3	CT224-5
CAO	.4	.1	.2	.2	.1	.3	.n	.2	.2	.n
MGO	44.5	46.7	40.6	38.4	37.9	44.6	42.5	46.9	45.9	42.8
MNO	.1	.5	.n	.1	.1	.3	.1	.6	.4	.1
FEO	4.8	1.4	10.9	13.6	14.2	3.8	7.8	.5	3.2	8.3
BAO	.n	.n	.n	.n	.n	.n	.n	.n	.n	.n
SRO	.n	.n	.n	.n	.n	.n	.n	.n	.n	.n
TOTAL	49.98	48.5	51.7	52.5	52.4	49.1	50.5	48.3	49.9	51.4

n = calculated concentration below accuracy (.1 wt %)

Carbonate

	CT224-6	AVERAGE	SD
CAO	.8	.2	.2
MGO	43.4	43.1	3.1
MNO	.1	.2	.1
FEO	4.8	6.6	4.6
BAO	.n	.n	.n
SRO	.n	.n	.n
TOTAL	49.3	50.4	1.4

Formula based on 6 O

Ca - 0.026
Mg - 5.479
Mn - 0.019
Fe - 0.476
Ba - 0.n01
Sr - 0.000

Magnetite

	AC8053-1
AL203	.n
CR203	.2
FE203	67.9
V203	.n
TIO2	.n
FEO	30.1
MGO	.n
MNO	.n
ZNO	.1
NIO	.5
TOTAL	99.0

	S054-1	S054-2	S054-3	S054-4	S054-5	S054-6	S054-7	S054-8	S054-9	AVERAGE
Al203	.n	.n	.n	.n	.n	.n	.n	.n	.n	.n
CR203	.n	.n	.n	.1	.n	.n	.n	.n	.n	.n
FE203	66.2	66.1	67.4	66.9	66.6	67.2	66.0	67.0	66.5	66.6
V203	.n	.n	.n	.n	.1	.n	.1	.1	.n	.n
TIO2	.n	.n	.n	.n	.n	.n	.n	.n	.n	.n
FEO	29.2	29.0	29.5	29.4	29.3	29.7	29.3	29.7	29.5	29.4
MGO	.n	.2	.n	.n	.1	.n	.n	.n	.n	.n
MNO	.n	.1	.n	.n	.n	.n	.n	.n	.n	.n
ZNO	.n	.n	.1	.1	.n	.n	.n	.n	.n	.n
NIO	.3	.1	.5	.7	.6	.6	.4	.5	.5	.4
TOTAL	96.n	95.8	97.7	97.6	96.8	97.7	96.1	97.5	96.8	96.9

n = calculated concentration below accuracy (.1 wt %)

	SD
AL203	.n
CR203	.n
FE203	.5
V203	.n
TIO2	.n
FEO	.2
MGO	.n
MNO	.n
ZNO	.n
NIO	.1
TOTAL	.7

Magnetite

	S055-2	S055-3	AVERAGE	SD
AL203	.n	.n	.n	.n
CR203	.5	2.0	1.3	1.0
FE203	66.3	64.4	65.4	1.3
V203	.1	.n	.n	.1
TIO2	.n	.n	.n	.n
FEO	29.5	29.6	29.6	.n
MGO	.1	.n	.n	.n
MNO	.n	.n	.n	.n
ZNO	.n	.n	.n	.n
NIO	.3	.4	.4	.n
TOTAL	97.2	96.7	97.0	.3

	MC228-5	MC228-13	MCA228-2	AVERAGE	SD
AL203	.n	.n	.n	.n	.n
CR203	.5	.8	.5	.6	.1
FE203	67.1	65.9	67.1	66.7	.6
V203	.1	.n	.n	.1	.n
TIO2	.n	.n	.n	.n	.n
FEO	29.9	29.5	29.8	29.7	.2
MGO	.1	.1	.1	.1	.n
MNO	.n	.n	.n	.n	.n
ZNO	.n	.n	.n	.n	.n
NIO	.4	.4	.4	.4	.n
TOTAL	98.5	97.1	98.4	98.0	.7

	S027-1	S027-2	S027-3	S027-4	S027-6	S027-7	S027-8	S027-9	S027-10-	S027-11
AL203	.n	.n	.n	.n	.n	.n	.n	.n	.n	.n
CR203	.3	.3	.2	.1	.1	.6	.n	.1	.1	.1
FE203	66.2	67.4	67.6	67.n	66.6	66.1	67.3	67.5	66.7	66.3
V203	.1	.n	.3	.n	.n	.n	.1	.1	.1	.1
TIO2	.n	.n	.n	.n	.n	.n	.n	.n	.n	.n
FEO	29.2	30.1	30.3	30.0	28.0	29.0	29.7	30.3	29.9	29.3
MGO	.1	.n	.n	.n	.5	.2	.n	.n	.n	.2
MNO	.n	.n	.n	.n	.n	.n	.n	.n	.n	.n
ZNO	.2	.n	.n	.n	.2	.n	.n	.n	.n	.n
NIO	.3	.4	.4	.2	.7	.6	.8	.2	.2	.3
TOTAL	96.8	98.4	99.0	97.6	96.5	96.8	98.1	98.4	97.4	96.5

Magnetite

	S027-12	S027-13	C027-14	S027-15	S027-19	S027-20	S027-21	AVERAGE	SD
AL203	.n	.n	.n	.n	.n	.n	.n	.n	.n
CR203	.4	.n	.2	.2	.n	.n	.1	.2	.n
FE203	67.0	67.1	66.3	67.3	67.7	67.1	67.5	67.0	.5
V203	.1	.2	.1	.3	.1	.1	.n	.1	.n
TIO2	.1	.n	.n	.n	.n	.1	.n	.n	.n
FEO	29.9	29.7	29.5	30.2	30.4	29.9	29.9	29.7	.5
MGO	.n	.n	.n	.n	.n	.1	.n	.1	.1
MNO	.n	.1	.n	.n	.n	.n	.n	.n	.n
ZNO	.3	.1	.1	.n	.n	.n	.n	.n	.1
NIO	.4	.3	.2	.3	.2	.2	.4	.4	.1
TOTAL	98.6	97.9	96.81	98.6	98.7	97.8	98.2	97.8	.8

n = calculated concentration below accuracy (.1 wt %)

Appendix III - Calculations

Calculation of rock norms

The normative mineralogy of the altered ultramafic rocks are calculated utilizing the whole rock and mineral chemical data. The method used involves solving a set of equations of the form

$$ax=b$$

in which a is the moles oxide/mole mineral (mineral data), x is the moles mineral/100 g rock, and b is the moles oxide/100 g rock (whole rock data). As an example, using the whole rock of sample NT-054, the serpentine and carbonate compositions determined for NT-054, and the average talc composition from those determined (note the little variation in serpentine and talc with variation in whole rock CO_2) the equations are:

	x_1 mt	x_2 mgs	x_3 serp	x_4 talc	=	rock(b)
[FeO]	x_1 1	x_2 .031	x_3 .161	x_4 .101	=	.0744
[CO_2]	x_1 0	x_2 1	x_3 0	x_4 0	=	.1784
[MgO]	x_1 0	x_2 .956	x_3 2.679	x_4 2.81	=	.9801
[H_2O]	x_1 0	x_2 0	x_3 2	x_4 1	=	.5725

In matrix notation, Ax=B, the equations are written

$$\begin{matrix} 1 & .031 & .161 & .101 \\ 0 & 1 & 0 & 0 \\ 0 & .956 & 2.719 & 2.81 \\ 0 & 0 & 2 & 1 \end{matrix} \times \begin{matrix} x_1 \\ x_2 \\ x_3 \\ x_4 \end{matrix} = \begin{matrix} .0744 \\ .1784 \\ .9801 \\ .5725 \end{matrix}$$

which is solved by the relation $A^{-1}B=x$ where A^{-1} is the inverse of matrix A. The result of this calculation is

x_1	=	moles magnetite/100 g rock	=	.0222
x_2	=	moles magneste/100 g rock	=	.1784
x_3	=	moles serpentine/100 g rock	=	.2764
x_4	=	moles talc/100 g rock	=	.0196

normalized to 100 %, the rock consists of, in moles:

56 % serpentine

36 % magnesite

4 % magnetite

4 % talc

Calculation of metasomatic gains and losses

The gain or loss of mass (M) of a component (n) in the alteration of an original rock 'A' to product rock 'B' is given by Gresens (1967) equation

$$M_n = [(V^B/V^A \times g^B/g^A) C_n^B - C_n^A] M^A \qquad (1)$$

where g = specific gravity

C = concentration

A = superscript for original sample

B = superscript for altered sample

M^A = reference mass of original sample

n = subscript for component

If, for an immobile component such as MgO in this study

$$M_{MgO} = 0 \qquad \text{and if } M^A = 1$$

$$(V^B/V^A \times g^B/g^A) C_{MgO}^B - C_{MgO}^A = 0 \qquad \text{and}$$

$$(V^B/V^A \times g^B/g^A) = C_{MgO}^A/C_{MgO}^B \qquad (2)$$

Substitution of equation 2 into equation 1 yields

$$M_n = (C_{MgO}^A/C_{MgO}^B) C_n^B - C_n^A \qquad (3)$$

from which the gains, losses, or immobility of the other components can be evaluated. Because the layered ultramafic rocks have a variable composition, this equation is also solved for the high and low concentrations of the element under consideration (high and low in the layered ultramafic rocks) thus forming a range reflecting the variable composition about 0 change.